NASA CR 166728

AIS-5
12 YEAR IN ORBIT
EVALUATION

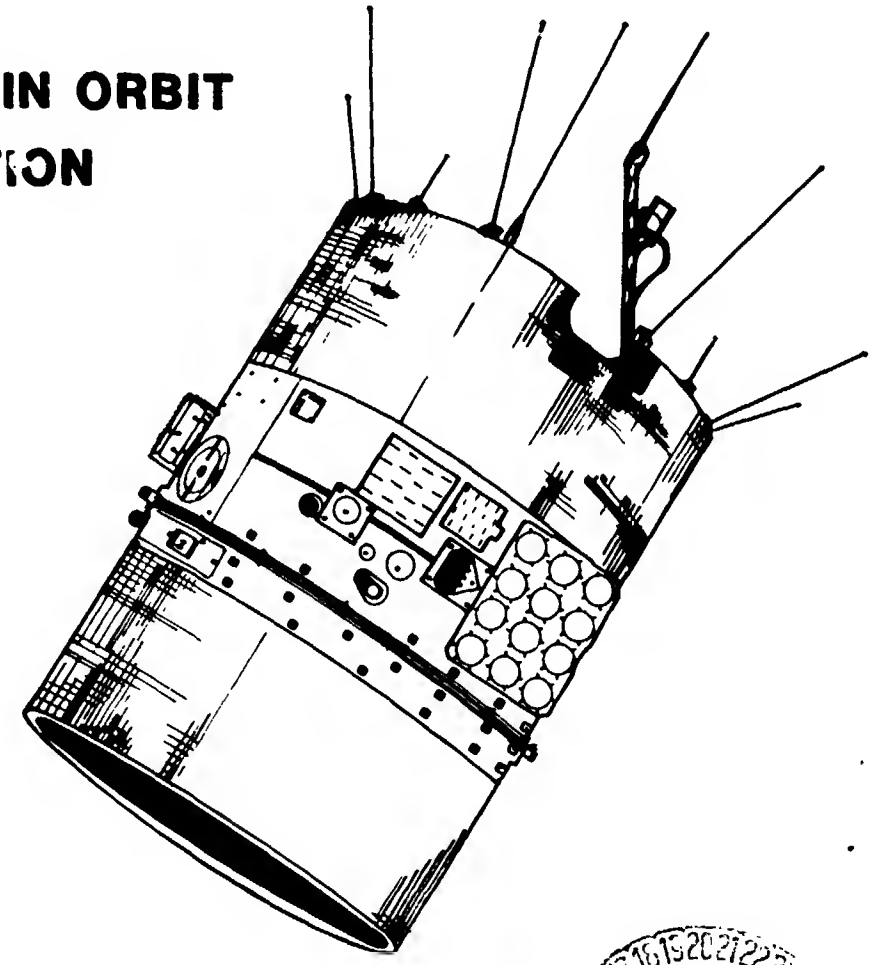

NAS 5 - 20825

SEPTEMBER 1981

NASA
Goddard Space Flight Center
Greenbelt Maryland 20771

TABLE OF CONTENTS

LIST OF ILLUSTRATIONS

LIST OF TABLES

ACRONYMS AND ABBREVIATIONS

2DLE	Two-directional Low Energy (Particle Detector, EME)
3DME	Three-directional Medium Energy (Particle Detector, EME)
ATS	Applications Technology Satellite
ATSOCC	Applications Technology Satellite Operations Control Center
C x L	C-Band (receive) to L-Band (transmit) Mode of Operation[1]
C/N_o	Carrier Power to Noise Power Density Ratio
CRC	Canadian Research Center (Ottawa, Canada)
EFE	Electric Field Measurements Experiment (EME)
EIRP	Effective Isotropic Radiated Power (referred to an isotropic antenna)
EME	Environmental Measurements Experiment
EOL	End-of-Life
FAA	Federal Aviation Administration
FT	Frequency Translation[1]
FTNB	Frequency Translation, Narrow Band[1]
GE	General Electric Co. (Schenectady, N.Y.)
Gnd Sta	Ground Station

GSFC	Goddard Space Flight Center
G/T	Antenna Gain to System Noise Temperature Ratio
IR	Infrared
L x L	L-Band (receive) to L-Band (transmit) Mode of Operation[1]
MA	Multiple Access[1]
ODHE	Omni-directional High Energy (Particle Detector, EME)
Omni	Omni-directional
PCM	Pulse Coded Modulation (spacecraft telemetry)
PWR	Power
RCVR	Receiver
RF	Radio Frequency
Rx	Receiver
S/C	Spacecraft
SRB	Solar Radio Burst Experiment (EME)
SSB/FM	Single Sideband (input) to Frequency Modulation (transmit) Mode of Operation[1]
TDA	Tunnel Diode Amplifier
T.V.	Television
TVCS	Television Camera System
TWT	Traveling Wave Tube

TWTA	Traveling Wave Tube Amplifier
Tx	Transmit
UDLE	Uni-directional Low Energy (Particle Detector, EME)
VSWR	Voltage Standing Wave Ratio
WBDM (WBD Mode)	Wide Band Data Mode[1]
CAL	Calculated
XMTR	Transmitter
BW	Bandwidth
RPTR	Repeater
I.P.	Ionosphere Propagation
Q.L.	Quick Look
DT	Data Tag
(C+N)/N	Carrier Plus Noise to Noise Ratio
B.P.	Band Pass
N.F.	Noise Figure
TDA	Tunnel Diode Amplifier

[1] Spacecraft operational modes are described in reference No. 3 (see Section 5). A brief description is also found in Appendix C.

FORWARD

This report was written with the intent of detailing the End-of-Life (EOL) performance of the ATS-5 spacecraft. The EOL test program was constrained in time by the fact that the Rosman Ground Station was scheduled to be closed at the end of December, 1980, thus ending all NASA C-Band capability. For this reason, tests requiring C-Band suport were performed, even though the spacecraft had not yet reached its end of life.

The reader may wish to substitute End-of-Mission (EOM) whenever reference is made to End-of-Life (EOL), since the spacecraft is continuing to function with its major subsystem operational.

It is expected that this document will provide the basis for an EOL report when the spacecraft is no longer useful.

The spacecraft is presently proving to be a valuable resource for VHF propagation studies by providing an RF beacon for experimenters (136 and 137 MHz telemetry downlink).

This report is submitted to Goddard Space Flight Center (GSFC by Westinghouse Electric Corporation in response to NASA Contract Number NAS 5-20825. Mr. Robert Wales is the GSFC Technical Officer. The report was written by F.J. Kissel with the assistance of J. Schaefer.

1.0 INTRODUCTION

1.1 PURPOSE

The purpose of this report is to present the results of the ATS-5 End-of-Life (EOL) tests performed June through December 1980. Whenever possible, the test data has been compared with prelaunch and/or inflight data. During the course of determining the prelaunch and inflight data, it became apparent that a significant portion of the ATS-5 historical data was available only in memos and letters which have received very little circulation. For this reason, pertinent memos and other informal documents have been included as appendicies. Pertinent documents which have received wide distribution and/or are avialable at the NASA/GSFC library are listed in Section 5 (References).

1.2 BACKGROUND

The history of the ATS-5 spacecraft is thoroughly described in the reference documents (Section 5). Especially noteworthy is the Post Launch Report (Reference 1) which discusses the events which culminated in the spacecraft rotating in the "wrong" direction. Details of the ATS-5 mission which are especially pertinent to this report are summarized as follows:

The ATS-5 spacecraft was launched August 12, 1969 into a near-perfect orbit with the vehicle spin-stabilized. The apogee motor was successfully fired for synchronous orbit insertion. After attaining synchronous orbit the spinning spacecraft with the apogee motor still

attached developed a rapid divergent nutation which could not be damped out. The spacecraft motion quickly degenerated into an unanticipated "flat" spin. When the apogee motor casing and adapter were jettisoned, the spacecraft resumed spinning about the normal spin axis, but unfortunately in the wrong direction. Consequently, the yo-yo despin mechanism could not be released to despin the spacecraft and the gravity-gradient stabilization system could not be deployed.

The communications subsystem contains two multimode repeaters. Repeater number 1 operates at C-band and may utilize the high gain (earth coverage) or omni-directional antennas. Repeater 2 operates at L-band and utilizes the L-band high gain antenna. Both the L and C-band high gain antennas were designed to operate with the spacecraft gravity gradient stabilized (one rotation per orbit) in synchronous orbit. The antennas were thus designed to illuminate the earth (half power beamwidth of approximately 20^{o}).

The C-band omni-directional antenna has a torriodal pattern which is near omni-directional normal to the spacecraft spin axis and significantly decreases in gain as the aspect angle moves away from 90^{o}.

The spacecraft presently has a spin period of approximately 765 msec about an axis of spin approximately parallel with the earth's axis. The spacecraft high gain antenna (both L and C-band) thus sweeps across the earth each spin period, illuminating each point within its area of coverage for about 50 ms (to the half-power points). The resulting "pulsing" effect presents great difficulty in performing accurate measurements of the spacecraft RF performance parameters.

1.3 DATA PRESENTATION AND DOCUMENTATION

In order to minimize duplication of effort, extensive use is made of references of previous ATS documents. In those instances where the referenced documents are not readily available, pertinent portions of the referenced document are included as an appendix. In general, the raw data is presented in an appendix, and the reduced data and/or results included in the main body of the report. Each section contains a description of the test(s), a discussion of the results and concluding remarks.

2.0 COMMUNICATION SUBSYSTEM TESTS

2.1 ANTENNA PATTERNS

2.1.1 C-Band Tests

Transmit Antenna Pattern

Transmit Antenna Patterns were measured using both the omni and planar array antennas. When measurements were made in the frequency translation (FT) mode, a 1 kw signal measured at the ground station transmitter output was uplinked to the ATS-5 satellite via the ground station 85' diameter antenna. This signal was enough to ensure that the spacecraft amplifiers were saturated and that the maximum output possible was transmitted from the satellite. When measuring in the WDBM, no uplink was required since the spacecraft developed its own downlink carrier. At the ground station, the downlink signal was viewed on stripcharts where the spacecraft transmitter antenna pattern could be measured.

Planar Array Transmit Antenna Patterns

The spacecraft was put into the wideband data mode, TWT 1 was turned on and a stripchart recording of the spacecraft transmit (Tx) antenna pattern was made. A portion of this stripchart is shown in Figure 2-1. Since the desired detail could not be acquired using only one channel, two channels were used to gain higher definition on the antenna pattern. The full Tx pattern was placed on channel 3. The lower portion of the pattern was placed on channel 5 and the upper portion was placed on channel 6. The stripcharts were later studied and translated to a polar coordinate Tx antenna pattern as shown in Figure 2-2. The power values

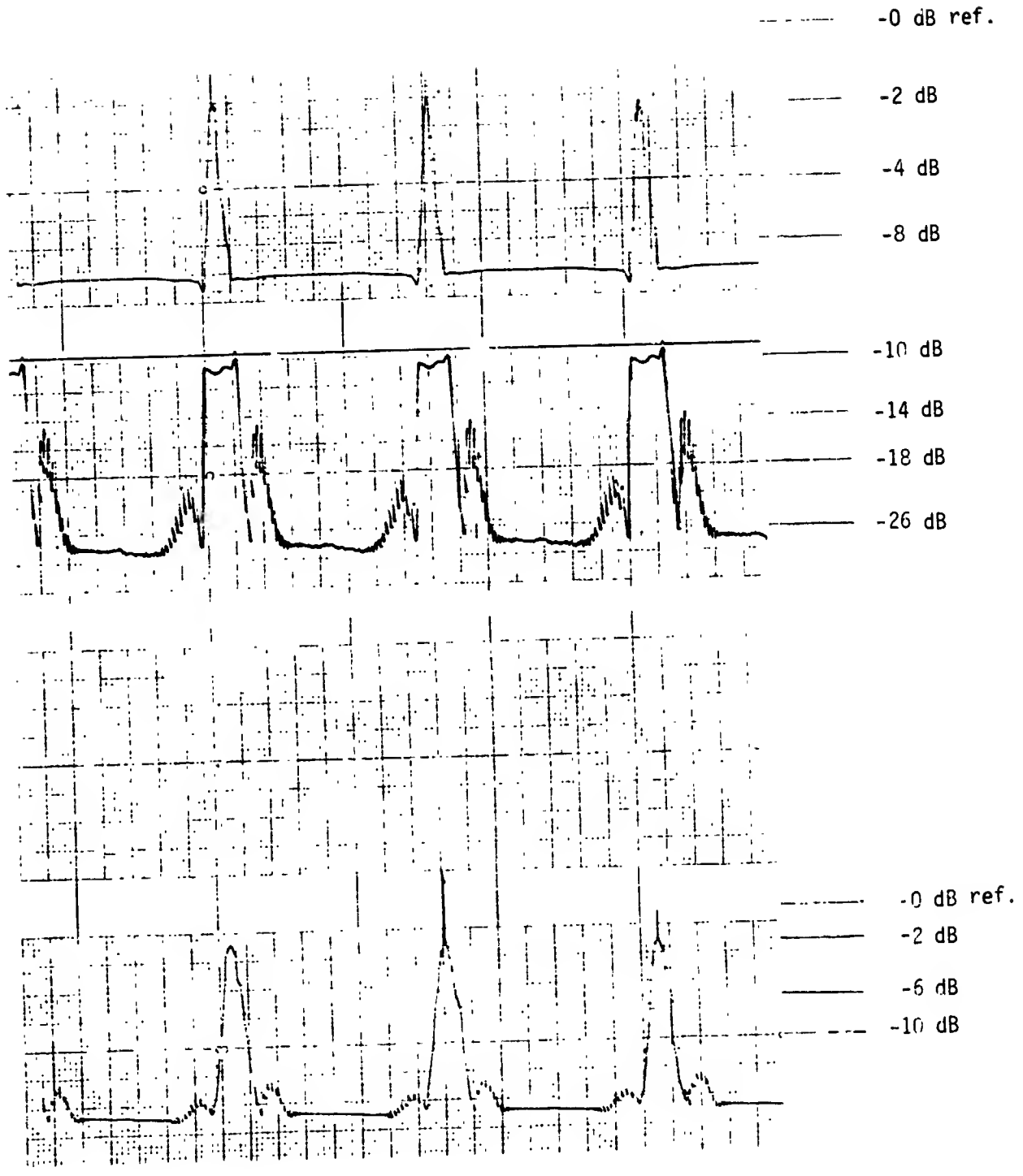

FIGURE 2-1

Planar Array TWT #1 Transmit
Antenna Pattern
Stripchart
(WBDM)

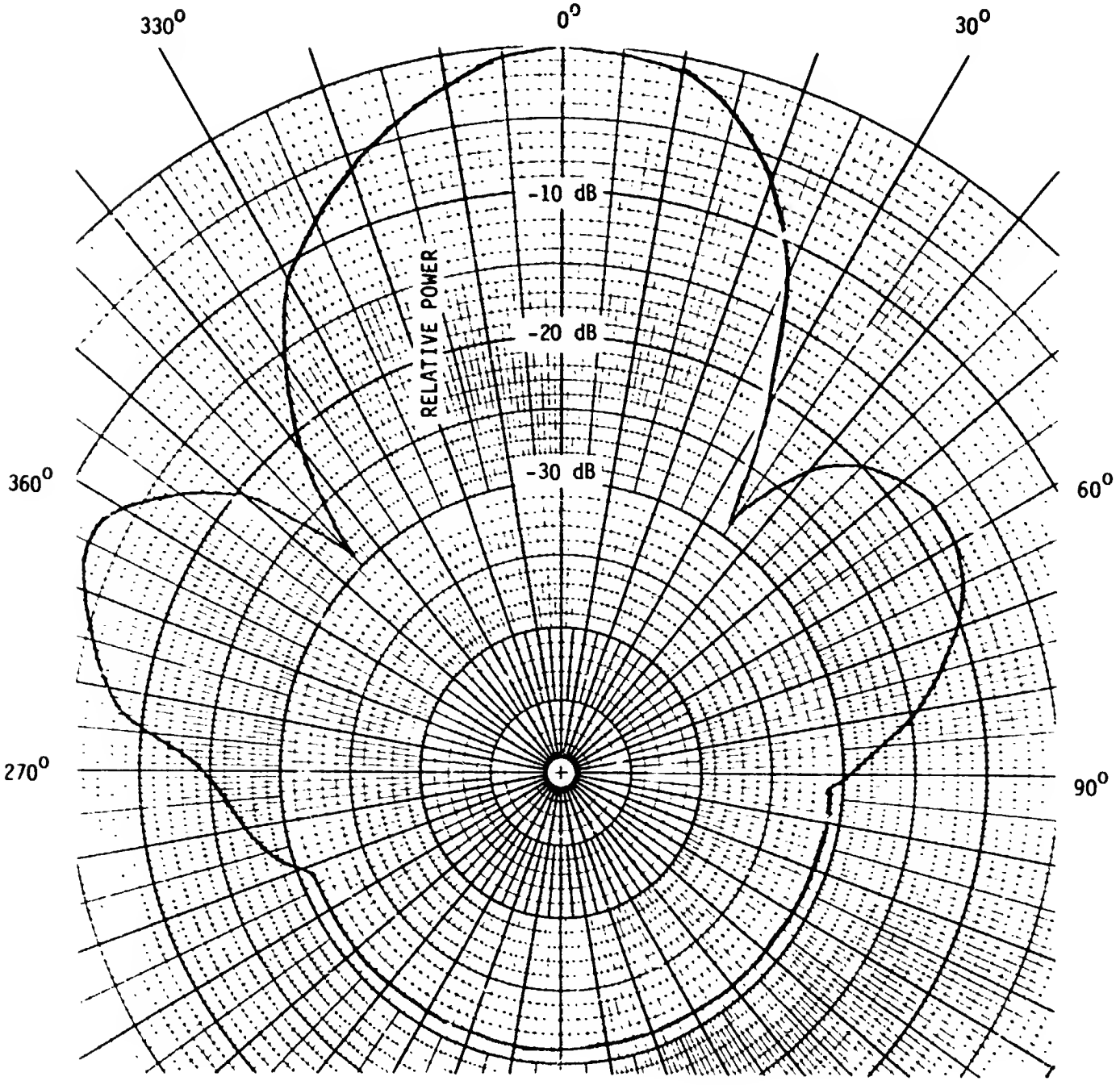

FIGURE 2-2

Plannar Array Transmit Antenna Pattern
(TWT 1, WBDM)

on the stripcharts include the receiving station antenna gain and stripchart calibration. After the recording of the antenna pattern was completed, TWT 1 was turned off and TWT 2 was turned on.

Stripcharts and polar plots were made as before. The results are presented in Figure 2-3 and 2-4. A third pattern was then recorded using TWT 1 and 2 simultaneously (approximately twice as much spacecraft EIRP). The stripchart and polar plot can be seen in Figures 2-5 and 2-6 respectively. Examination of the stripcharts shows that the patterns obtained using the TWTs separately and together are essentially identical (slight differences in the polar plots are due to manual translation uncertainties).

Omni-Directional Antenna Transmitting Patterns

The spacecraft was put into the wideband data mode, TWT 1 was turned on and a stripchart recording was made as with the Planar Array Tx tests. However, with the omni-directional antenna patterns, the entire waveform could be adequately represented on one stripchart channel. Using the information on the stripchart, the polar coordinate antenna pattern could be determined. The stripchart and its polar representation are shown in Figures 2-7 and 2-8 respectively.

The spacecraft was then set to the C-band FT mode and both TWT 1 and 2 were used to measure the omni antenna transmit pattern. The stripchart and polar plot are given in Figures 2-9 and 2-10 respectively.

C-Band Test Results

In the course of the investigation for the ATS-5 C-band tests, previously measured transmit antenna patterns were acquired for comparison purposes. This data is given in Appendix A. In comparing the Appendix A stripcharts to those given in the text, no major pattern

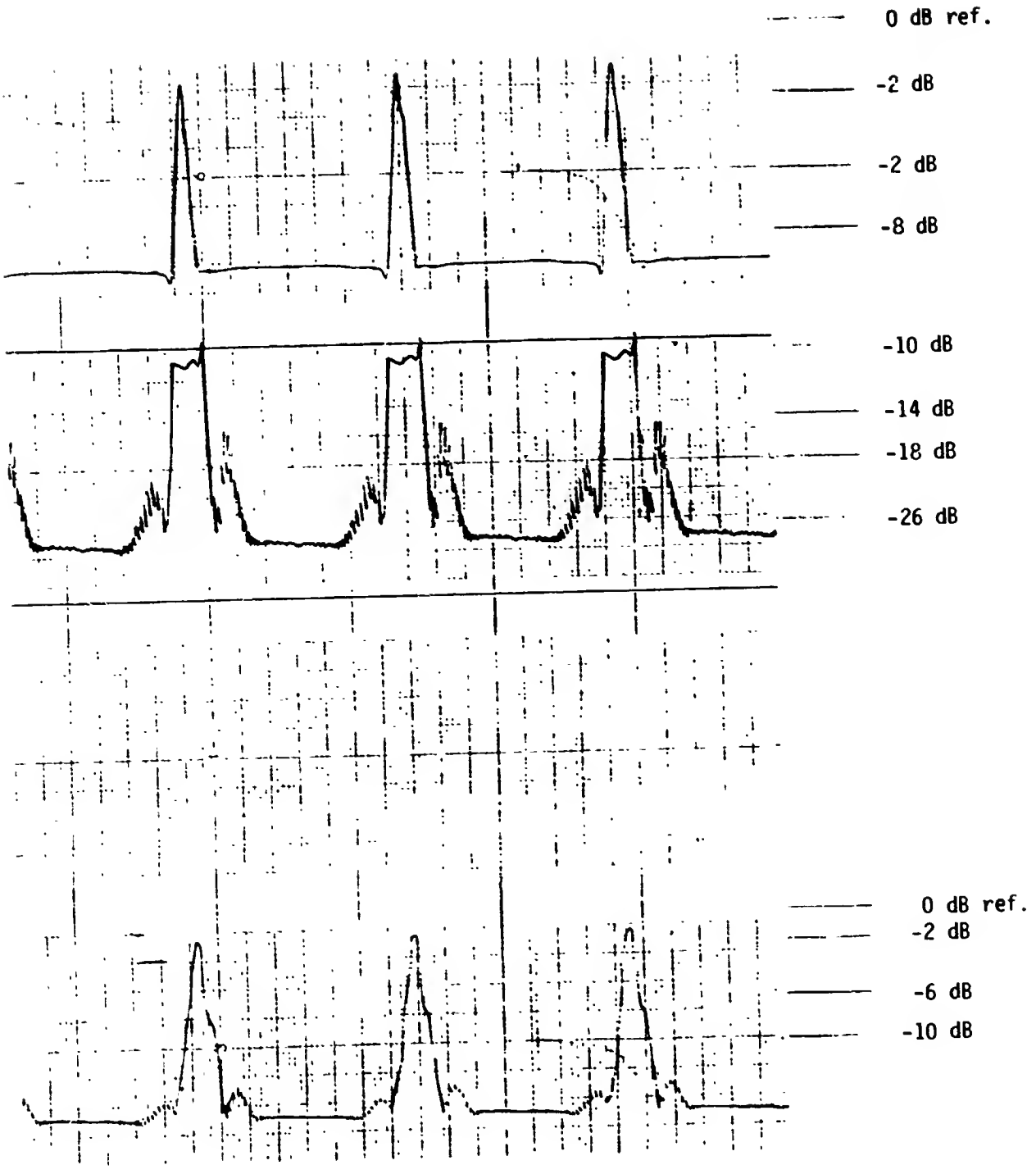

FIGURE 2-3

Planar Array TWT #2 Transmit
Antenna Pattern
Stripchart
(WBDM)

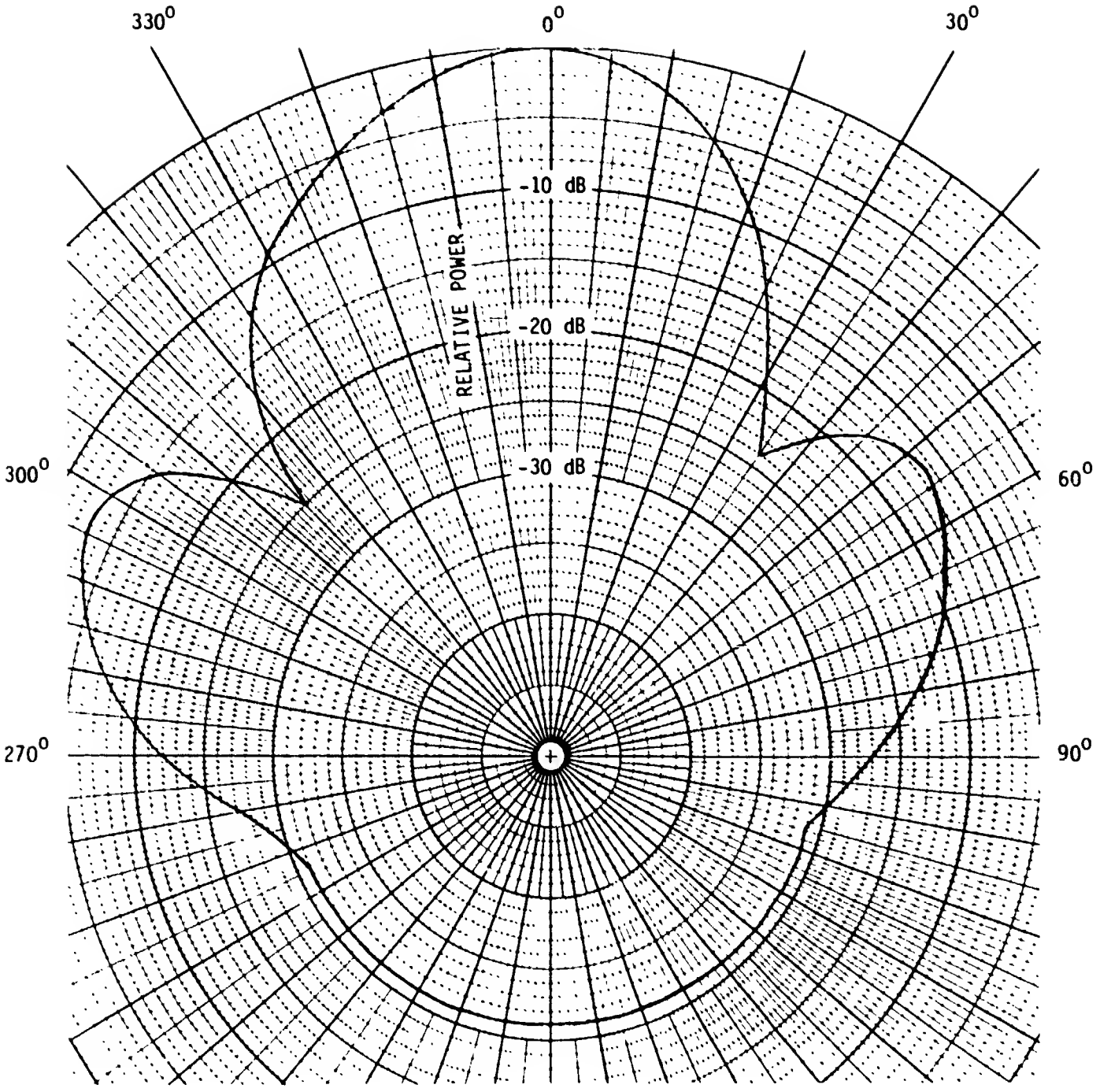

FIGURE 2-4

Planar Array Transmit Antenna Pattern
(TWT 2, WBDM)

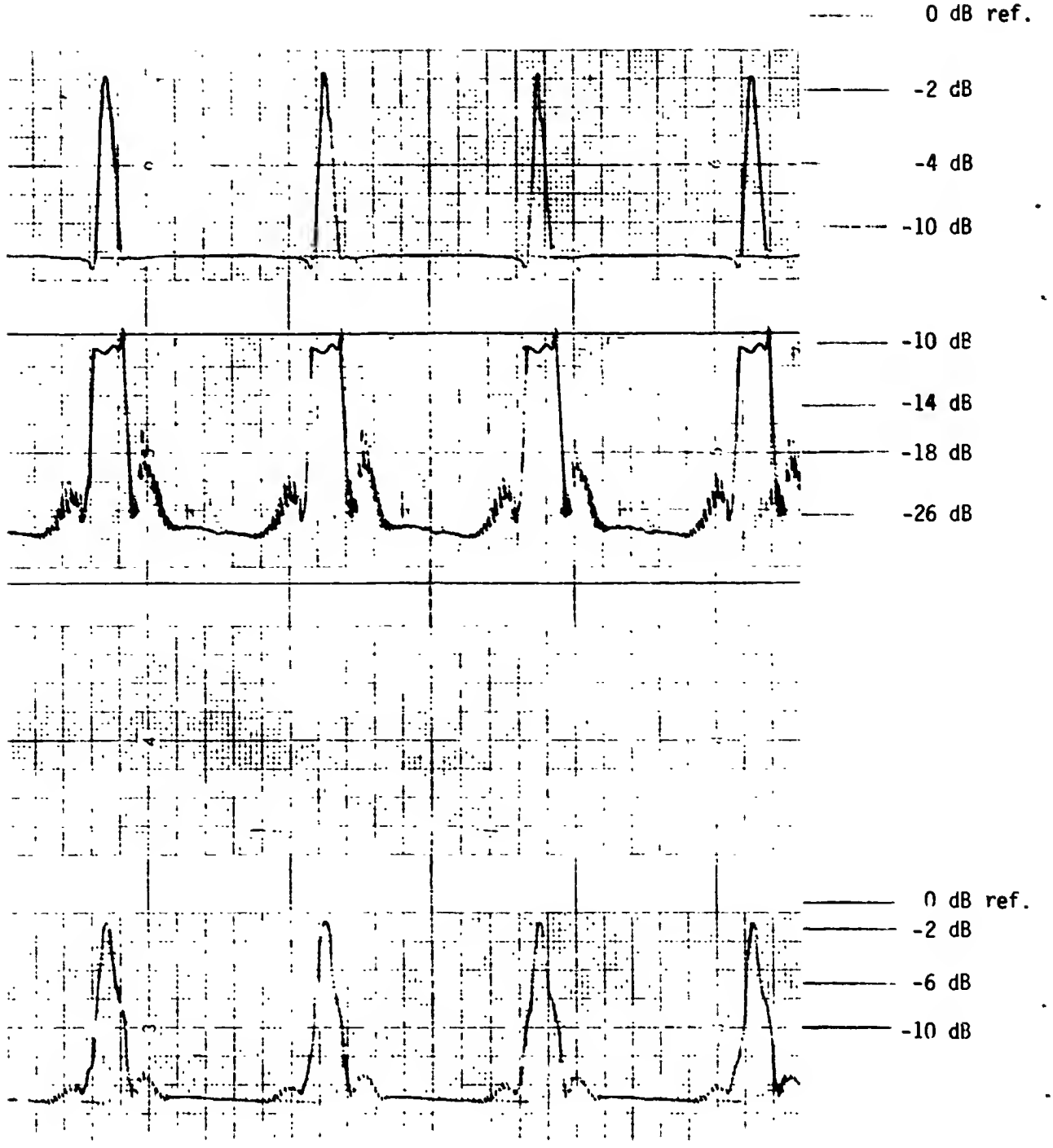

FIGURE 2-5

Planar Array TWT #1 and #2 Transmit

Antenna Pattern

Stripchart

(WBDM)

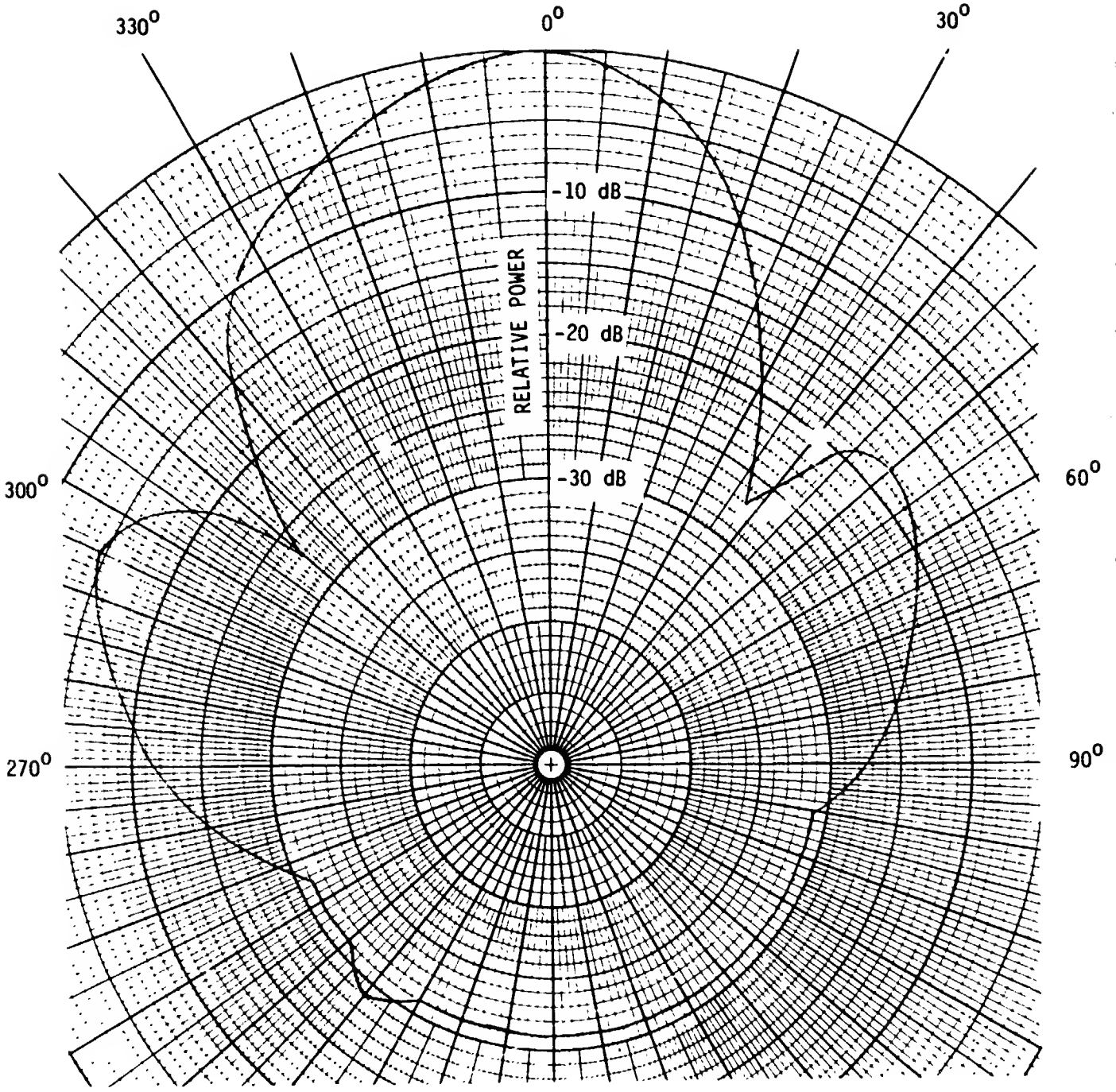

FIGURE 2-6

Planar Array Transmit Antenna Pattern

(TWT 1 and 2, WBDM)

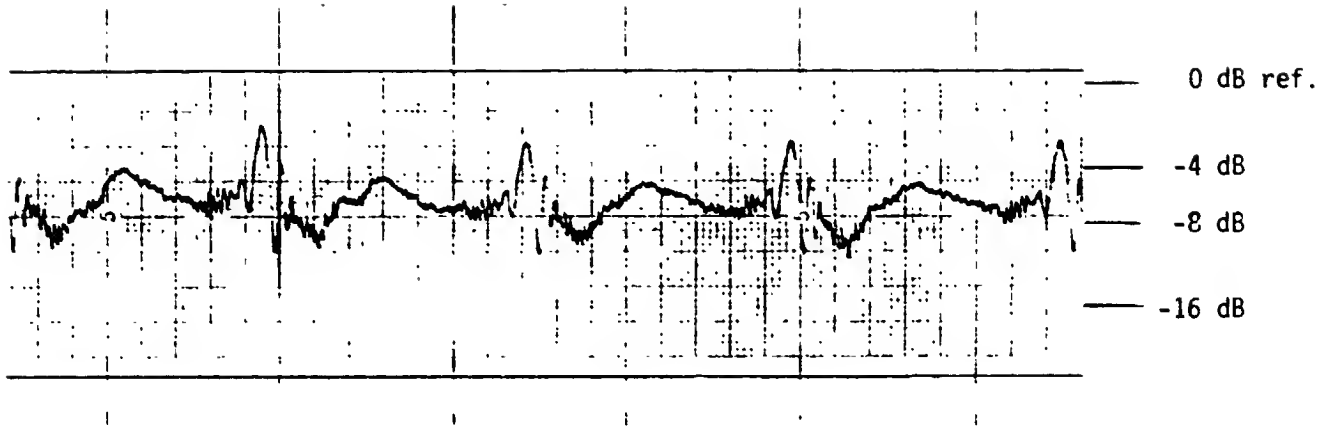

FIGURE 2-7

Omni Antenna TWT #1 Transmit
Antenna Pattern
Stripchart

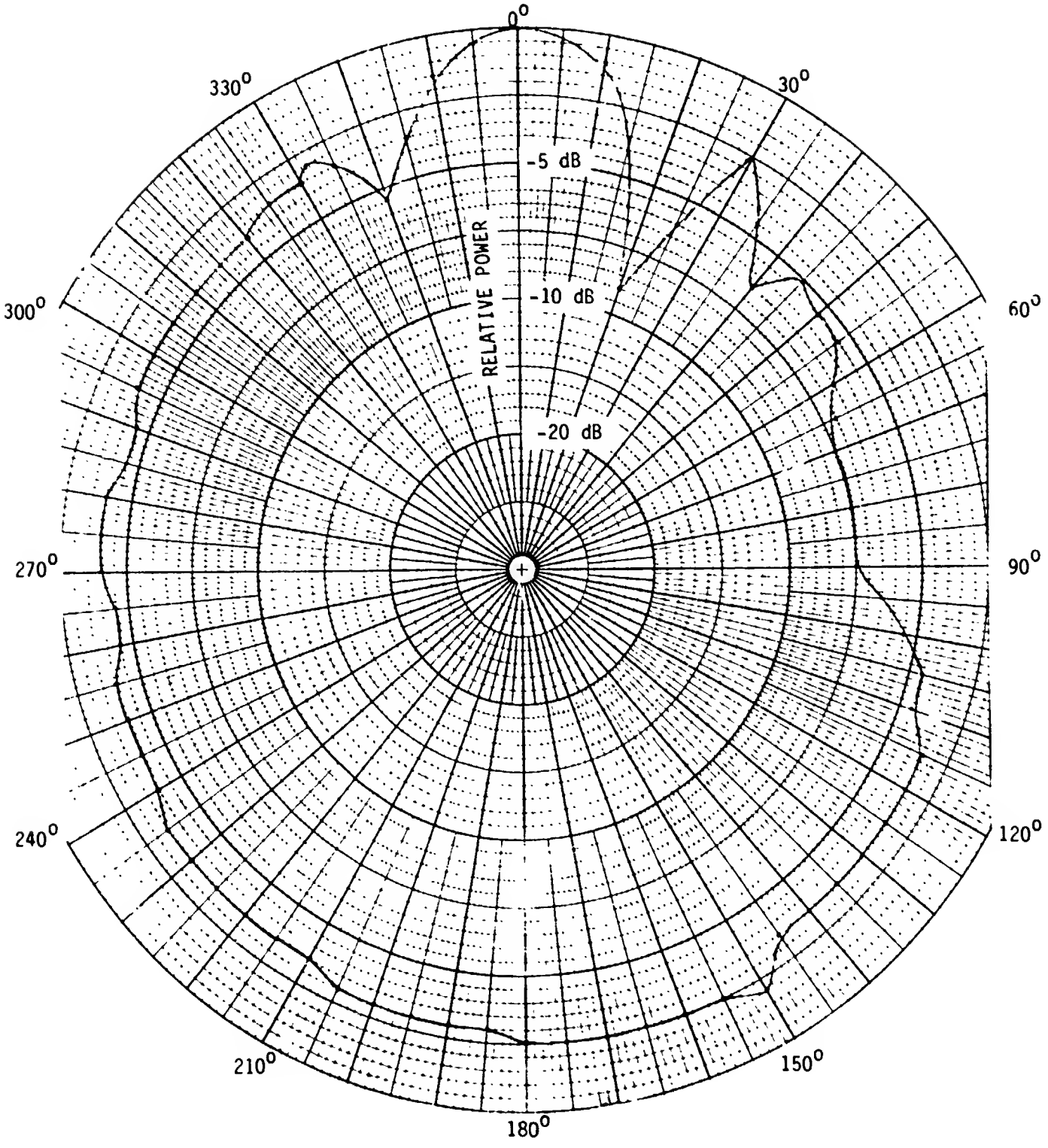

FIGURE 2-8

Omni Transmit Antenna Pattern

(TWT 1, WBDM)

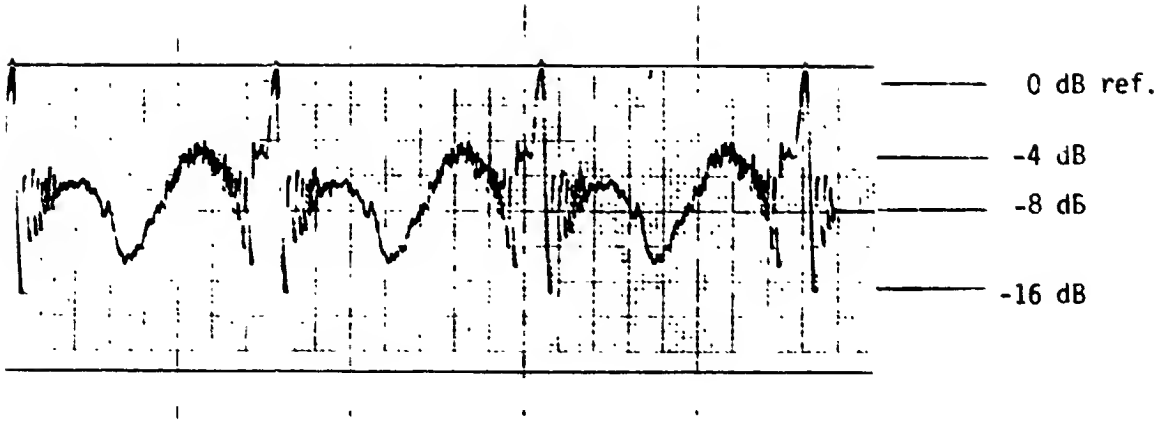

FIGURE 2-9

Omni Antenna TWT #1 & #2
Transmit Antenna Pattern
Stripchart
(FT Mode)

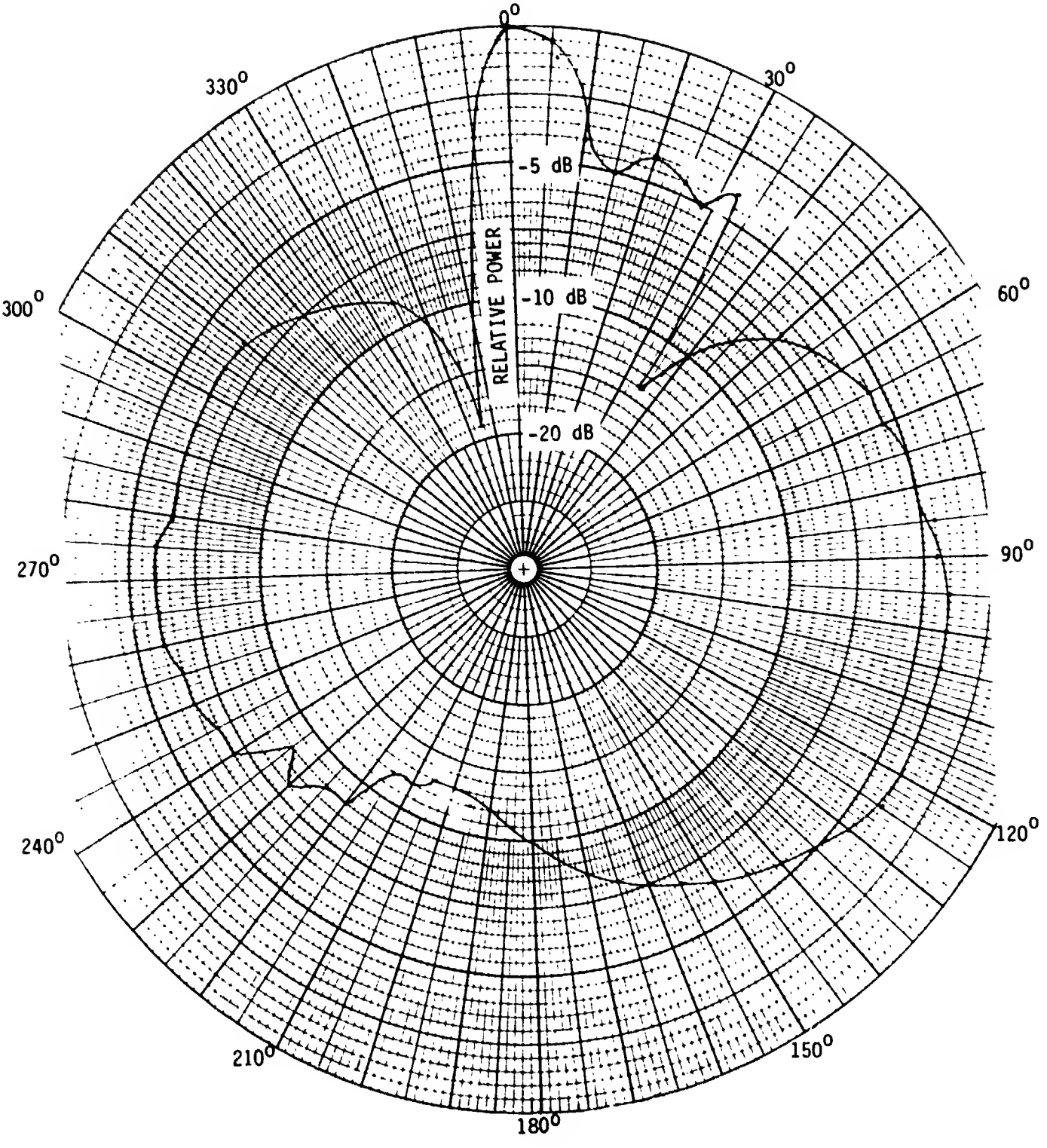

FIGURE 2-10

Omni Transmit Antenna
Pattern
(TWT 1 and 2, FT Mode)

changes were noted. The planar array antenna patterns of Figures 2-2, 2-4, and 2-6 all show the peak of the two first side lobes at about 55^{0} and 295^{0} respectively.

Also, the nulls between the main lobe and the side lobes are at least 24 dB down from the main lobe peak power in each plot. It will be noticed from comparison between Figures 2-1, 2-3, and 2-5 that when both TWT 1 and 2 are on, a 3 dB improvement is shown in the transmission signal strength which was anticipated.

The omni antenna patterns (Figures 2-9 and 2-10) provided dramatic evidence of interaction of the planar array and the omni antennas. This is due to the low isolation of the RF switch used to select the C-band antennas. In Figure 2-10 the planar array influence in the omni antenna pattern has produced a pattern with two nulls centered about a pseudo main lobe. This effect had been previously noted during ATS-5 operations.

The configuration of the ferrite RF switch is shown in Figure 2-11. Additional information regarding the RF switch and the effects of low isolation can be found in Appendix B.

2.1.2 L-Band Tests

At the time that the ATS-5 EOL tests were performed, the L-band capability had been removed from the Rosman ground station, thus severely limiting the L-band testing capability. Two former L-band experimenters, the General Electric Company in Schenectady, New York and the Canadian Research Center in Ottawa, Ontario were contacted and agreed to limited

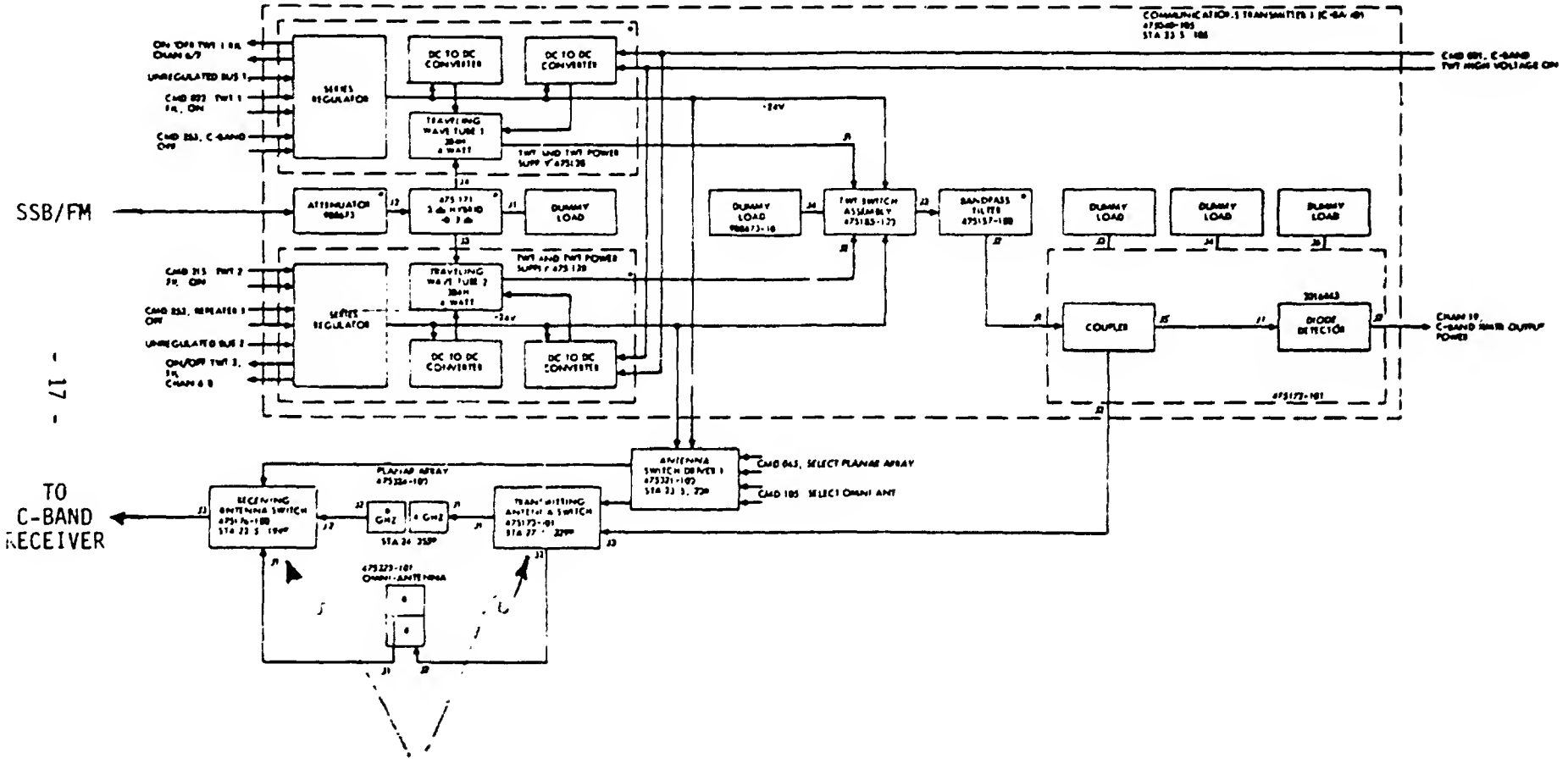

FIGURE 2-11

C-Band Communications Transmitter

participation in the EOL tests. A further impediment to L-band testing was the failure of the L-band receiver and one of the two TWTs. See Appendix C for discussion on the L-band equipment malfunctions.

Transmit Antenna Pattern

The receiver at Ottawa was tuned to the L-band beacon at 1565.82 MHz. In this configuration, with no uplink signal, the L-band beacon caused near saturation of the L-band TWT. This provided a down-link signal to measure the antenna pattern. The recorded stripchart is shown in Figure 2-12. In this test, the upper channel of the stripchart was used for greater definition of the peak of the signal whereas the lower channel of the stripchart was used to show the entire waveform. The power values presented with the stripcharts are relative values. Figure 2-13 is the polar coordinate transformation of the stripchart given in Figure 2-12. Appendix D presents the calibration method used by CRC in Ottawa.

The spacecraft was then placed in the FT mode with the C x L configuration. The planar array antenna was used on the uplink. The ground station at Ottawa received the downlink at 1553.77 MHz in a 50 KHz bandwidth. Figure 2-14 shows a section of the stripchart obtained and Figure 2-15 shows the polar coordinate transformation of the received antenna pattern.

L-Band Test Results

The antenna pattern of Figure 2-13 may be compared with that of the L-Band transmit pattern (WBDM) in Appendix C. Although the

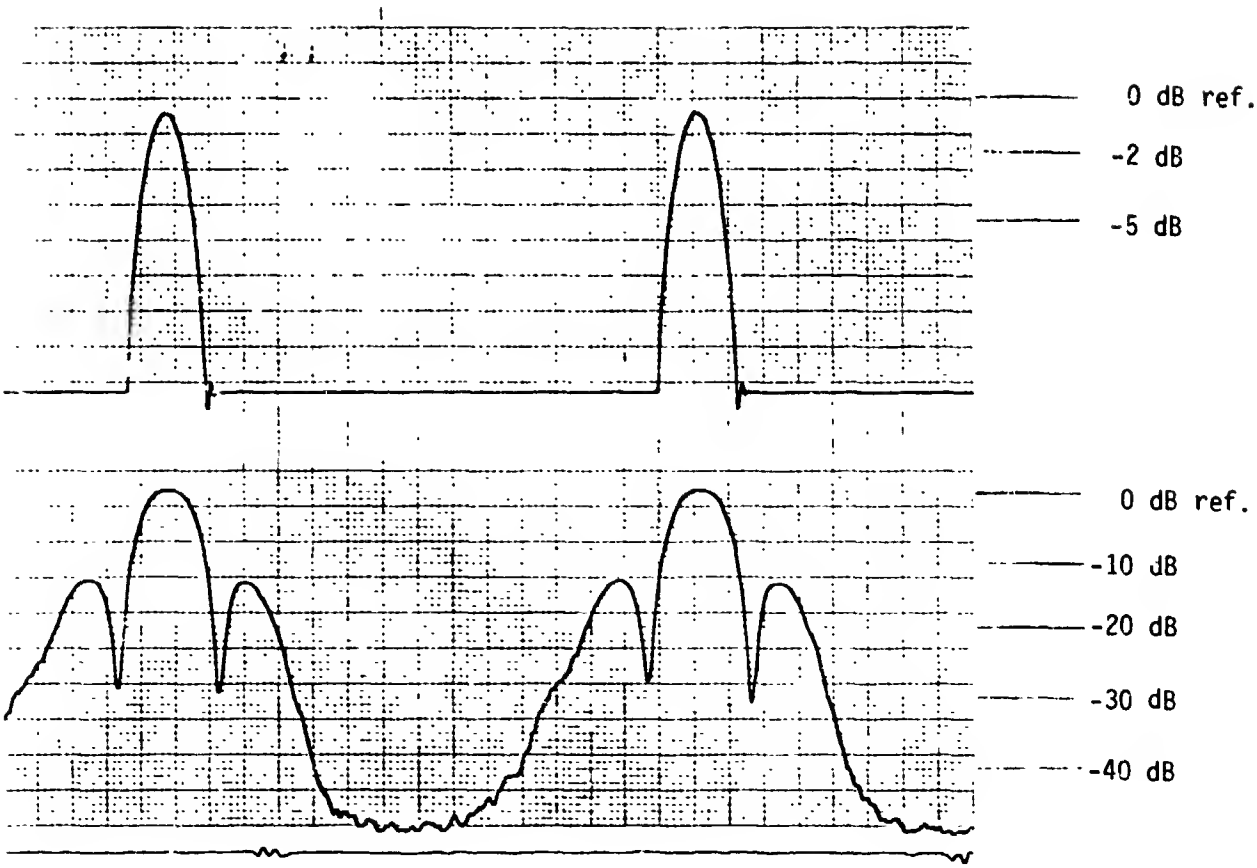

FIGURE 2-12

L-Band Beacon Transmit Antenna Pattern
Stripchart
(1565.82 MHz)
Beacon Downlink

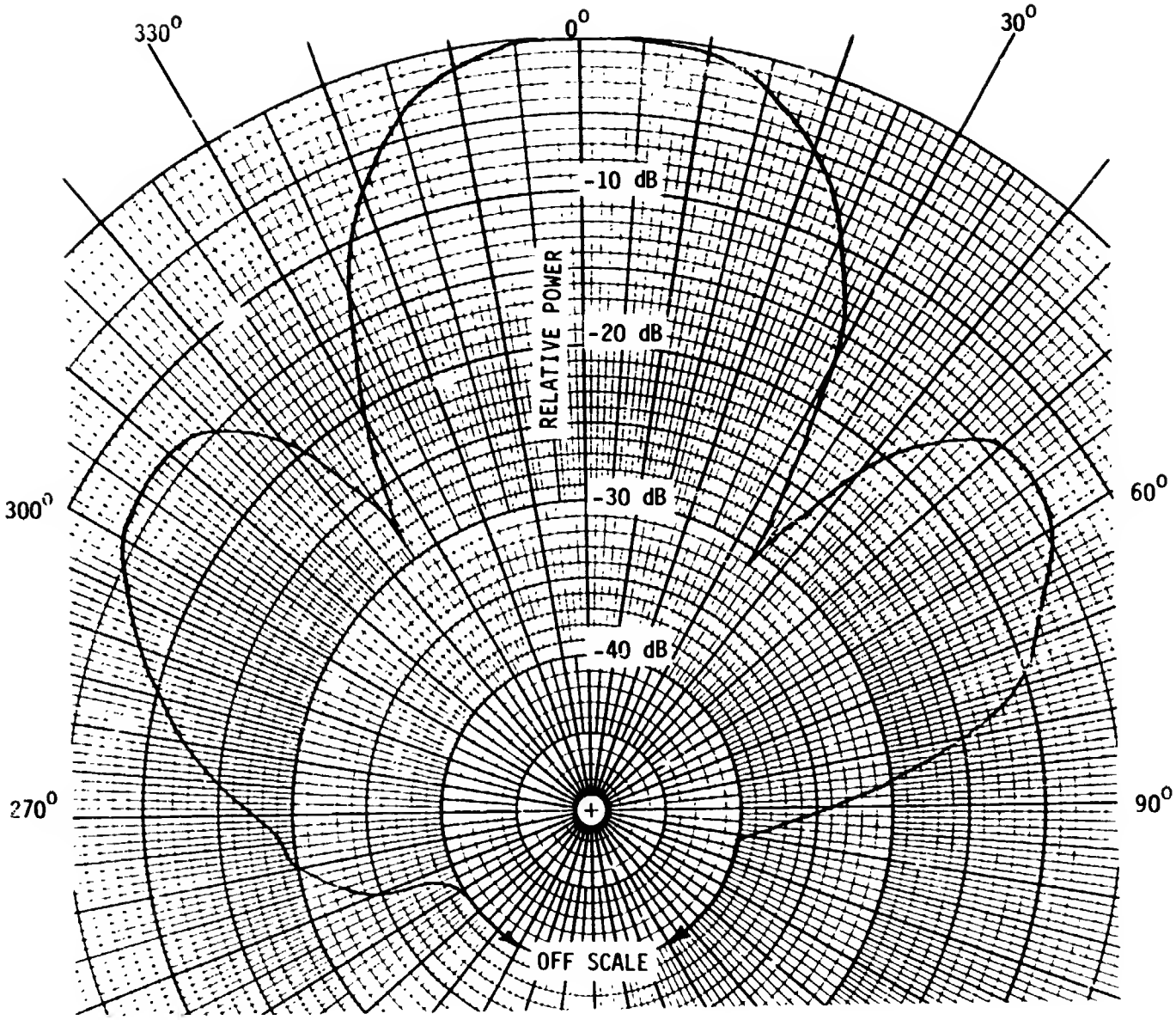

FIGURE 2-13

L-Band Transmit Antenna Pattern

Beacon Downlink

(1565.82 MHz)

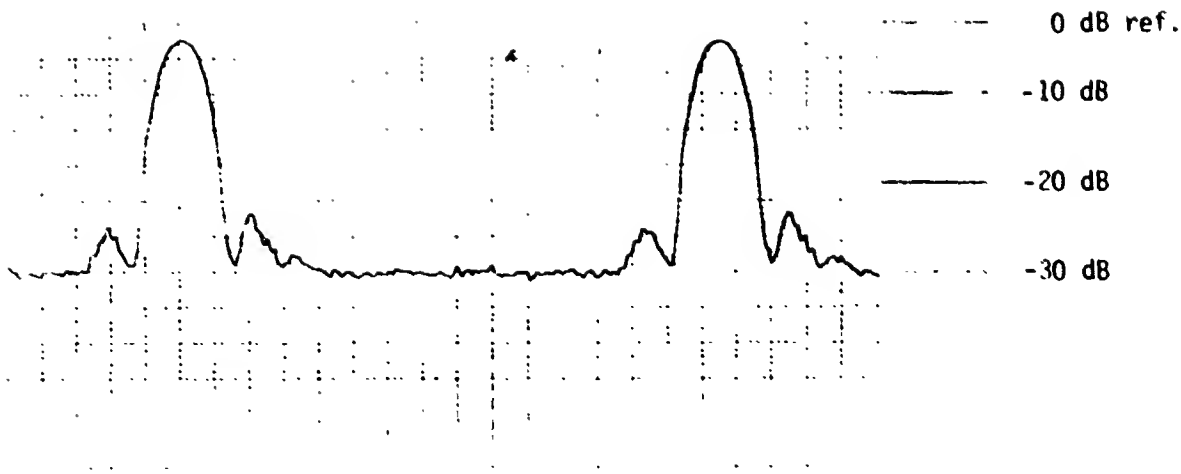

FIGURE 2-14

L-Band Transmit Antenna Pattern Stripchart
with the Planar Array
in the FT C x L Mode

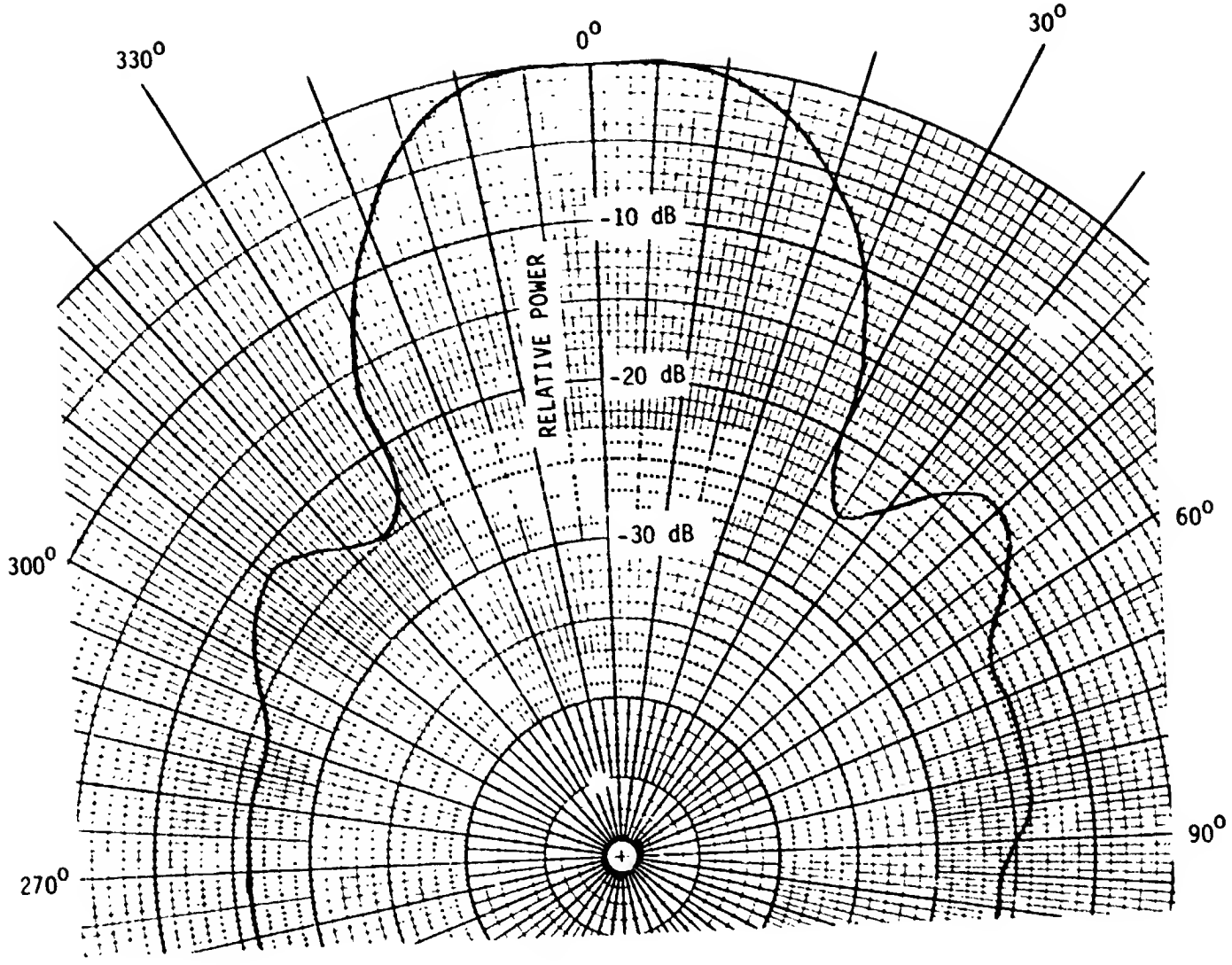

FIGURE 2-15

L-Band Transmit
Antenna Pattern using the
FT C x L Mode

(Planar array on C-band uplink)

frequencies of the patterns recorded differ slightly (1555.82 MHz for beacon, and 1550.48 MHz for the WBDM), the two can be compared. Both have first nulls at about 35^{0} and 325^{0}. Additionally, the side lobes are down 15 dB from the main lobe in both cases. A comparison can also be made between the C x L antenna pattern of the test and that of the C x L stripchart in Appendix C. The C-band planar array was used to develop the stripchart of Figure 2-14 and the C-band omni was used for the stripchart in Appendix B. The only difference here is the noteable low isolation effect of the RF switch in the C-band transponder. Figure 2-14 shows no perturbations but the stripchart of the C x L test in Appendix B does show perturbations. See Reference 2 for a presentation of previous L-band measurements.

2.2 RF PERFORMANCE PARAMETERS

2.2.1 Introduction

The spacecraft RF parameter measurements were restricted to the C-band EIRP and G/T because of the limited ground station facilities and test equipment. Measurements of L-band downlinks were provided by General Electric (in Schenectady, N.Y.) and the Canadian Research Center (Ottawa, Canada). These measurements provided a means of determining the L-band EIRP and also verification of the failure of the L-band preamplifier.

It should be noted that all values assigned to the spacecraft are dependent upon the calibration accuracy of the ground station. Thus some discrepancy may be expected among prelaunch, in-orbit, and EOL test results.

The test results are summarized in Tables 2-1 through 2-3 which include prelaunch and in-orbit values as well as specification limits.

The specification limits shown in Table 2-1 through 2-3 were obtained from References 3 and 4; the preflight values were measured in 1969 as part of the Hughes Aircraft Co. Long Form tests (Reference 5). The in-orbit values were determined from various operational tests conducted primarily during 1971-72 period over the lifetime of the spacecraft. The EOL values shown in Tables 2-1 through 2-3 represent the best estimate of the true value, often derived from an average of several measurements made when tests were performed during the fall of 1980.

2.2.2 Spacecraft EIRP

The C-band and L-band EIRP calculated values are shown in Table 2-4. Measurements were made for vairous combinations of spacecraft mode and antenna configurations. The C-band EIRP values were calculated from C/N_0 measurements made at the Rosman ground station. The L-band EIRP value was calculated from the measured value of received signal strength reported by CRC (Canada). Sample EIRP calculations are presented in Appendix E. The spacecraft Tx power output was reported via spacecraft telemetry during each EIRP test (as shown in Table 2-4). Using the EIRP spacecraft Tx output values; it was possible to determine the apparent net antenna gain (as shown in Table 2-4). Variations in net antenna gain are attributed to the ferrite switch (discussed in conclusions subsection).

2.2.3 Spacecraft G/T

The G/T (antenna gain to system noise temperature ratio) of a receiving system is a figure-of-merit of the system performance. A method of measuring the in-orbit G/T has been developed (Appendix F) which requires

a known signal level to be transmitted to the spacecraft coupled with accurate determination of the variation of the resultant spacecraft transmitted carrier output. The technique requires sufficient uplink power to cause saturation of the spacecraft transmitter. The resultant downlink receive carrier was then used to establish a reference level and the uplink power is decreased and measured for various decreases in the downlink carrier from reference level. A sample calculation of G/T is shown in Appendix E.

Table 2-5 shows the measured G/T data for the C-band omni and planar array antennas. Several values of G/T are measured for each antenna, and averaged to determine a best estimate. No L-band G/T measurement could be made because of the failure of the spacecraft L-band receiver front end (see Appendix C for a comprehensive discussion of the L-band front end failure).

2.2.4 Conclusions

2.2.4.1 Summary

- The C-band EIRP has degraded significantly (up to 6.1 dB) from prelaunch measurements
- The C-band G/T is essentially unchanged from prelaunch values
- The L-band TWT 4 EIRP is essentially unchanged from prelaunch values (TWT 3 failed 30 Jan 74)

2.2.4.2 C-Band Tx RF Parameters

Examination of the EOL test results (Table 2-4) shows a variation of measured EIRP of 1.5 dB (planar array, 2 TWT's). This variation may well be due to ground station parameter changes and measurement accuracy.

Another possibility is that the ferrite switch which selects either the omni or planar array antennas (Figure 2-11) is erratic in operation. Evidence for the latter is seen in the spacecraft Tx power output telemetry which shows higher than nominal values, an effect which may occur if the spacecraft power output detector received significant reflected power from the antenna switch.

Table 2-1 is a summary of the C-band Tx RF parameters. The prelaunch values were the results of measurements made by the Communications Subsystem Contractor (Hughes Aircraft Co.) and reported in the Long Form tests (Reference 5). The in-orbit and EOL values of EIRP were calculated from measurements of ground station received power. The in-orbit and EOL values of Transmitter Output Power were determined from spacecraft telemetry. The net antenna gain (including all line losses), is calculated by subtracting the spacecraft Tx power from the EIRP; the resulting 3.1 dB apparent variation of net antenna gain (10 to 13.1 dB; EOL tests) is attributed to variations in the VSWR of the antenna ferrite switch; the variation of net antenna gain over the life of the spacecraft (from a prelaunch value of 15.8 dB) is attributed to changes in the spacecraft transmission network losses (see Figure 2-11).

The effect of the ferrite switch was first observed during post launch tests (Appendix G) and is also discussed in Appendix B with regard to omni-to-planar array antenna isolation.

2.2.4.3 C-Band Receive RF Parameters

The C-band G/T measured values show little change from the prelaunch values (see Table 2-2). The prelaunch and spec G/T values were calculated from RCVR noise figure and line losses (sample calculations in Appendix E).

The available inflight data was not adequate to determine G/T values for the C-band receivers.

Of particular interest in the results shown in Table 2-2 is the difference in gain between the omni and planar array G/T. The EOL gain difference is 19.4 dB while the prelaunch value is 19.0 dB. This is remarkable and indicates that virtually no degradation has occurred in the spacecraft receive subsystem.

2.2.4.4 L-Band RF Parameters

The only EOL L-band RF parameter avialable for measurement was the EIRP using TWT 4. This required the assistance from the Canadian Research Center (CRC) to measure the downlink from the saturated spacecraft transmitter output. The measurements was performed using the FTNB mode with no uplink (in this mode the onboard beacon oscillator causes saturation of the L-band TWTA). The spacecraft output power (via telemetry) was used to determine the net antenna gain. As seen in Table 2-3, no significant changes in EIRP, TX power output or antenna gain have occurred. TWT 3 failed 30 Jan 1974 (prior to EOL testing); however, in-orbit measurements prior to its failure indicated nominal performance.

Because of the failure of the L-band receiver (Appendix C) no EOL G/T measurements could be made; however, inflight data was obtained which indicated a 3 dB decrease in G/T since prelaunch measurements. The 3 dB decrease could be due to measurement errors, or actual degradation of the L-band preamp.

An attempt was made to characterize the current performance of the L-band receiver. General Electric (Schenectady, N.Y.) provided an uplink EIRP of approximately 90 dBm (approximately -84 dBm at the spacecraft preamp input). The resultant output was recorded by CRC (Ottawa, Canada) and is shown in Figure 2-16. CRC reported the GE return

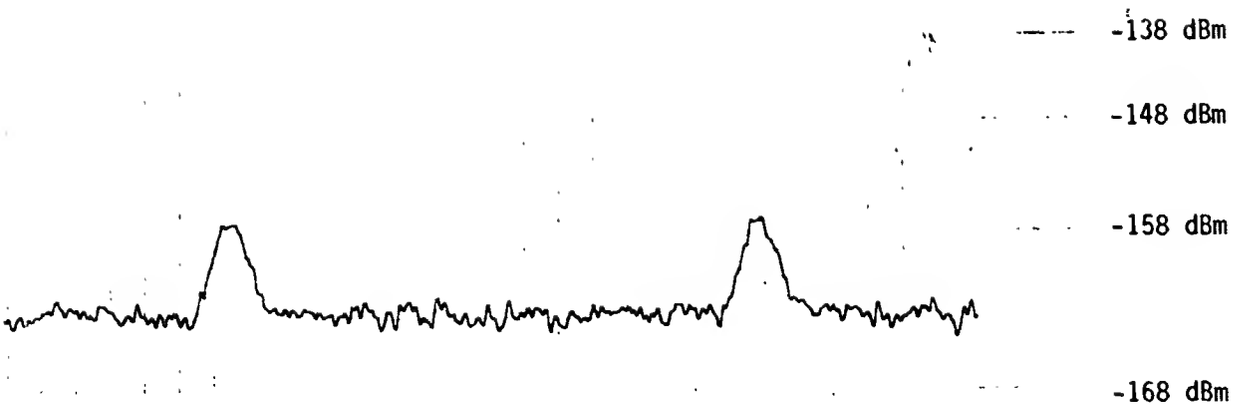

Ground station received signal strength.

Figure 2-16

L-Band Repeater Response, FTNB Mode

(shows effect of failed L-band RCVR preamplifier)

GE L-Band Tx 100w (EIRP = 90 dBm)

CRC L-Band Receive (-158 dBm)

level to be -158 dBm (a decrease of 21.5 dB from their measurement of spacecraft saturated output power). Based on post launch tests (Appendix G) the observed performance indicates a decrease in the L-band RCVR gain of approximately 33 dB. This value is consistant with previously observed values (see Appendix C).

Table 2-1

ATS-5 C-Band Tx RF Parameters

	Spec	Prelaunch	In-Orbit	EOL
Transmitter Ouptut Pwr				
TWT 1 (dBm)	35.3 min.	35.9		
TWT 2 (dBm)	35.3 min.	35.9		
TWT 1 & 2 (dBm)	38.3 min.	38.4	38.7	38.9 to 39.8
Transmit Antenna Gain[1]				
Omni (dB)		0.8	2.8	-0.2 to -1.5
Planar Array (dB)	16.7 min.	15.8	16.3	10.0 to 13.1
EIRP				
Omni Antenna				
TWT 1 (dBm)			38.5	
TWT 2 (dBm)		36.2	38.5	
TWT 1 & 2 (dBm)			41.5	37.8 to 39.3
Planar Array				
TWT 1 (dBm)	50.4 min.	51.7	52.0	47.8
TWT 2 (dBm)	50.4 min.	51.2	52.0	46.3
TWT 1 & 2 (dBm)	53.4 min.	54.4	55.0	48.3 to 49.8

(1) net gain (includes line losses)

Table 2-2

ATS-5 C-Band Receive RF Parameters

	Spec.	Prelaunch	EOL
RCVR Noise Figure (dB)	6.2 max.	6.16	
Receive Antenna Gain			
Omni (dB)		1.3	
Line Loss (dB)		3.3	
Net Gain (dB)		-2.0	
G/T (dB)		-35.7	-36.9
Planar Array			
Line Loss (dB)	2.7 max.	2.45	
Net Gain (dB)	16.3 min.	16.6	
G/T (dB)	-17.3 min.	-16.7	-17.5

Table 2-3

ATS-5 L-Band RF Parameters

	Spec.	Prelaunch	In-Orbit	EOL
Transmitter Output Pwr				
TWT 3 (dBm)	41.0 min.	40.8	40.0	
TWT 4 (dBm)	41.0 min.	39.8	41.0	40.8
TWT 3 & 4 (dBm)	44.0 min.	43.4	43.9	
Transmit Antenna Gain (dB)	14.0 min.	14.7		
Diplexer & Line Loss (dB)	3.5 max.	1.1		
Net Gain (dB)	10.5 min.	13.6	11.6	12.3
EIRP				
TWT 3 (dBm)	51.5 min.	53.7	52.1	
TWT 4 (dBm)	51.5 min.	53.4	52.3	53.1
TWT 3 & 4 (dBm)	54.5 min.	56.4	55.4	
Receive Antenna Gain (dB)	15.0 min.	15.6		
Diplexer & Line Loss (dB)	2.3 max.	1.3		
Net Gain (dB)	12.7 min.	14.3		
RCVR Noise Figure (dB)	5.5 max.	4.8		
Antenna G/T (dB)	-19.8	-16.5	-19.6	

Table 2-4

ATS-5 EIRP Test*

Spacecraft Parameters					Gnd Sta Measurement		Cal S/C Parameters	
	Mode	TWT	Ant	Tx Pwr (dBm)	Tx Pwr (dBm)	C/N_0 (dB)	Net Tx Ant. Gain (dB)	EIRP (dBm)
C-Band 20 Nov 80	WEDM	1 & 2	Omni	39.6	-	74	-0.3	39.3
	FT	1 & 2	Omni	38.9 39.5	0 60	74	-0.2	39.3
	FT	1 & 2	Array	39.8	60	83	8.5	48.3
	WBDM	2	Array	34.5		81	11.8	46.3
	WBDM	1	Array	34.7		82.5	13.1	47.8
	WBDM	1 & 2	Array	9.7		84.5	10.1	49.8
4 Jun 80	WBDM	1 & 2	Omni	39.3		74	-1.5	37.8
	WBDM	1 & 2	Array	39.3		85.5	10.0	49.3
L-Band 4 Jun 80	FTNB	4	Spiral Array	40.8			12.3	53.1

* C-Band EIRP calculated from Rosman Gnd Sta C/N_0 measurement
L-Band EIRP calculated from CRC Gnd Sta measured received signal strength

Table 2-5

ATS-5 EOL C-Band G/T Determination

	Ros Tx Pwr (dBm)	Downlink Carrier (dB)	Noise[1] Sharing Correction Factor, (C.F.) (dB)	Calculated[2] G/T (dB)
Planar Array	60	0 (REF)		
	45	-0.5		
	43	-1.0	-5.2	-17.5
	40	-2.0	-2.2	-17.5
	37	-4.0	1.2	-17.9
	34	-6.0	3.4	-17.1
				-17.5 average
Omni	60	0 (REF)		
	59	-2.0	-2.2	-36.5
	57.8	-3.0	-0.2	-37.3
	56	-4.0	1.2	-36.9
	54	-6.0	3.4	-37.1
				-36.9 average

(1) C.F. is a correction factor which accounts for the noise power sharing of the spacecraft transmitter output. Its value is a function of the carrier suppression (refer to Appendix F).

(2) Appendix F describes the calculation of G/T and presents a sample calculation

3.0 POWER SUBSYSTEM TESTS

3.1 INTRODUCTION

In the ATS-5 spacecraft, N on P silicon solar cells provide the primary source of electrical energy while nickel-cadmium batteries provide power during transient loads and solar eclipses. The solar array and batteries are divided into two independent solar array subsystems.

Each main solar cell array directly powers an unregulated bus, with a voltage range maintained between -32 to -24.5 volts. The lower limit is controlled by bus voltage limiters and the upper limit by a battery discharge control unit. Each battery is charged directly by a small solar cell battery charge array connected in series with the main array. A command-operated bus relay is included in the spacecraft which allows interconnecting the two unregulated supplies to accommodate fluctuating and asymmetrical loads. An automatic feature causes unparalleling of the two busses whenever the magnitude of the bus voltage falls below a nominal value of about 22 volts.

The system includes several current sensors which function to provide the telemetry encoders with voltage analogs of the bus and the battery charge/discharge currents. This power supply status information is then telemetered to the ground station.

A current control unit is included which places a fixed load into two additional dedicated bus voltage limiters upon command. Its purpose is to provide thermal heating inputs at key locations in the spacecraft during the worst-case eclipse conditions, utilizing energy from the battery.

The power subsystem is fully described in Reference 6 (see section 5). Pertinent details are shown in the power subsystem block diagram given in Figure 3-1.

3.2 POWER CONSUMPTION

3.2.1 Background

The electrical package loads on ATS-5 are distributed roughly equally between the two battery busses. Communication subsystem packages are shared between the two busses. For example, telemetry transmitters 1 and 3 are electrically connected to Bus 1, while telemetry transmitters 2 and 4 are electrically attached to Bus 2. The basic load packages and their bus assignments are given in Table 3-1.

3.2.2 Test Activities and Results

Power consumption tests were conducted at the GSFC ATSOCC by successively turning on electrical packages and noting the corresponding change in the appropriate unregulated current bus telemetry word. It was soon discovered that the power consumption of the electrical packages on Bus 2 could not be accurately measured. This is due to fluctuating telemetry readings acquired from Bus 2. The fluctuations are attributed to the damage to the aft solar array which resulted from apogee motor jettison. Thus, ..o meaningful Bus 2 power consumption results were obtained.

Bus 1 current telemetry values also fluctuate but the deviations are lower in magnitude. Table 3-2 presents a comparison of EOL test measured values and prelaunch values for electrical package current consumption. Some electrical loads were not measured due to possible adverse effects upon the spacecraft.

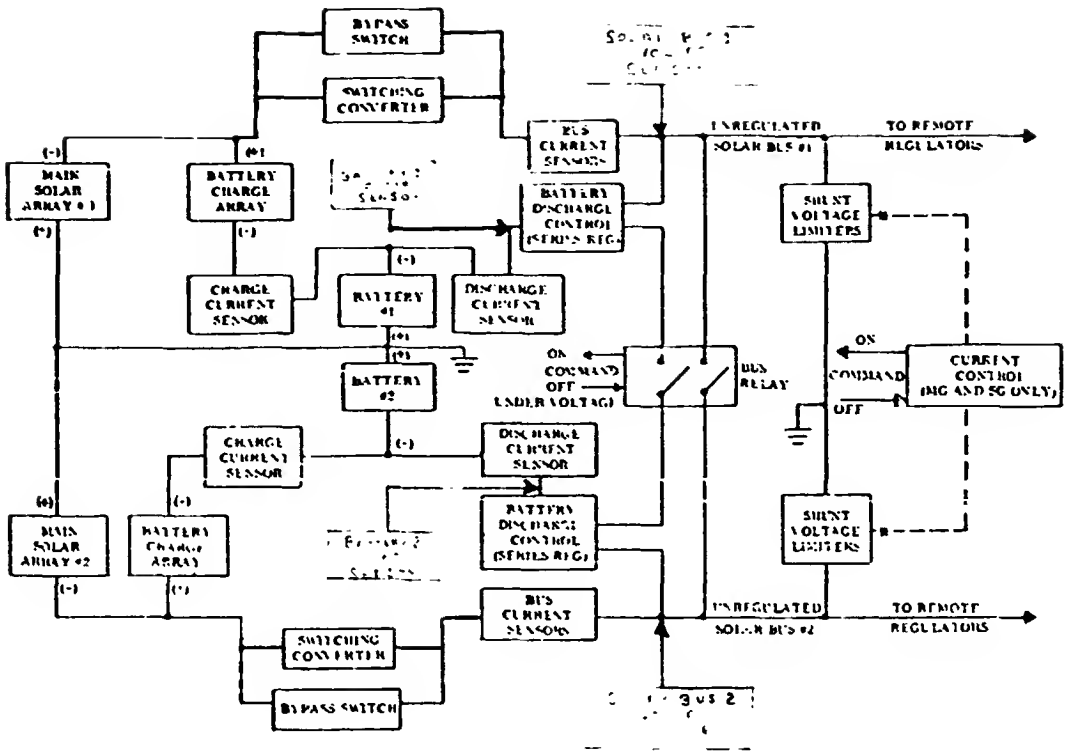

FIGURE 3-1 ATS-5 Power Subsystem

ORIGINAL PAGE IS
OF POOR QUALITY

Table 3-1

Basic Electrical Package Bus Assignments

ITEM	BUS 1 ASSIGNMENTS (ma)	BUS 2 ASSIGNMENTS (ma)
Telemetry Transmitters 1, 3	190	
Telemetry Transmitters 2, 4		190
Telemetry Encoder 1 (PCM)	115	
Telemetry Encoder 2 (PCM)		115
Telemetry SCO 1	50	
Telemetry SCO 2		50
Command Subsystem 1	100	
Command Subsystem 2		100
Clock (from Command Regulators)	15	15
Clock (from either bus)	60	60
C-Band Repeater MA Mode	185	
C-Band Repeater FT Mode	220	
C-Band Repeater WBD Mode	240	
C-Band TWT No. 1 Filament	125	
C-Band TWT No. 2 Filament		125
C-Band TWT No. 1 High Voltage	635	
C-Band TWT No. 2 High Voltage		660
L-Band TWT No. 3 Filament	175	
L-Band TWT No. 4 Filament		175
L-Band TWT No. 3 High Voltage	2060	
L-Band TWT No. 4 High Voltage		1875
L-Band Driver 1	300	
L-Band Driver 2		300
Current Control Unit	500	500
Subliming Solid Engines 1 and 2		
1) Conditioning Mode	610	610
2) Thrust Mode (first 12 minutes)	875	875
3) Extended Thrust	680	680
4) Shutdown (for both engines)	35	35

Table 1

Basic Electrical Package Bus Assignment

(continued)

ITEM	BUS 1 ASSIGNMENTS (ma)	BUS 2 ASSIGNMENTS (ma)
Gravity Gradient Regulator		20
IR Earth Sensor		285
T.V. Subsystem		380
Solar Aspect Sensor		160
Millimeter Wave Regulator 1	1580	
Millimeter Wave Regulator 2	1180	
Third Harmonic Generator Regulator		50
Solar Cell Experiment Regulator		280
Magnetic Damper Regulator	50	
Magnetic Damper Coils (each)	210	
Resistojet Experiment	420	
Ion Engine 1 and 2 (maximum)	1450	1500
Magnetometer Regulator	50	
Environmental Measurements Regulator		250
EME Bus Power		33
3 DME		300
ODHE		140
2 DLE		230
UDLE		50
SRB		130
EFE		80

Table 3-2

ATS-5 Current Consumption

ITEM	BUS 1 CURRENT (MA) MEASURED (EOL) VALUES	BUS 1 CURRENT (MA) PRE-LAUNCH VALUES
Telemetry Transmitters 1, 2, 3, and 4	†	190
Telemetry Encoders 1 and 2 (PCM)	†	115
Telemetry SCO 1 and 2	†	50
Command Subsystem 1 and 2		100
Clock (from Command Regulators)		15
Clock (from either bus)	†	60
C-Band Repeater MA Mode	200	185
C-Band Repeater FT Mode	210	220
C-Band Repeater WBD Mode	240	240
C-Band TWT No. 1 Filament	120	125
C-Band TWT No. 1 High Voltage	650	635
L-Band TWT No. 3 Filament	170	175
L-Band TWT No. 3 High Voltage	000	2060
L-Band Driver 1 and 2	†	300
Battery Discharge Control 1 and 2	not testable	25
Current Sensors Bus 1 and 2 (Connected to battery charge bus)	not testable	20
Current Control Unit	490	500
Subliming Solid Engines 1 and 2		
1) Conditioning Mode	460	610
2) Thrust Mode (first 12 minutes)	†	875
3) Extended Thrust	†	680
4) Shutdown (for both engines)	†	35
Millimeter Wave Regulator 1	1600	1580
Millimeter Wave Regulator 2	1000	1180
Magnetic Damper Regulator	44	50
Magnetic Damper Coils (each)	210	210
Resistojet Experiment	†	420
Ion Engine 1 and 2 (maximum)	†	1450
Magnetometer Regulator	†	50
† Not Tested		

Examination of the data shows that most measured values are close to the recorded prelaunch values. The differences may be due to onboard analog-to-digital converter components changing values because of age, or actual component value changes in the instrument itself. The one instrument that was measurable which showed no current drain, was the high voltage power supply for the L-band TWT 3. This device failed completely on January 30, 1974 during normal spacecraft operations. See Appendix C for a detailed report of the failure.

3.3. BATTERY DISCHARGE TESTS

3.3.1 Background

Battery discharge tests are useful to determine the approximate amp-hour capacity of batteries. Normally, discharge test results on spacecraft batteries are compared to discharge test results of a similar earthbound battery. The earthbound battery is a like battery made by the same manufacturer using the same technology as the flight battery. Similar batteries to that of ATS-5 were monitored and tested for about 11 years by the Naval Weapons Support Center, Evalaution Program for Secondary Sapcecraft cells in Crane, Indiana. The earthbound testing was discontinued in October 1978 when on an average 1 to 5 cells failed in each test battery. The earthbound test batteries had utilized mid 1960's technology and could be used as a standard comparison with many similar batteries flown in other satellites launched at that time. However, the earthbound test batteries were normally tested with a depth of discharge of about 40%. It has been approximated that the ATS-5 batteries have normally been discharged heaviest during eclipse periods to approximately a 15 to 20%

depth of discharge. Since the flight batteries have been discharged much more lightly then those of the earthbound test batteries, no immediately direct comparison of the two would be reliable. Consequently, the discharge tests that were performed on ATS-5 must be evaluated without the aid of controlled, standard test results.

The first battery discharge test was completed 12/08/80 on both of the 6 amp-hour batteries on ATS-5. The test was repeated on 12/19/80 but an undervoltage condition was encountered on battery 1 which resulted in a termination of the discharge tests on both batteries. Therefore, two battery discharge tests were completed on battery 1 while only one discharge test was completed on battery 2. It is suggested that the undervoltage condition on battery 1 was caused by the partial failure of the battery; three of the 22 cells have apparently shorted resulting in a -25 volt battery versus the nominal -29 volts. Additional tests will be performed at a later date to fully characterize battery performance.

3.3.2 First Battery Discharge Test and Results

The first battery discharge test was conducted on 12/08/80. Normally, the batteries were indirectly paralleled via their solar busses for load sharing purposes. However, during the discharge tests, the solar busses were unparalleled. Initially, the unregulated busses had to be loaded by turning on electrical packages to first exceed the solar array current capacity and second to load the batteries until they were discharging at a C/2[1] rate. Since the batteries originally had a 6 ampere hour capacity, approximately 3 amps of constant load current was drawn from the batteries.

[1] C/2 rate is one half of battery rated ampere hour capacity.

Each battery consists of 22 cells and it was assumed that a low-end discharge voltage of -1.05 volts per cell could be safely reached. This corresponds to a -23.1 volt battery terminal voltage. The test was terminated when downlinked telemetry momentarily displayed the low-end voltage.

Figure 3-2 shows a plot of discharge voltage versus discharge time. The normal no-load battery 1 voltage before the test started was -28 volts, but as load current was drawn from the battery the voltage fell to about -27.2 volts as Figure 3-2 indicates. Figure 3-3 is a plot of discharge current versus time. The time scales on Figure 3-2 and 3-3 are the same and direct correlations can be made between the two. The load current of battery 1 seemed to fluctuate during the bulk of the test. It has since been determined that this apparent fluctuation is due to non-symmetric weakness in the solar cell main and charge arrays which are supplying current to the unregulated bus and battery, respectively (see Appendix H).

In inspecting Figure 3-3, the numerical average of the discharge current for the bulk of the test is 2.3 amperes. The total discharge time is approximately 26 minutes. From this, the approximate amp hour capacity of battery 1 is as follows:

$$2.3 \text{ amps} \times 26 \text{ minutes} \times \frac{1 \text{ hour}}{60 \text{ min.}} = 1.0 \text{ ampere hours}$$

Battery 2 was also discharged at the same time battery 1 was discharged. The same procedure was used on battery 2 that was used on battery 1. Approximately 3 amperes of battery current was continuously drawn to discharge the battery at a C/2 rate. Figure 3-4 shows a plot of

FIGURE 3-2

BATTERY 1

VOLTAGE VS TIME

FIRST DISCHARGE

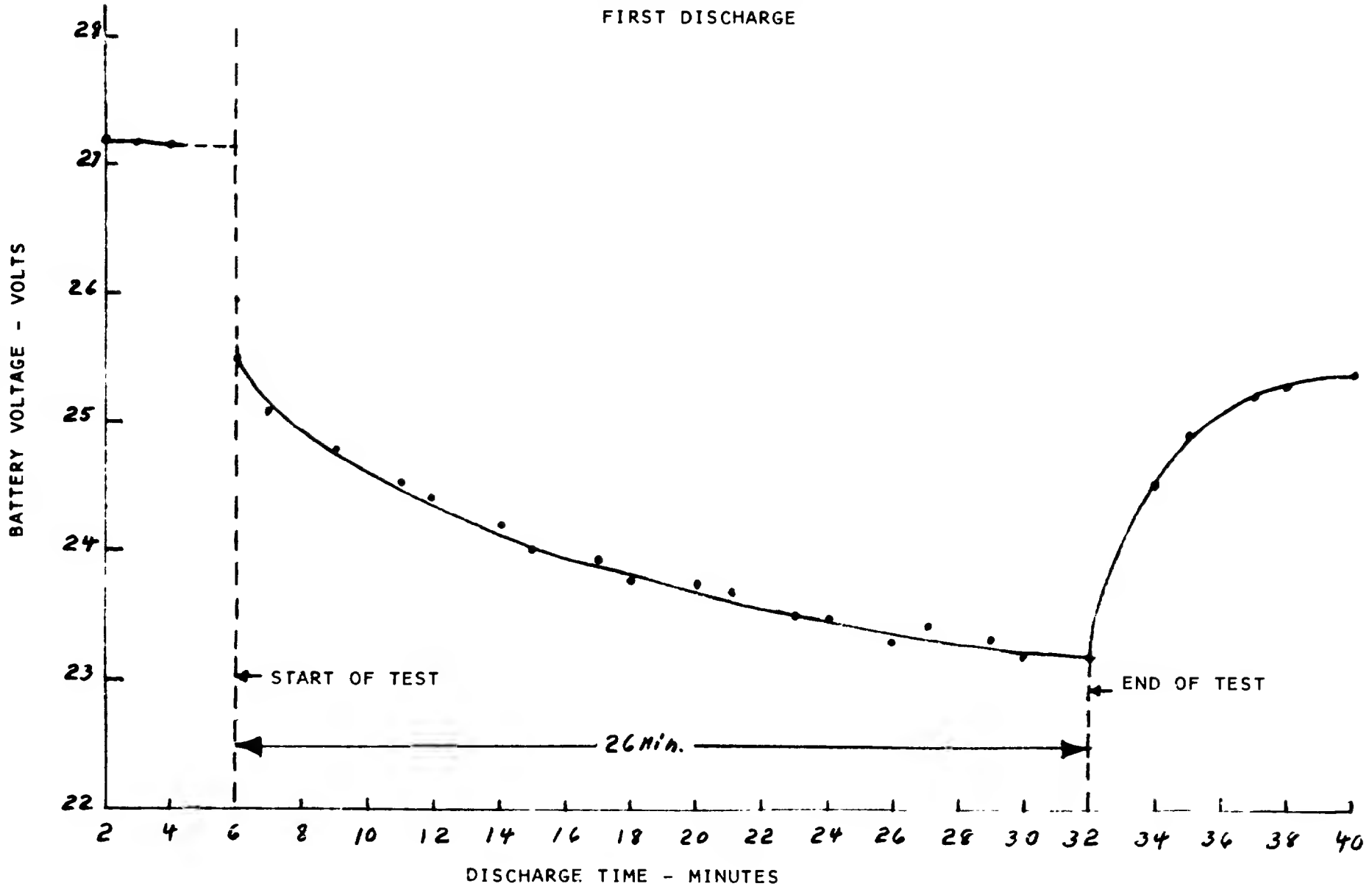

FIGURE 3-3

BATTERY 1
LOAD CURRENT VS TIME
FIRST DISCHARGE

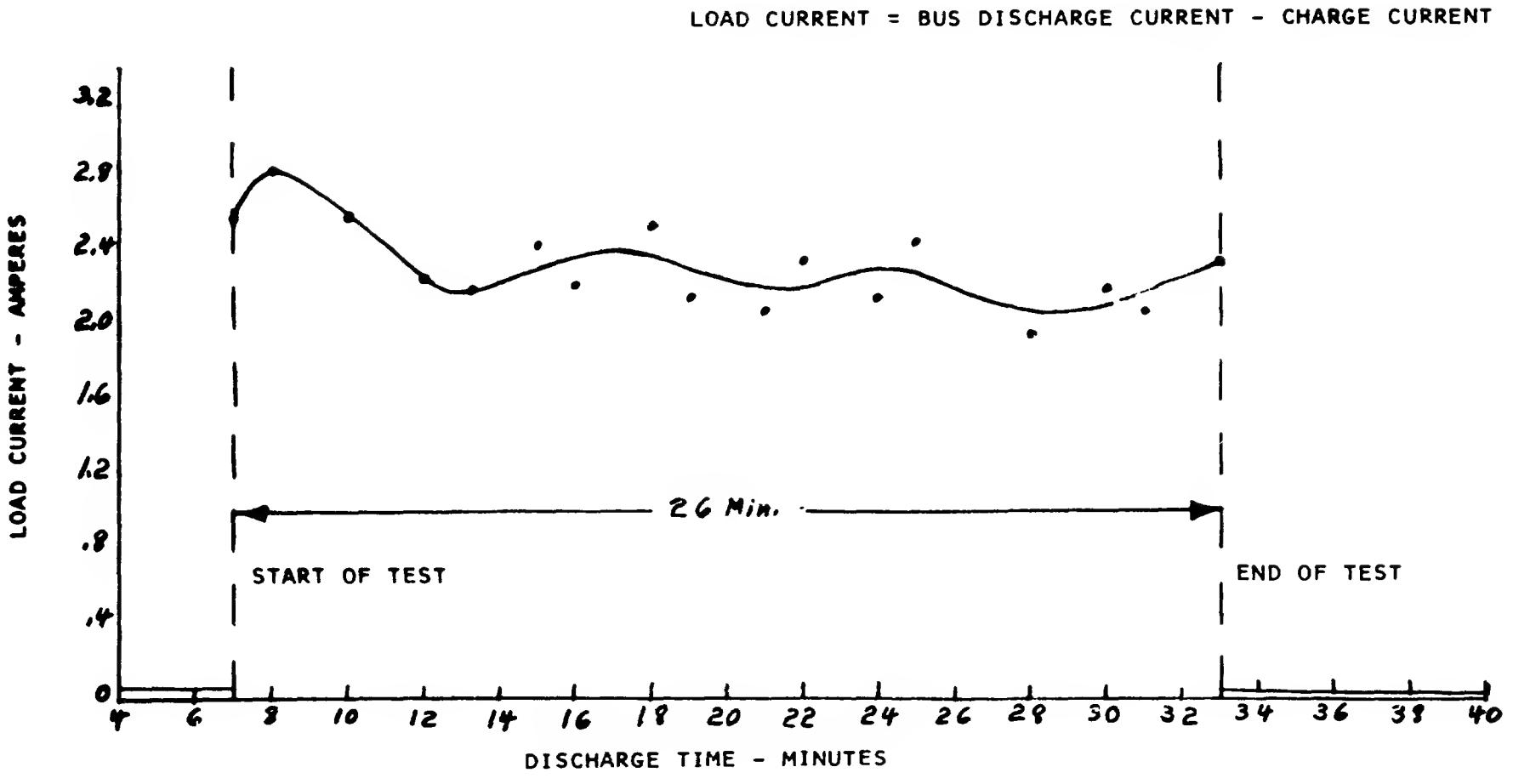

FIGURE 3-4

BATTERY 2
VOLTAGE VS TIME

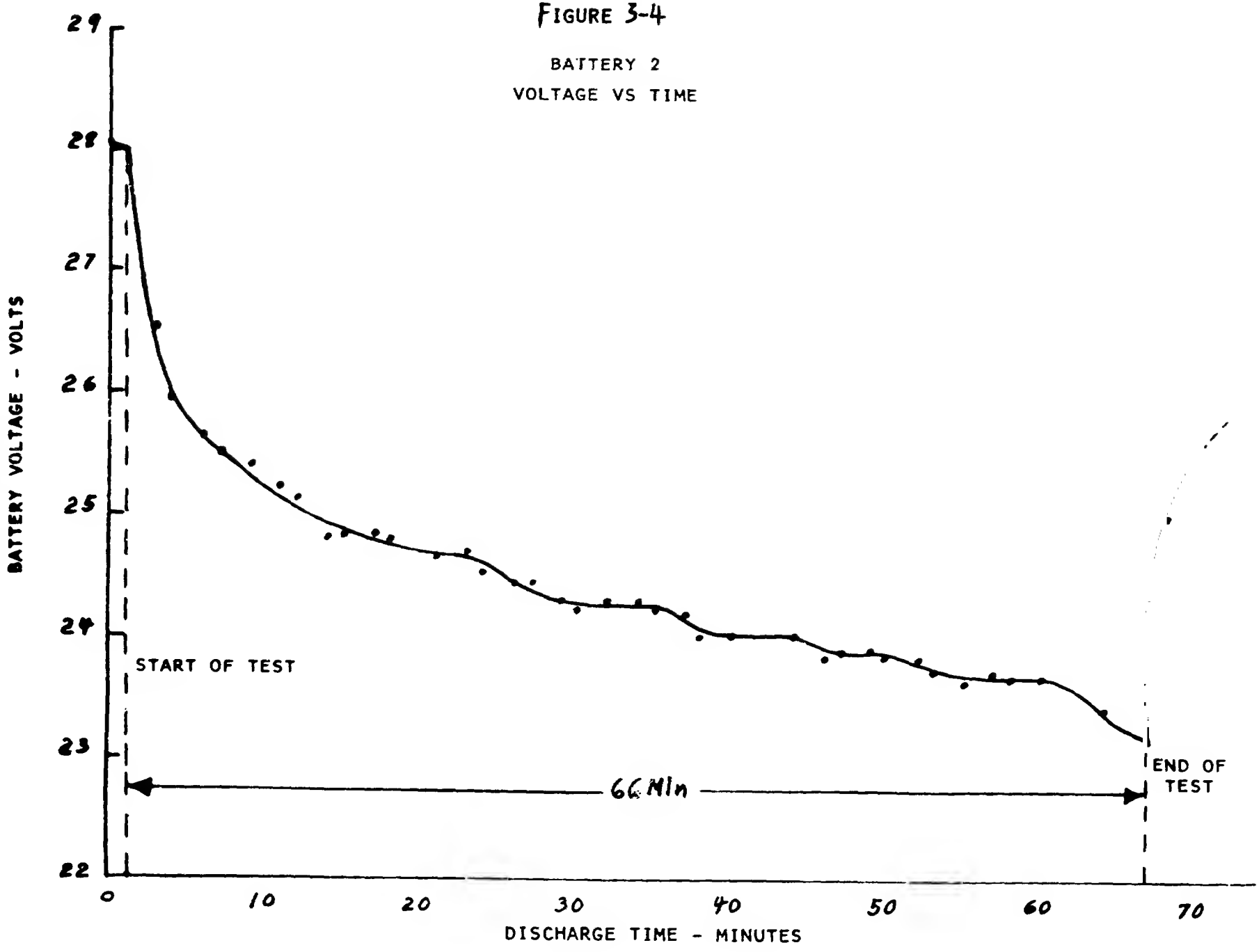

battery 2 voltage versus discharge time. Figure 3-5 shows a plot of battery discharge load current versus time and denotes large current fluctuations. These fluctuations are on the order of about 600 mA and are the result of aft end solar array damage which occurred when the apogee motor was jettisoned. As the spacecraft rotates and
the damaged portion of the solar array faces the sun, a current surge from the battery is seen. When the undamaged portion of the solar array faced the sun, the solar array added power to the unregulated bus which reduced battery load and thus resulted in lower battery current drain values.

The satellite is spinning at a spin period of approximately 765 milliseconds per revolution and the onboard telemetry updates every 2.97 seconds. Thus the telemetry from the satellite is "spin" modulated. Add to this the 2 minute sample interval factor used for this discharge test and the curve of Figure 3-5 is obtained. This curve definitely indicates solar panel damage. This characteristic was observed more clearly in the second discharge test.

The average current used to estimate the amp-hour capacity of battery 2 was obtained by numerically integrating under the curve of Figure 3-5. The estimated amp-hour capacity was then calculated as follows:

$$1.7 \text{ amps} \times 66 \text{ minutes} \times \frac{1 \text{ hour}}{60 \text{ min.}} = 1.9 \text{ amp-hours}$$

3.3.3 Second Battery Discharge Test and Results

On 12/19/80, a second battery discharge test was conducted. This discharge test was planned to duplicate the conditions of the first test. However, an undervoltage condition was reached on battery 1 which resulted in an immediate termination of the discharge tests. Since the discharge

FIGURE 3-5

BATTERY 2
LOAD CURRENT VS. TIME

LOAD CURRENT = BUS DISCHARGE CURRENT - CHARGE CURRENT

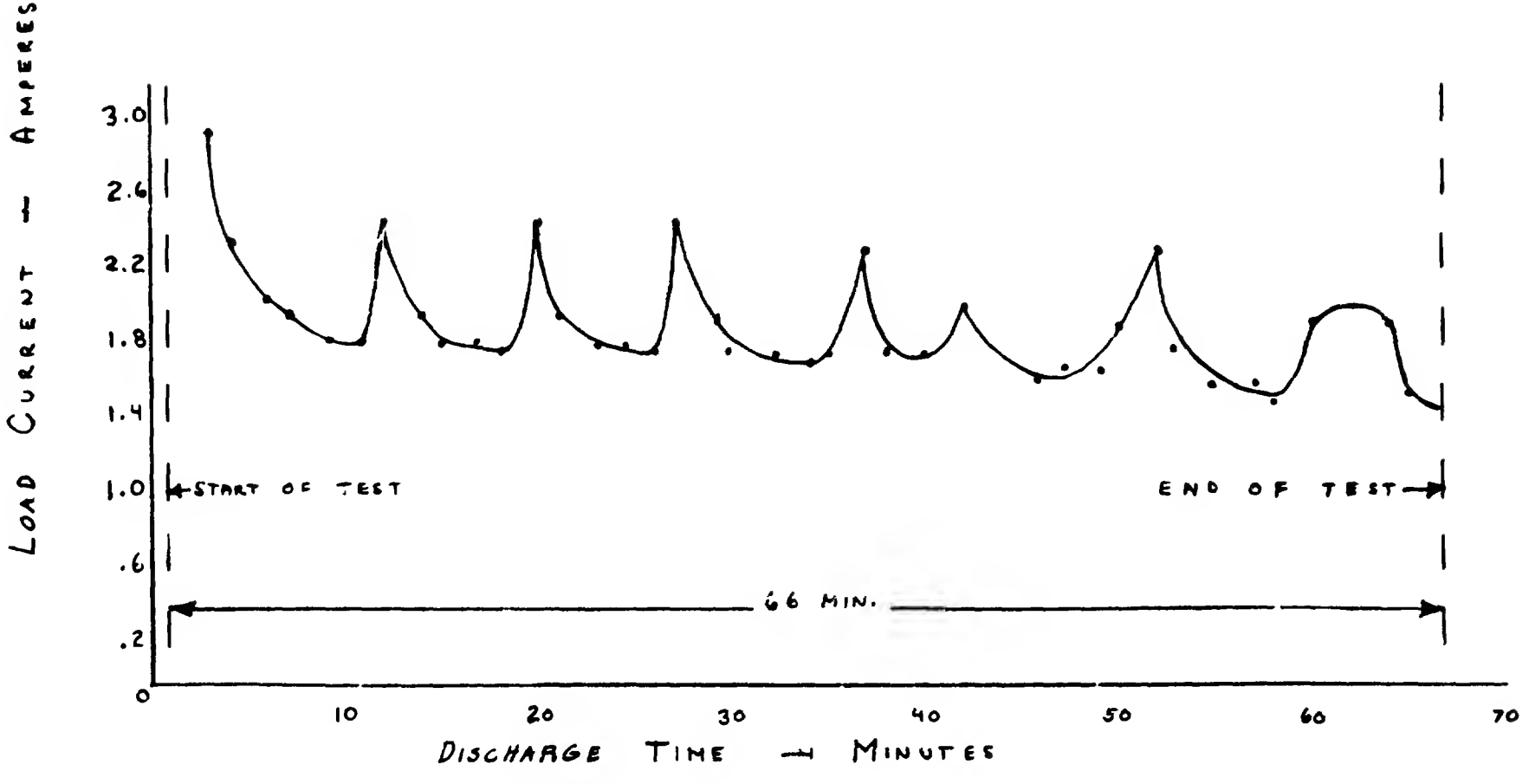

data on battery 2 was incomplete, results are not presented here. However, battery 1 discharge data is complete.

Figures 3-6 and 3-7 show battery 1 voltage and current respectively versus time. The elapsed time scale is the same on both plots so a direct comparison can be made. As can be seen in Figure 3-2, the battery 1 voltage dropped at least 0.6 volts with even mild (50 milliamp) loading. As In Figure 3-7, there was about an 18 minute delay from the time the battery was initially current loaded until it was fully loaded at about a C/2 rate. This 18 minute delay was required to execute the proper commands in order to load the spacecraft busses for the discharge test. When all the electrical loads were finally on, the spacecraft was allowed to discharge without disturbance for an additional 47 minutes. The discharge current shows a steady decrease as time progresses. This is probably a function of the regulators of the individual electrical loads on the spacecraft. From Figure 3-7, a capacity estimate can be made for battery 1. During the 18 minute low discharge period, an average of 0.8 amperes were being drawn from the battery. During the 47 minutes C/2 discharge rate, the numerical average of the current being drawn was 2.0 amperes. Thus, the capacity of battery can be approximated by:

$$(0.8 \text{ amps}) \frac{(18 \text{ minutes})}{\frac{60 \text{ minutes}}{1 \text{ hour}}} + (2.0 \text{ amps}) \frac{(47 \text{ minutes})}{\frac{60 \text{ minutes}}{1 \text{ hour}}} = 1.8 \text{ amp-hours}$$

The calculated 1.8 amp-hour capacity is consistant with the previous 1.0 amp-hour capacity result acquired in the first discharge test as follows:

Figure 3-2 may be redrawn so as to extrapolate the curve to the trip point of -22 volts; thus showing an additional 30 minutes

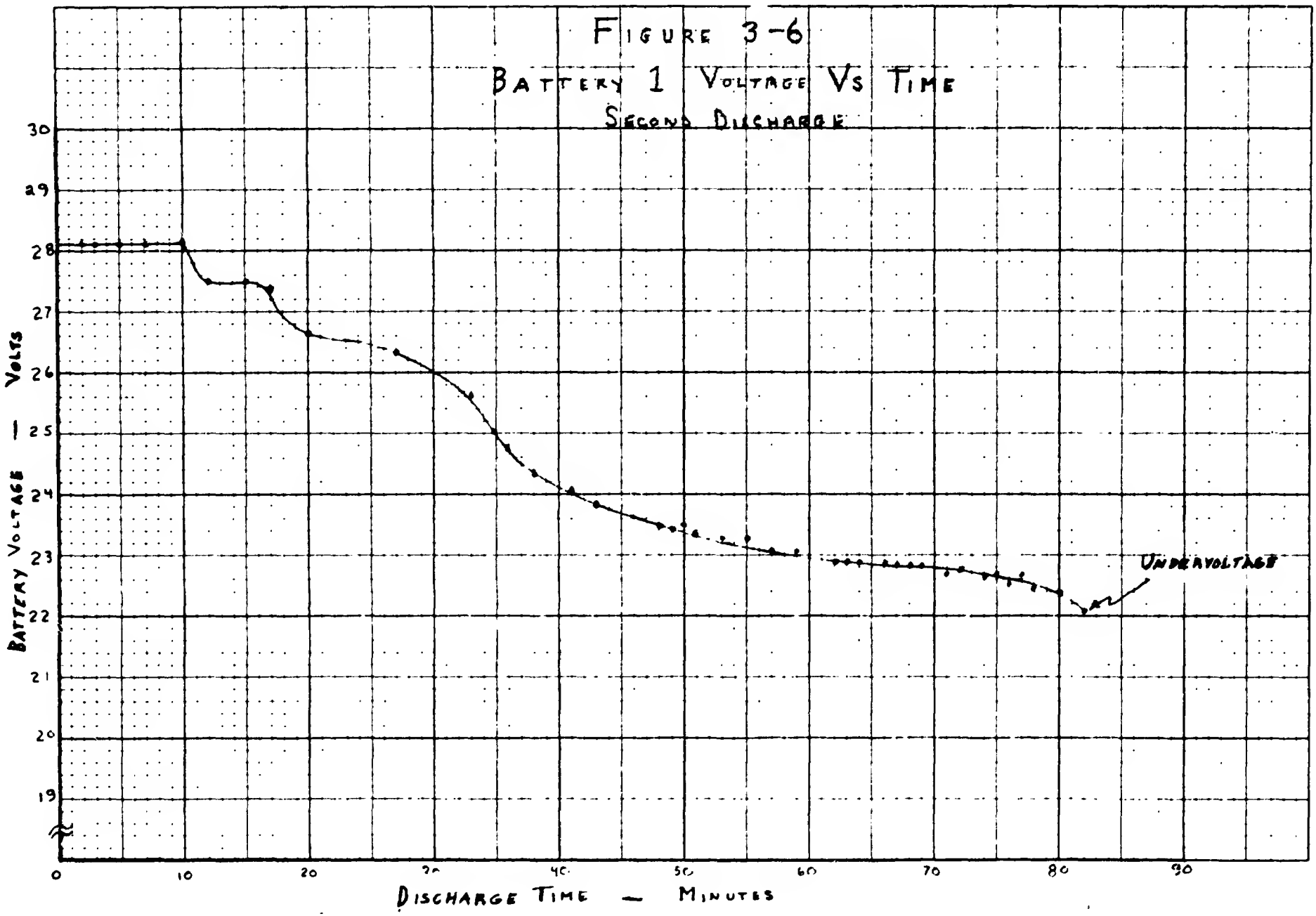

FIGURE 3-7

BATTERY 1 LOAD CURRENT VS TIME
SECOND DISCHARGE

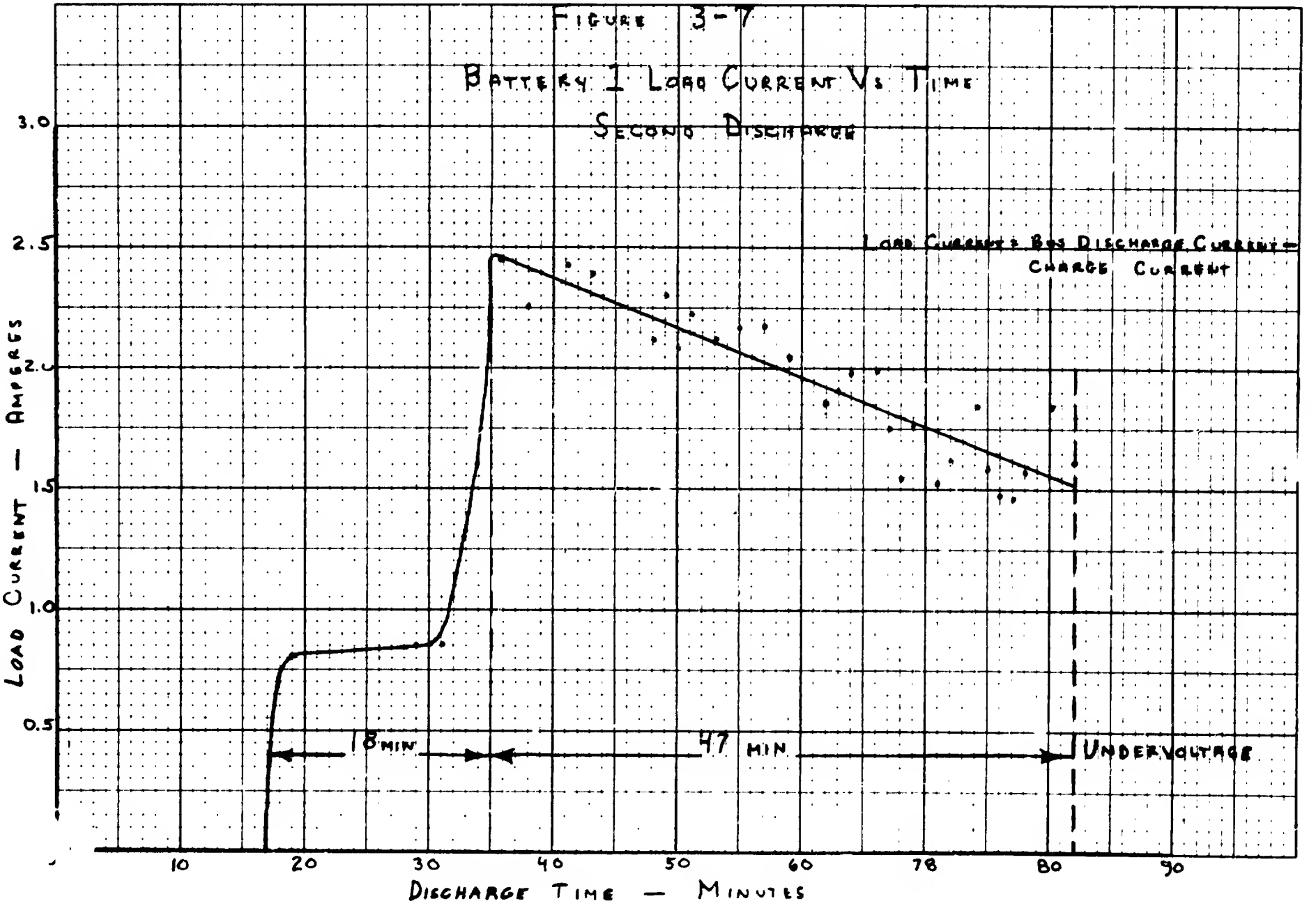

of discharge time (see Figure 3-8). At an average discharge current of 2.3 amperes, an additional 1.2 ampere hours is added to the previously der d figure of 1.0 amp-hours. Thus, from Figure 3-2, an extrapolated capacity of 2.2 ampere hours down to -22 volts is shown. This compares closely with the 1.8 ampere hours measured from the second discharge test on battery 1.

In consideration of the differences between the first and second discharge tests on battery 1, it is estimated that battery 2 has as much as a 3.0 amp-hour capacity.

3.4 SOLAR ARRAY PERFORMANCE

As discussed in Para 1.2, ATS-5 went into a "flat" spin after the Apogee Motor Burn (spacecraft spinning about an axis normal to the Z axis). Since the apogee motor was actually mounted somewhat "inside" the S/C structure, it was inevitable that the motor would impact the spacecraft case during the apogee motor jettison. This is because jettison is accomplished by moving the apogee motor along the Z axis. The release mechanism cannot move the apogee motor fast enough to avoid impact with the aft end of the spacecraft as it spins, thus causing damage to the aft solar array (solar array #2). The damage has not adversely affected operation of the aft solar array as it continued to charge battery 2 and supply power to unregulated bus 2. The results of the damage can be seen as fluctuations in the battery 2 bus current when it is under load. Such a condition occurred during the discharge test. Figure 3-9 is a plot of battery 1 and 2 current versus time. The data is from a rawdump of telemetry data when the two batteries were loaded to approximately a C/2 rate. Every 2.97 seconds, the telemetry updates. Every 765 milliseconds, the spacecraft rotates once.

FIGURE 3-8

BATTERY 1 VOLTAGE VS TIME
EXTRAPOLATION

(FROM FIGURE 3-2, FIRST DISCHARGE)

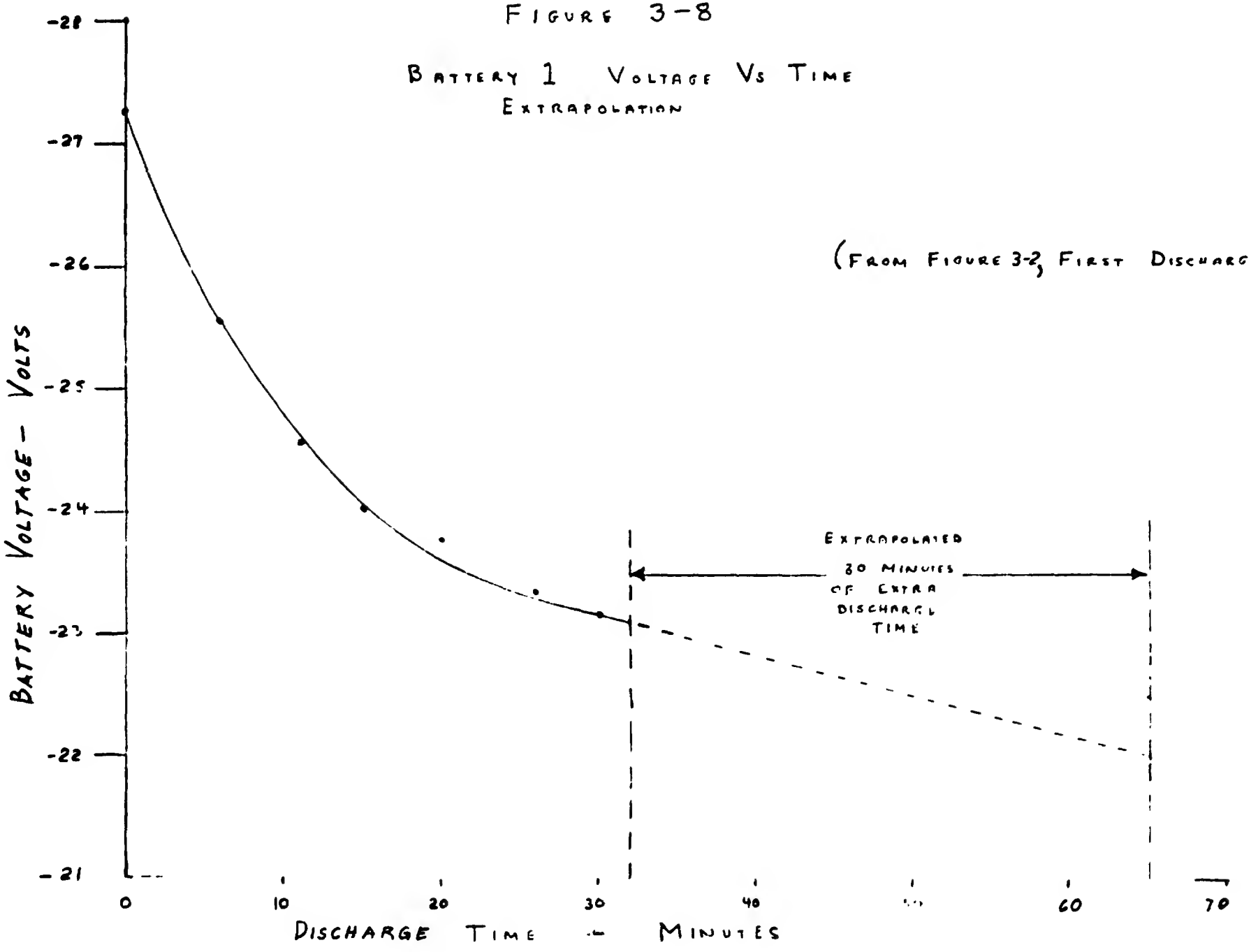

FIGURE 3-9

CURRENT VS. TIME
BATTERY 1 AND 2 (FINAL DISCHARGE)

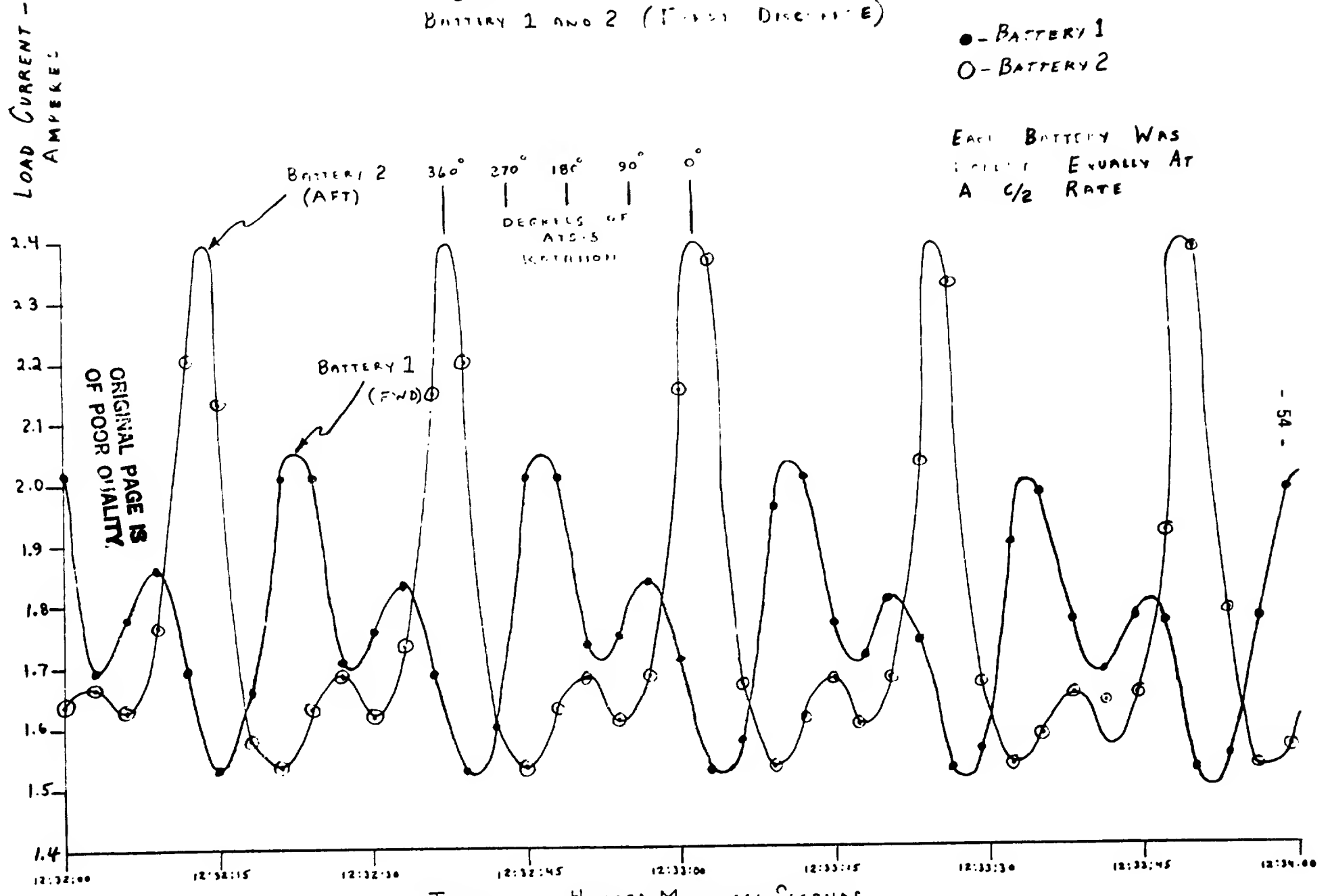

Therefore the spacecraft completes 3.88 rotations between telemetry updates, with the sun illuminating a different portion of the solar array each time the telemetry is updated. From the foregoing, it is determined that each data point represents approximately -43^{o} of spacecraft rotation.

This provides a means of determining the periodic current versus time characteristics form the data shown in Figure 3-9. The lower scale gives the actual data sample times, the upper scale shows the approximate waveform per spacecraft rotation. The plot shows the effect of damage and weakness of each solar array. The low points on the curves indicate that the solar arrays are strongest at that point. The maximum elements of the curves indicate where the solar array was damaged or weakened and thus more battery current must be drawn.

Figure 3-9 indicates that solar array 2 shows greater current variation than that of array 1. This is to be expected since the aft solar array (array 2) is the one that was damaged. The current variation noted in solar array 1 could be due to degraded strings of cells within the array or possibly by damage to a lesser degree by the impact with the apogee motor.

The forward array maximum current capacity has been measured to be approximately 2.1 amperes. The aft solar array maximum current capacity has been estimated to be approximately 1.7 amperes. Both values were determined from test data on 5 December 1980 at a sun angle of 68^{o}. Normalizing the foregoing values to a 90^{o} sun angle (as would occur at equinox) yields normalized values of 2.26 and 1.83 amperes for the forward and aft arrays, respectively. Using the normalized values for the present capability and an original capability of 4.4 amp for each array, the forward solar array

demonstrates a 49% degradation and the aft solar array depicts a 58% degradation from the design current capacity. The estimated degradation is 40%, determined as follows:

Some data relating to solar array performace in synchronous orbit was collected on ATS-5 by L.A. Gibson of the Aerospace Corporation. From this information, the solar cells of ATS-5 degraded about 4% due to initial travel through the Van Allen Belt. In August of 1972, a large solar flare occurred which slightly damaged the solar cells of all spacecraft. The recorded damage reduced the ATS-5 solar cell maximum power by about 3% (references 8 and 9). Additionally, the power loss estimated on the basis of trapped electrons is 3% per year for similar ATS-5 technology solar cells. By combining these factors, one can make a first order estimate of the solar cell power degradation as follows:

Year	Precent Loss	Cause
1969	4%	Van Allen Belt Passage
1972 (August)	3%	Solar Flare
1969-1980	33% (@ 3%/year)	Trapped Electrons
TOTAL	40%	

This 40% predicted degradation can be used as a basis for the comparison of the 49% forward array capacity loss and the 58% aft array current capacity loss. Considering the forward array, the estimated and sun angle normalized values differ by 9%. The difference could easily be accounted for by additional solar flares which have occurred since August of 1972 (only 3 flares of that same magnitude would produce the observed effects). Additional causes of power loss can be a possible deposition of a contaminant on the cell cover slides and low energy protons entering from the edges of the cells or from the back of the cell through Kapton fiberglass substrate (Reference 10). Considering the aft solar array, the predicted loss value and the measured

loss value differ by 18%. The reason for the difference may be the same as those for the forward array in addition to the physical damage which resulted from the collision with the apogee motor casing during jettison.

A series of tests were performed from which solar bus current dwell telemetry was obtained for solar bus 1 and 2. The data is presented in Appendix H and clearly shows the result of the damage solar cells.

4.0 GRAVITY GRADIENT TVCS TESTS

4.1 BACKGROUND

The gravity gradient television camera system (TVCS) consists of a camera unit and an electronics unit. The original purpose of the TVCS was to provide observations of the dynamics of the primary booms. The camera provides a standard 525 line raster which can be displayed on commercial TV monitors.

The camera unit contains the videcon tubes, its associated circuitry, and the horizontal deflection, blanking, beam current, and vidicon protective circuits. A protective sun shutter, also provided, is mounted on the camera unit.

An electronics units contains all necessary circuitry to process the video signal generated in the camera. The video output of the camera system can be channeled directly to the spacecraft wideband C-band transmitter for downlink transmission. See Reference 7 for a full description.

4.2 TESTS AND RESULTS

Tests were conducted in August 1980 to determine the status of the TVCS. To ensure sun shutter closure, the end of the test was to be performed while the spacecraft was eclipsed by the earth. This was necessary to ensure sun shutter closure using the automatic sun shutter control electronics.

After eclipse, the TVCS was again turned on in an effort to obtain a stronger signal and thus a clearer picture. These efforts failed as no picture quality improvement was seen. At the end of the TVCS test, it was discovered that the sun shutter was not operative. Thus, the sun shutter had to be left open when the TVCS was finally shutdown. However, the damage to the videcon tube due to sun exposure will be minimal. It was later conjectured that the failure of the sun shutter was due to the spin of the spacecraft. The sun shutter was not designed to operate on a spinning spacecraft thus the sun shutter actuator cannot overcome the force of spin and consequently cannot close.

A final test of the TVCS was made in November 1980. There was no apparent degradation of picture quality and thus no damage to the videcon tube due to occasional solar view.

It was suggested that the TVCS be used if possible to observe boom deployment after ATS-5 is deorbited. However, accurate measured quantities of boom deployment should not be expected from the availabl video downlink. It may, however, be possible to derive qualitative information on the Gravity Gradient System by utilizing the TVCS.

5.0 REFERENCES

1. ATS-V Post Launch Report (Preliminary), GSFC, 1969
2. L-Band Performance Characteristics of the ATS-5 Spacecraft, NASA/GSFC X-731-70-51, FEB, 1970 (Revised May 1970)
3. Application Technology Satellite ATS-E System Description NASA/GSFC S-II-037, AUG, 1969
4. Spacecraft Communications Subsystem, ATS-E Specification NASA/GSFC S2-0131, April, 1969
5. Hughes Aircraft Company, ATS-5 Long Form Tests, May, 1969
6. ATS Series Vol. 2 Systems and Technology, NAS 5-21548, July, 1973
7. ATS-E Gravity Gradient Orbit Test Handbook, NAS 5-9042, July, 1969
8. B.E. Anpauth, "ATS-5 Solar Cell Experiment after 699 days in Synchronous Orbit," Conf. Rec. of the 9th IEEE Photovoltaic Specialists Conf., 308, 1972
9. B.E. Anpauth, "ATS-5 Solar Cell Experiment after 6½ years in Synchronous Orbit," Conf. Rec. of the 12th IEEE Photovaltaic Specialists Conf., 191, 1976
10. H.Y Tada, J.R. Carter, Jr. "Solar Cell Radiation Handbook" NASA-JPL, November, 1977

APPENDIX A

C-Band Antenna Patterns

This appendix presents C-band planar array and omni transmit antenna patterns measured October 27, and 28, 1969. The data includes calibration measurements and stripchart recordings which are used for comparison purposes in the C-band EOL experiments. The omni antenna pattern shows the effect of the RF leakage through the C-band antenna select switch. This effect is further detailed in Appendix B.

Scope

The planar array antenna pattern, with its corresponding calibration curve, is presented in Figure A-1 as a stripchart recording and was measured on October 27, 1969. When the same antenna pattern was measured on October 28, 1969 the omni antenna pattern was also recorded on a stripchart as shown in Figure A-2. This pattern was the result of RF leakage through the C-Band antenna select switch.

2TW2, DOWNLINK, OCTOBER 27, 1969

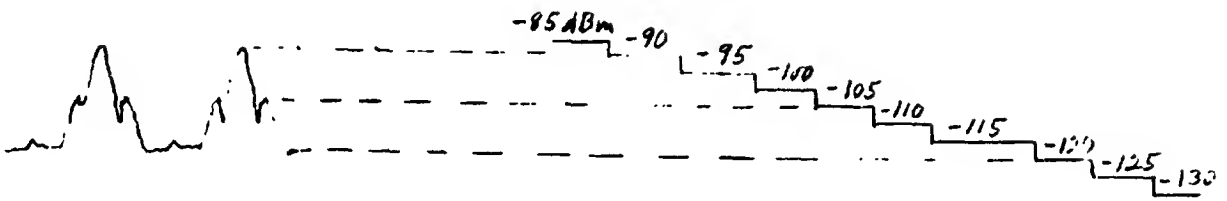

FIGURE A-1 ATS-5 PLANAR ARRAY ANTENNA PATTERNS AND CALIBRATION

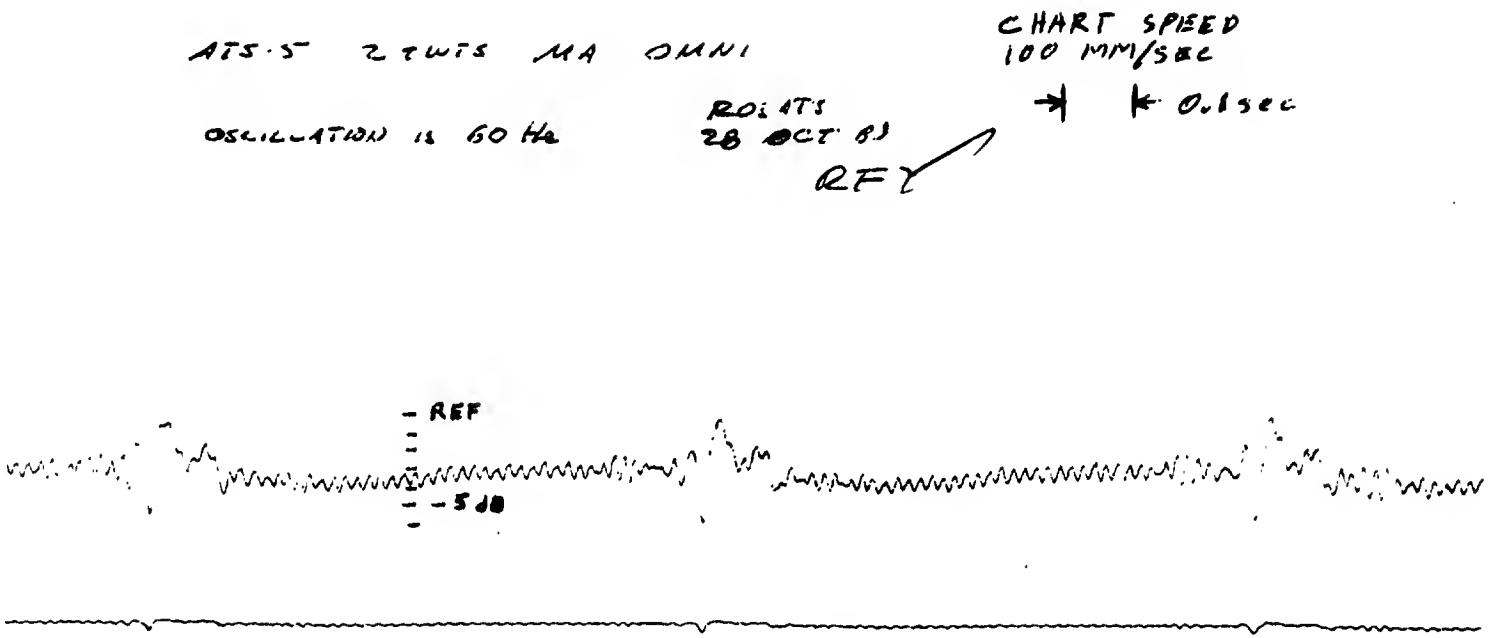

FIGURE A-2 ATS-5 OMNI-DIRECTIONAL ANTENNA PATTERN (RF SWITCH LEAKAGE)

APPENDIX B

RF Antenna Select Isolation

This appendix consists of the following documents.

Page B-2, B-3

Letter from Hughes Aircraft Company to NASA/GSFC detailing the RF switch and its effect on the C-Band and planar array antennas.

Page B-4

Stripchart from an FAA/BOEING Test completed March 9, 1972 showing the effect of the leakage in the C-Band receive antenna select switch.

Page B-5

Discussion explaining basic geometrical considerations in determining position of nulls in the C x L antenna patterns using the omni antenna.

HUGHES AIRCRAFT COMPANY

AEROSPACE GROUP

SPACE SYSTEMS DIVISION

EL SEGUNDO, CALIFORNIA

13 March 1968

IN REPLY REFER TO:
68H(22)3017/A3498

SUBJECT: Omni/Planar RF Switch Leakage

TO: National Aeronautics and Space Administration
Goddard Space Flight Center, Code 460
Greenbelt, Maryland 20771

ATTENTION: Mr. Don V. Fordyce
Spacecraft Manager
Applications Technology Satellite Project

REFERENCE: TWX from D. V. Fordyce dated 7 March 1968,
Subject: Omni/Planar 3 db Variance

The test data for omnidirectional antenna patterns taken on F-4 show an increase in power of approximately 3 db when the planar array comes into view of the test receiving antenna (for about 20 degrees). The reason for this is that the RF switch used to select between the planar array and the omni antenna (Figure 1) does not have perfect isolation. When the omni is selected a signal approximately 20 db down goes to the planar array. When antenna gains and cable losses are considered the following situation exists.

		Repeater 1 (1 TWT) (dbm)	Repeater 2 (1 TWT)
Omni Antenna Selected:	ERP of the omni is	+32.9	+33.6
	ERP of the planar is	+31	+32
Planar Array Selected:	ERP of the omni is	+13	+13.5
	ERP of the planar is	+50.9	+51.6

The power loss due this low isolation is about 0.1 db so that the ERP of the spacecraft will not be impaired and as the test data shows, the valves obtained are 0.5 and 1.2 db above the spec. values for planar array.

This isolation characteristic is one which is due to the design and not to a defective RF switch. Antenna patterns will be checked again during the final long form test to verify that the system has not degraded during environmental testing.

J. P. Wrzesinski, Manager
Systems Engineering Department
Applications Technology Satellite Program

JPW:LGMartinson:rm

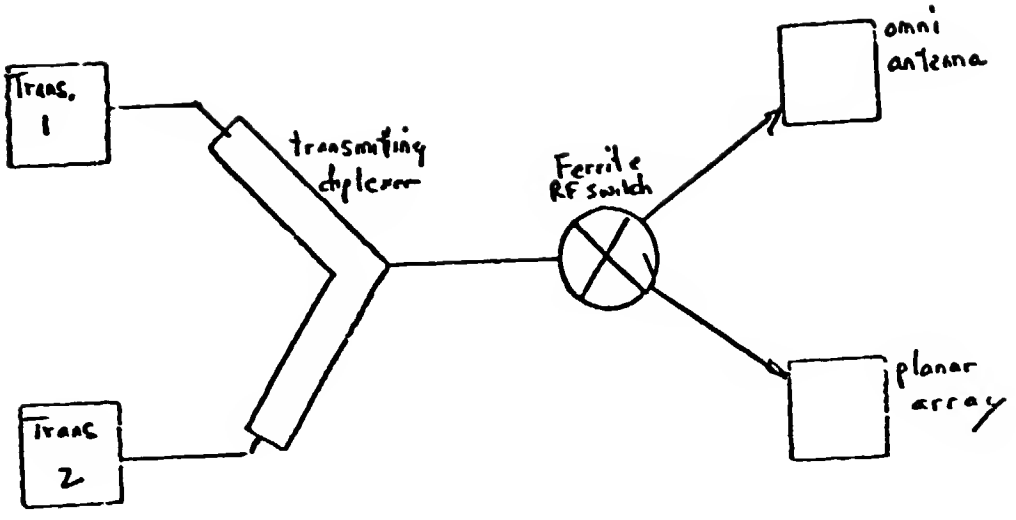
Trans. 1
Trans 2
transmitting diplexer
Ferrite RF switch
omni antenna
planar array

Fig 1.

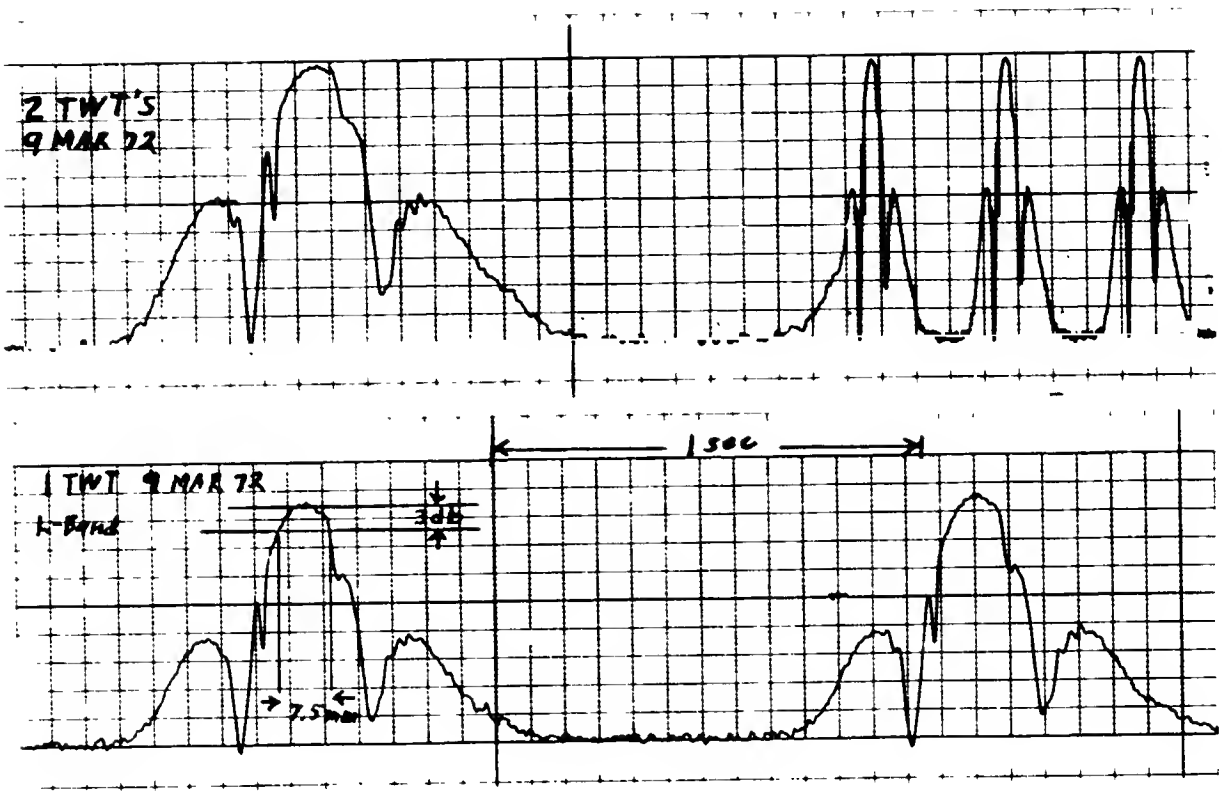

FAA/BOEING TEST

ATS-5 85' Dish Uplink

C x L Mode 125 mm/sec

C-Band Omni Antenna

Main lobe distortion is due to feed through in the C-Band antenna select switch

Analysis of Antenna Nulls

The C x L antenna stripchart on page B-4 demonstrates the effect of spacecraft rotation on the production of nulls when the omni antenna is used in the C x L configuration. The spacecraft was designed to be gravity gradient stabilized. Thus the communications subsystem was designed so that both the plannar array and the omni antenna receive an incident C-band wavefront in phase while in the orientation shown below.

Wave cancallation occurs when the received wavelengths are 180^0 apart this happens in ½ λ periods. At 6212.094 MHz, ½ λ = .95 inches.

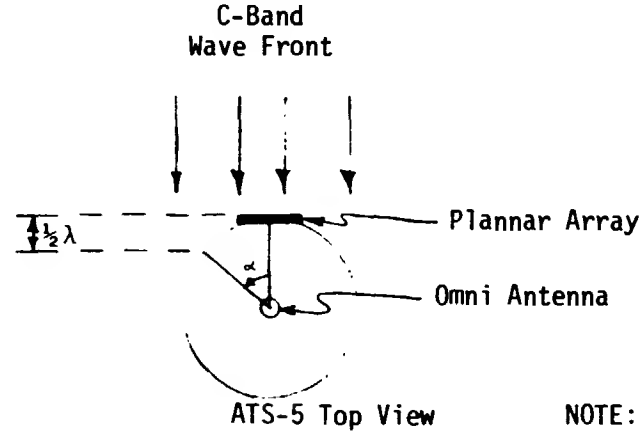

ATS-5 Top View NOTE: S/C radius = 56.6"

As the spacecraft rotates, a point is reached where the distance between the plannar array and the omni antenna differ by ½ wavelength. By referring to the above diagram and applying standard trigonometric principles, the angle of a ½ λ rotation calculates to be-14.8^0. In an analysis of the C x L stripchart of page B-4, the nulls occur at a spacecraft rotation of 20 degrees. These angles compare closely considering the probable errors resulting from the lack of spacecraft attitude information in the calculations.

APPENDIX C

L-Band Receiver Malfunction

This appendix presents the only known chronicle of the L-band receiver malfunction on ATS-5.

Pages C-2 thru C-15

Report of L-band repeater malfunction and events through 16 May 1972.

Page C-16

Report describing L-band receiver faulure occurring in August 1974.

Page C-17

Report describing the events leading to the last and apparently final malfunction of the L-band receiver.

REPORT ON ATS-5 L-BAND REPEATER MALFUNCTION

INTRODUCTION

This report contains the history to date of the L-band repeater malfunction together with as much background as is required for an understanding of the problem. The report is divided into the following sections:

1. Repeater Description

   A. Modes of Normal Operation (Nomenclature)
   B. Block Diagram (Input Pwr. Monitor)
   C. Characteristics (Frequency, BW, Pwr. input required for Saturation)

2. History of Malfunction

   A. Summary
   B. Detailed Description

3. Characteristics of Malfunction Mode

4. H.A.C. Simulation

5. Conclusions

Original report dated 8/23/72

1. Repeater Description

A. Modes of Operation

The L-band repeater normally is capable of operation in one of six modes as follows:

Wideband, Frequency Translation (FTWB)

Spacecraft receives at L-band, down converts to an IF frequency of approximately 67 MHz, and then upconverts to the L-band transmit frequency. There is no remodulation in this mode. The full repeater bandwidth (25 (MHz) is utilized for this mode.

Narrowband, Frequency Translation (FTNB)

Same as FTWB except that a 2.5 MHz filter is in the IF and an additional 10 dB of IF gain is provided.

Single Sideband to Frequency Modulation Mode (SSB/FM)

This is a remodulation mode in which the uplink L-band signal is linearily amplified in the S/C, and down converted to baseband (500-600 KHz). The baseband signal is used to frequency modulate an onboard voltage controlled oscillator (VCO) which has a nominal center frequency of 67 MHz. The VCO output is heterodyned to L-band for retransmission.

Wideband Data Mode (WBDM)

In this mode the onboard VCO provides the source for the downlink L-band signal. The input to the VCO is selected from one of four onboard experiments: Gravity Gradient TV (GGTV), Millimeter Wave Experiment (MWE), L-band front end (L-band), or Infa-red Earth Sensor (IRES). If the selected experiment is not powered, then the VCO will free run with no modulation, thus providing an unmodulated L-band source (in this discussion the free running, unmodulated VCO configuration will be referred to a WBDM). If the L-band is selected, then the SSB/FM configuration is obtained (when the L-band front end is energized).

L-Band to C-Band Cross-strap (LXC)

This mode is identical to the SSB/FM except that the received baseband signal (500 to 600 KHz) is used to FM the C-band repeater VCO in lieu of the L-band VCO.

C-Band to L-Band Cross-strap (CXL)

The uplink C-band signal is down converted to IF, and routed to the L-band upconverter to provide the downlink.

B. Repeater Characteristics

The repeater characteristics are as follows:

	FTNB	FTWB	SSB/FM	WBDM	LXC	CXL
Uplink Freq.(MHz)	1651.50	1651.02	1650.55		1650.55	6214.94
Downlink Freq.(MHz)	1550.48	1550.00	1550.48	1550.48	4119.60	1553.79
Bandwidth(MHz)	1.5*	25.0*	0.1	6.0	0.1	6.6*
Saturated Input(dbm)	-83.0**	-73.0	-93.0		-93.0	-80.0

*Front end saturated
**Increase of 2 db uplink pwr. produces 1 db increase in downlink pwr. Refer to Figure 1 for saturation curves.

C. Repeater Block Diagram

Referring to the block diagram, it may be seen that four modes (FTWB, FTNB, SSB/FM and LXC) all share a common L-band front end, downconverter, and IF amplifier. It is these modes which are inoperable when the malfunction is present. As seen in the block diagram, all five L-band downlink modes share a common post amp (at IF) as well as the limiter/amp. The limiter amp, prior to limiting, provides a sample of the signal which is detected and encoded for PCM telemetry to the earth station. Normally RCVR front end noise will cause an octal readout of 001 or 002 when the S/C is in the FTNB mode, thus providing a means of qualitatively determining from PCM telemetry if the L-band RCVR is operating normally.

One further point concerns the switching mechanism. The VCO select switches are mechanical, all other switching is performed with diode switches. The diode switches are used to apply (or withold) DC bias voltage from various transistor stages.

2. History of Malfunction

In this discussion the terminology repeater ON or OFF refers to D.C. power applied to (or withold from) appropriate modules.

A. Summary of Events

DATE	RCVR STATUS	COMMENT
27 Oct. 70	First indication of malfunction	Malfunction was cleared by commanding S/C RPTR On/Off
Oct. & Nov. 70	Malfunction reoccurred and cleared several times	Malfunction was increasingly difficult to clear
04 Nov. 70	Malfunction reoccurred	Malfunction could not be cleared (several cmd sequences were used)
09 Nov. 70	Malfunction cleared	Malfunction cleared during a S/C test. Return to normal occurred 10 mins. after execution of a S/C cmd (C-band hi-lo select). The exact time was determined from PCM. RPTR was left in "On" configuration

25 May 71	Malfunction reoccurred	The main difference between this reoccurrence and others is that in this instance the malfunction occurred while the repeater was energized (the repeater has remained energized since 9 Nov. 70).
01 Jun 71	Malfunction cleared & reoccurred	Malfunction cleared for approx. 30 mins. (as indicated by PCM). Malfunction reoccurred before ground station could verify status with L-band measurements
22 Jul. 71	Malfunction cleared	Malfunction cleared by itself (the S/C was not being commanded)
07 Sept. 71	Malfunction reoccurred	No S/C operations or PCM recording was being performed at the time.
08 Dec. 71	Malfunction cleared	Cleared during normal S/C operations.
26 Jan. 72	Malfunction reoccurred	The RPTR was inadvertently turned Off, and the malfunction was present when the S/C was commanded back On.
28 Jan. 72	Malfunction cleared	The malfunction cleared during a S/C investigation test. Time of clearing was 5 mins. 11 secs. after the last cmd. At the time the S/C power system was heavily loaded and it was possible for the first time to accurately measure load currents. When the malfunction cleared, the bus current increased 230 ma, which is approximately equal to the repeater nominal load current.
24 Feb. 72	Malfunction reoccurred	RPTR was OK at 2351:40 on 23 Feb. when switched to WBDM for I.P. test. Next Q.L. at 0536 showed reoccurrence of malfunction.
16 May 72	Malfunction Cleared	Malfunction cleared sometime between 15/1241 and 16/0303.

A plot of failure occurrence vs. time, temp., and sun angle is shown in Figure 1. No correllation has been established.

B. Detailed Description of Events

Oct.-Nov. 1970

After operating satisfactorily for over a year, an apparent malfunction occurred in the S/C L-band receiver. The malfunction was first experienced 0110Z 27 October 1970 when a signal could not be passed through the S/C in the FTWB mode. The problem cleared after turning off the L-band repeater and bringing it up again.

The problem reoccurred 2230Z 27 October when the L-band repeater was turned on for another test (again in the FTWB mode). The problem cleared when the repeater was shut off and turned on again. The malfunction reoccurred 2200Z 28 October when the repeater was turned on (this time in the FTNB mode). The problem cleared with no S/C commands being sent. The problem did not reoccur until 2230Z 29 October even though the S/C was operated in different modes, and the repeater was turned on and off several times. When the malfunction reoccurred 2230Z 29 October, the S/C was in the FTWB mode and several combinations of mode changes and on/off sequences did not clear the problem. Later the same evening the S/C operated normally. A similar performance was observed 30 October with the malfunction first occurring during an "Off" to "On" configuration of the L-band repeater. Several mode changes and S/C repeater On/Off commands were unsuccessful in restoring normal operations. The problem then cleared for subsequent tests.

Normal L-band operation was obtained 31 October, and 03 November. The malfunction reoccurred 04 November and could not be cleared. Several command sequences were executed over a period of several days in an effort to clear the malfunction. None was successful. The problem cleared itself 09 November 23:18.43. The exact time (within 3 seconds) was determined from PCM data which was being recorded at that time as part of a special L-band investigation test. The return to normal operation occurred 10 minutes after the execution of a C-band hi/lo select command and is thus not associated with a command execution.

The repeater was in the WBDM when the fault cleared. It was switched to the FTWB mode where it remained for several weeks. Also, the repeater was kept in the "On" condition (the TWT amplifiers were turned on and off, as required, but the L-band receiver was left on).

After operating in the WBFT mode, the S/C mode was successfully changed to all other modes. The repeater, however, was never turned off (until 25 May after the malfunction again occurred).

May-June 1971

The ATS-5 L-band repeater experienced a malfunction similar to the malfunction which occurred during October and November of 1970. The problem was manifest in a loss of gain in the L-band receiver front end, thus causing the FTNB, FTWB, SSB/FM, LXC cross strap modes to be inoperable. The WBDM and CXL cross strap modes operate normally.

The main difference between this malfunction occurrence and those of 1970 is that in this instance the malfunction occurred while the repeater was energized (the repeater had remained energized since 9 November 1970 when the malfunction last cleared. The malfunction was first recognized as having occurred 25 May when the FAA reported that they were not receiving a signal through the S/C (FTNB mode). Several On/Off and mode change sequences were performed in an effort to return the S/C to normal operation. None of the sequences allowed the receiver to be Off more than a few minutes.

On 1 June a sequence was begun which allowed the receiver to be Off for two hours, then turned On. The second time the sequence was performed, the repeater came up in what was apparently normal operation (PCM telemetry indicated 001 on data tag 43, indicating that the L-band receiver front end noise was being detected by the signal strength monitor). The Mojave station was immediately requested to bring up their L-band transmitter so that quantitative measurements could be performed, however, the malfunction reoccurred before such tests could be made (the malfunction was cleared for about 30 minutes). PCM telemetry confirmed that a signal level equivalent to front end noise had been received from22:56:25 until 23:28:03 (31 mins. and 38 secs.). The reoccurrence of the malfunction was not associated with any mode change or command. Numerous similar mode change and On/Off sequences were performed to no avail until 22 July, when the malfunction cleared.

July 1971

The L-band receiver malfunction cleared during the A.M. of 22 July (PCM recording was analyzed to determine the exact time).

A test was performed P.M. of 22 July to quantitatively characterize the L-band repeater in various modes.

Canada (CRC) radiated L-band from Ottawa and A.I.I. received the downlink L-band signal at Wallops Island (A.I.I. was currently performing a C to L-band cross strap experiment and had two receiver systems set up at Wallops). The tests showed that the S/C was operating essentially nominally in the FTNB mode (saturated power output is obtained with nominal input level, and nominal 2.5 MHz. BW was achieved). The S/C was switched to the FTWB, WBDM and cross strap modes with no difficulty. The mode was switched to FTNB and nominal performance was achieved.

Sept. 1971

The L-band receiver on ATS-5 experienced a malfunction 7 Sept. (the exact time is not known since PCM has not been recorded). The malfunction indication was observed on PCM telemetry (data tag 043 dropped to 000). A test was performed 8 Sept. with Canada (CRC) monitoring the L-band downlink with the S/C in the L-L, MA mode. No front end noise was observed, indicating a loss in gain of at least 30 to 40 db.

Dec. 1971

The L-band receiver front end came on 8 Dec. (DT 43 read 002 octal). The S/C had been configured in the WBDM for the IP test. At 0600:20Z, the S/C was commanded into the FTNB mode. At that time the PCM showed 002 for DT 43, thus indicating normal operation of the L-band receiver. A test was performed by CRC and MOT (Canada) to checkout the S/C characteristics. Preliminary results show nominal S/C operation in the FTNB mode. After the Canadian test was completed, the S/C was put into the L-CX strap mode. Rosman detected approx. 1 db carrier suppression of the C-band downlink due to L-band receiver front end noise; this is nominal for normal operation.

Jan. 1972

The L-band receiver was inadvertently turned off 26 Jan. at 0015:25 when Cmd. 374 (L-band xpndr off) was sent instead of Cmd. 312 (L-band xmtr off). The 374 Cmd. is an interlocked cmd., however, the interlock at Rosman had been bypassed due to relocation of the MCC which was taking place out as part of the ATS-F GSI. The repeater was immediately brought back up in the FTWB mode and then switched to the WBDM for the I.P. test. The repeater stayed in the WBDM until 04017 when it was switched to the FTNB mode.

At this time it was noted by PCM that DT 43 was 000, indicating that the S/C receiver malfunction had reoccurred. A test was performed 26 Jan. which verified the malfunction had occurred, after which repeated attempts to clear the malfunction were made during the next two days by turning the repeater On/Off and switching between FTNB, FTWB and WBDM modes.

Another test was performed 28 Jan. using Canada (CRC) radiating to the S/C, and the L-band mobile at Rosman receiving. The test was to determine the extent of the S/C loss in the FTNB and SSB/FM modes. In the midst of the test, the PCM indicated that the receiver malfunction had cleared. A subsequent check of the PCM (which had been recorded throughout the test) showed that the malfunction cleared at 20:44:37Z which was 5 mins. 11 secs. after the last cmd. to the S/C had been executed. The repeater BW and linearity was then measured in the FTNB mode and the sensitivity was measured in the SSB/FM mode. Both tests confirmed nominal operation.

At the time the malfunction cleared, TWT 3 and 4 were both on, thus both S/C batteries were being discharged. This provided an opportunity to measure the load current fairly accurately before and after the malfunction. The total load current increased 0.25 amp when the malfunction cleared. The nominal load current for the FT mode is 0.2 amp thus indicating that little or no extra power was being used by the receiver in the failure mode. This aspect of the problem will be investigated further.

Feb. 1972

The L-band rcvr. malfunction reoccurred sometime between 23/2351:40Z and 24/0536. The exact time is not known. The sequence of events follows:

TIME	EVENT	COMMENT
23/2351:40Z	RPTR switched to WBDM from FTNB	DT 43 reads 002. Prior to Cmd. execute (per PCM).
24/0400:00	Stop PCM recording	PCM recording stopped to support ATS-3 eclipse.
24/0400:45	XMTR Off (cmd. 312)	TWT turned off after I.P. test.
24/0401:05	RPTR switched to FTNB	No reading was made of DT 43.
24/0536	Q.L. recorded	First indication of malfunction occurrence.

PCM provides an indication of the RPTR condition (malfunction or cleared) only when the RPTR is in the FTNB mode; thus the PCM recordings from 23/2351:40 to 24/0400:00 provides no clue as to the time of the malfunction.

CRC (Canada) monitored the L-band downlink while the S/C was in the WBDM and the L-band front end was selected. If the S/C was operating normally, noise sidebands approx. 10 db down from the carrier should have been visible with carrier suppression of approx. 2.2 db (CRC reported possible suppression at 0.2 db, however signal was noisy).

The Westinghouse transmit/receive terminal (Baltimore, Md.) was used 25 Feb. to further confirm the malfunction. Westinghouse transmitted 200 watts (10 ft. dish) which is sufficient to saturate the L-band front end (in normal operation) in the FTNB mode. No downlink was observed (S/C with 2 TWTs), thus indicating S/C gain was down at least 25 dB (the Westinghouse terminal normally has a 25 to 30 dB (C+N)/N).

The tests performed by CRC and Westinghouse, as well as S/C PCM, all indicate that the S/C was in the failure mode.

May 1972

The malfunction cleared sometime between 15/1241 and 16/0303. The exact time is not known. A PCM Q.L. taken at 16/0303 indicated that the front end was in the FTNB mode Subsequent RF tests verified normal operation. The sequence of events preceeding the return to normal operation was as follows:

13/0600-15/1241	S/C in FTNB mode. PCM recording indicates malfunction present.
15/1241-16/0005	S/C in CXL mode for FAA/Boeing Test. PCM cannot provide indication of L-band receiver status (whether or not malfunction is present). There were some S/C configuration changes during this period in support of test.
16/0005-16/0301	S/C is WBDM for IP Test. PCM cannot provide indication of L-band malfunction status.
16/0301	S/C switched to FTNB mode. PCM Q.L. indicates malfunction cleared.

3. Characteristics of Malfunction Mode

The characteristics of the ATS-5 L-band repeater when operating in the malfunction condition are as follows:

a) FIWB (LxL) No detectable signal through S/C with max. ground transmitter power of 1 mW (-83 dbm at S/C).

b) FINB (LxL) Signal level depressed approx. 39 db. S/C not usable for experiments.

c) WBDM (L-band downlink only) Normal operation.

d) SSB/FM (LxL) Multiple access mode signal level depressed approx. 42 db (based on LXC measurements) S/C not usable.

e) L x C Cross-strap (SSB/FM) Signal level depressed approximately 42 db. S/C not usable.

f) C x L Cross-strap (FM/FM) Normal operation.

From the above, it may be concluded that the gain decrease due to the malfunction is approximately 39 to 42 db. This correlates well with the decrease in gain of 40 db measured November of 1970.* The foregoing measurements are probably only accurate to within 3 or 4 db.

Using the LXC mode, it was possible to measure the decrease in front end noise which appears at the VCO input when the L-band receiver is selected. This decrease was measured to be 20 db (identical to the decrease in front end noise measured November 1970).

4. Hughes Aircraft Company (HAC)

HAC utilized the ATS-5 breadboard modules to perform tests to simulate various module failures. The simulated failure involved removing D.C. power

*Another measurement made November of 1970 showed the decrease in gain in the FINB mode to be about 25 db. This measurement has been repeated and now indicates a 39 db loss in gain.

from the module (in one case the L.O. signal was removed). Following is a summary of the simulation results:

MODULE	GAIN(db)	N.F.(db)	NOISE PWR (DBM/MHz)
T D A	15	5.5	-109
b.P. Filter	-.5		
Mixer	-7		
Pre Amp	23 to 25	4	-110(-120 due to TDA)
Attenuator	-5 to -6		
IF Amp	23 to 25	6	-108(-84 due to TDA, -92 due to Pre Amp)

Measurements were made of beacon to carrier (B/C) and carrier to noise (C/N) ratios with various modules energized as follows (only one module was de-energized at any one time).

CONFIGURATION(INPUT-73 dbm)	B/C (db)	C/N (db)	COMMENT
Normal, everything on	-18	42	
TDA Off (DC removed)	-13	30	Carrier dropped 4 db. Noise drops 13 db.
Pre Amp Off			Carrier completely disappears (gain down at least 42 db). Noise is same as normal.
L.O. Removed			Noise drops 20 db.
Post Amp Off			Lose both signal and noise.

5. Conclusions

Measurements made with the S/C in the malfunction mode were compared with normal operation conditions (pre-measured), as well as with the HAC simulation measurements. By measuring the decrease in gain and the decrease in front end noise, it is possible to make an educated guess as to which module may have experienced the malfunction (assuming that the malfunction is due to loss of DC power and not due to a transistor being shorted, or open or a thousand other possible failures not simulated).

a) Loss of Local Oscillator

The observed decrease in front end noise of 20 db correlates exactly with the HAC simulation of removing the L.O. signal. Assuming that the L.O. were partially present, it is conceivable that the signal could be suppressed by 40 db.

b) DC Power Loss to TDA and Pre-amp

If the TDA and pre-amp both lost DC power, the loss in gain (at least 42 dB) and increase in front end noise (calculated to be about 17 dB) would correlate well with measured S/C data including the 230 ma increase in DC load current when the malfunction cleared 28 January 1972.

It is doubtful that the failure is due to the IDA alone, since pre-flight tests show that the insertion loss whether shorted or open circuit, is on the order of 5-6 db. Thus the net loss in gain would be approximately 20 db.

(Original signed by F.J. Kissel 8/23/72)

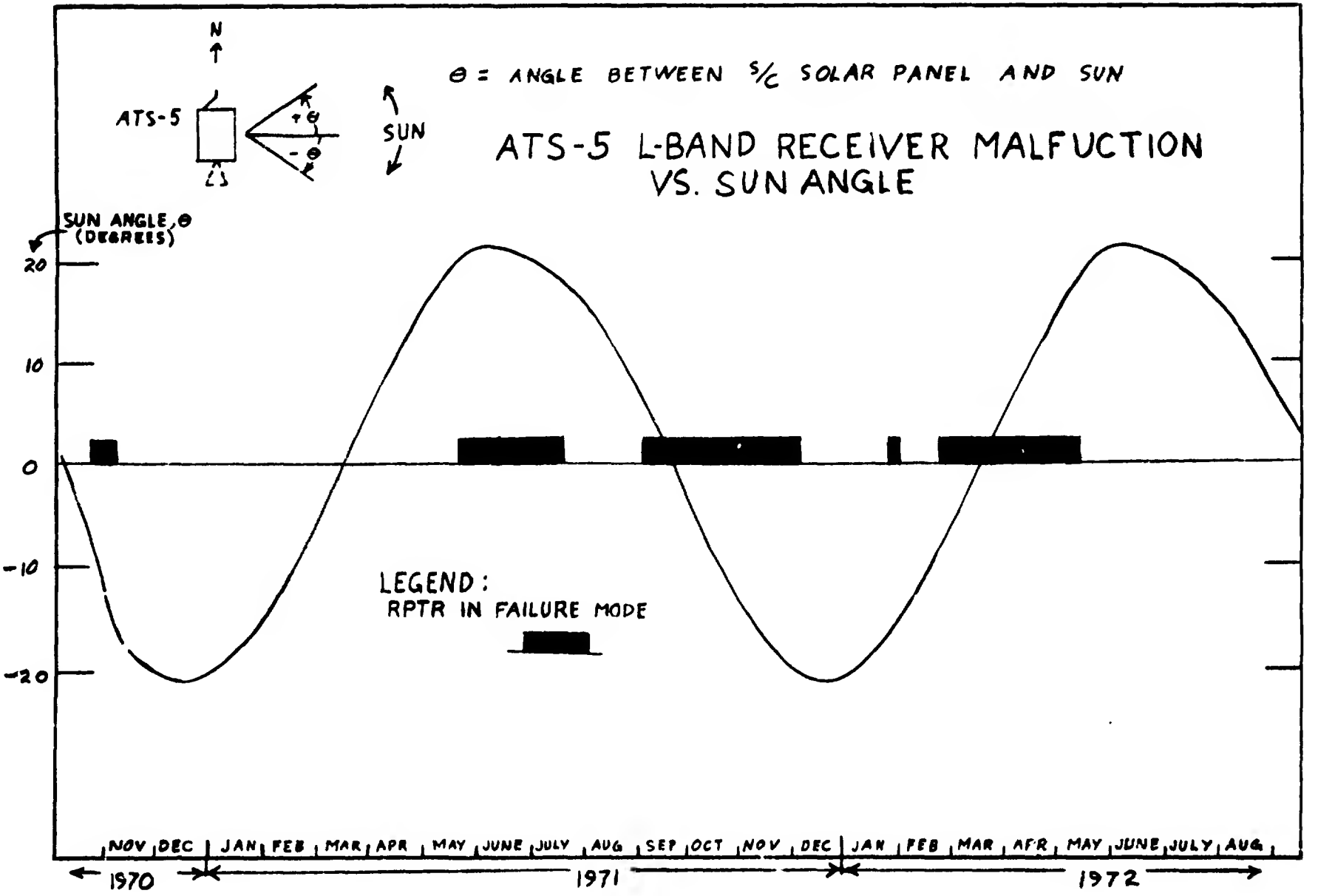
N
ATS-5
+θ
-θ
SUN
θ = ANGLE BETWEEN S/C SOLAR PANEL AND SUN
ATS-5 L-BAND RECEIVER MALFUCTION VS. SUN ANGLE
SUN ANGLE, θ (DEGREES)
20
10
0
-10
-20
LEGEND:
RPTR IN FAILURE MODE
NOV DEC JAN FEB MAR APR MAY JUNE JULY AUG SEP OCT NOV DEC JAN FEB MAR APR MAY JUNE JULY AUG
1970
1971
1972

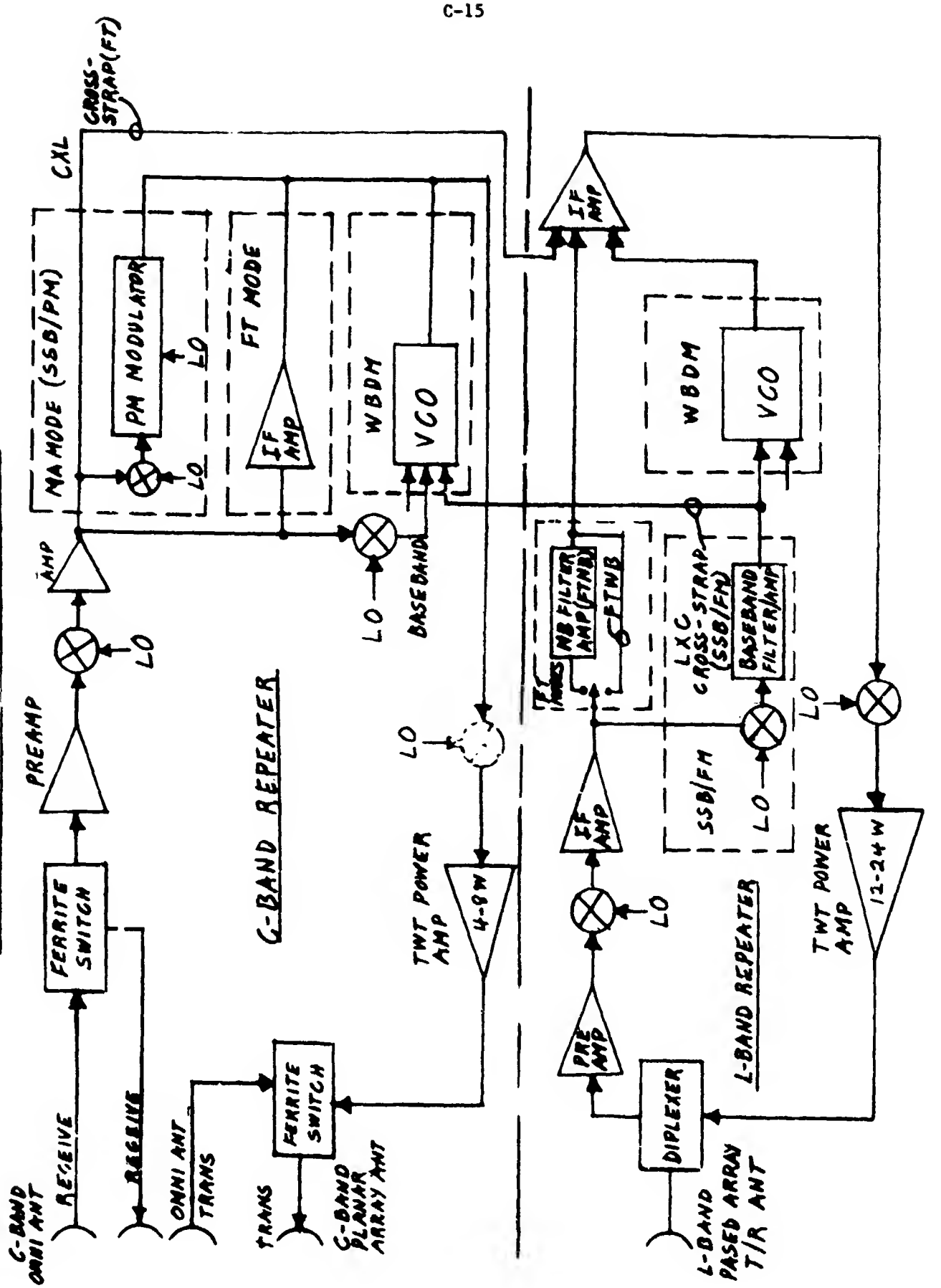
ATS-5 L + C-BAND REPEATERS
C-BAND REPEATER
L-BAND REPEATER
CROSS-STRAP(FT)
CXL
MA MODE (SSB/PM)
PM MODULATOR
LO
FT MODE
IF AMP
WBDM
VCO
BASEBAND
AMP
PREAMP
FERRITE SWITCH
RECEIVE
TRANS
C-BAND OMNI ANT
OMNI ANT
C-BAND PLANAR ARRAY ANT
TWT POWER AMP
4-9 W
NB FILTER AMP (FTNB)
SETNB
LXC CROSS-STRAP (SSB/FM)
BASEBAND FILTER/AMP
SSB/FM
PRE AMP
DIPLEXER
L-BAND PASED ARRAY T/R ANT
12-24 W

L-Band Receiver Failure

In August, 1974 the L-band receiver failed to operate due to excessive battery current drain. The L-band transponder, which had been in operation, was planned to be disabled over a weekend to allow C-band ranging to be performed. Unfortunately the C-band transponder was disabled by mistake. This resulted in a limited performance of ranging which continued until the signal strength was no longer acceptable. The telemetry performance also began to deteriorate. Subsytems were then turned off but the quality of the telemetry continued to decay.

Telemetry data was lost and then recovered. At the time of telemetry recovery the battery voltage was at a low value of 20.4V.

(memo to F.J. Kissel from ATSOCC/Baker, 14 April 76)

5 March 1976

TO: H. Pedolsky/D. Moore

FROM: ATSOCC/R. Baker

(Nov 4 1976)

On Julian Day 063 of this year the L-Band receiver turned off due to excessive battery drain caused by operation of the Ion Engines on ATS-5. The lowest battery voltages recorded were 25.9 v for battery #1 and 25.8 for battery #2. I do not believe that it was solely battery drain, but rather a combination of load current, battery voltage, and possibly temperature that caused the L-Band receiver the cycle off.

Post eclipse and return of Rosman support will be required to enable a second turn on.

NOTE: This was the last time that the L-Band repeater operated nominally

FJK, 1/23/81

APPENDIX D

L-Band Experiment Calibrations (CRC, Ottawa, Canada)

This appendix presents the calibration technique used by the Canadian Research Center in Ottawa, Canada for the EOL L-band tests. It is provided as supplementary information to the L-band test experiment.

MEASUREMENTS OF ATS-5 FOR N.A.S.A.

4 JUNE 1980

E.E. Matt

Rx CALIBRATION SYSTEM

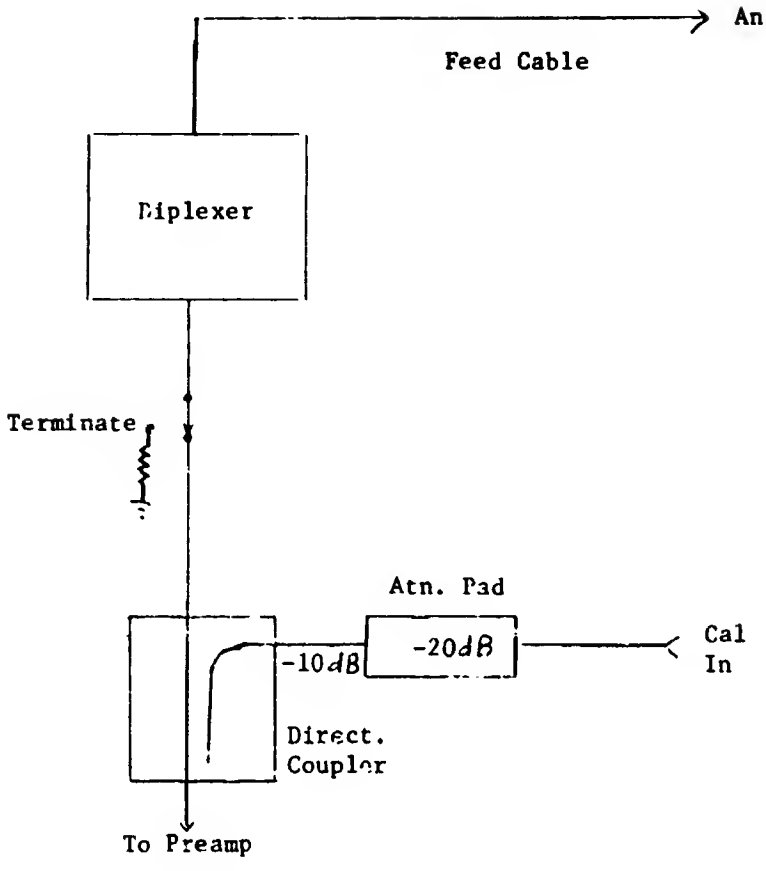

Injected +10 dBm into preamp port of coupler (1550.48 Mc).

Measured with hp 436 A power meter

Out of Cal. cable -20.05 dBm

Out of Ant. Cable +6.6 dBm

By reducing the hp 8660 C generator to -16.5 (from +10)

Measured -20.05 dBm out of antenna cable

These reading correspond with a measurement of 26.5 dB that was used as a cal factor in Mar 77

Cal Factor to input of preamp = 30 dB, to dish in 66.5 dB.

PREAMP NOISE FIGURE MEASUREMENT JUNE 1980

Avantek Model AM1600N Serial #21

Gain to Spec. Ana.		53 dB
Measured Noise Level		-116 dB/Hz
Effective Noise at Input of Amp.		-169 dB/Hz
Noise of 50Ω load at 290°K		-174 dB/Hz
∴ Amplifier N.F.	=	5 dB

Xx SYSTEM NOISE CALCULATIONS

Factor	Contribution
Sky temp - into ant.	100°
Transmission loss - feed cable + couplers - 3.4 dB	-158°
Preamp N.F. - 5 dB	640°
System Noise Temp -	898°
Effective noise at the input of preamp	-171 dB/Hz

When Terminated

50Ω load	290°
Pream N.F. - 5 dB	640°
System Noise Temp -	930°
Effective noise at the input of preamp	171.1 dB/Hz

OTTAWA STATION SPECIFICATIONS

Antenna - 28' parabolic - gain 40 dB at 1650 MHz

Note: 38.5 gain used in AEROSAT experiments included feed loss - these are now included in cal. factors.

Receive System - Calibration Factors

- Cal. gen. to input of preamp	30	dB
- Cal. gen to input of dish	66.5	dB
- Preamp N.F.	5	dB
- Feed + coupler losses	3.4	dB
- Effective noise at preamp input	-171	dBm/Hz

Transmit System - Calibration Factor

- Monitor point to output of dish	79	dB
- Maximum E.R.P.	+88	dBm

C-2

0025-0037 - Tuned to 1550.17 Rx signal (Wide-Band Data)
- Ant.Update -31minE, 2°S
- Signal level -74 dBm
- Rx,in 50 kHz IF B.W., 10Ms T.C.

0110-0218 - Tuned to 1565.82 MHz Rx signal (beacon)
- Rx in 10 kHz B.W.
- Ant Update -31minE, 2.7°S
- Signal level -70 dBm, -100 at preamp
  signal should be 171-100 = 71 dB above noise
- On hp 8568A - peak signal -48
  noise -118.2 dB/Hz
  Measured C/No = 70.2 dB/Hz

0220-0241 - Tuned to 1550.48 (GE downlink)
- Rx in 50 kHz B.W.
- Ant Position 31minE, 4.2°S
- Signal level -88 dBm, -118 at preamp

0250-0335 - Tuned to 1553.77 (C to L)
- Rx in 50 kHz B.W.
- Ant.Update 31minE, 5.6°S
- Signal level -73 dB, -103 at preamp
- C/No - measured 67, calculated 68

APPENDIX E

Sample Link Calculations

This appendix includes the following:

Table E-1 Rosman Ground Station Parameters

Table E-2 Spacecraft - Earth Station Geometry

Table E-3 Sample EIRP Calculation

Table E-4 Sample Spacecraft G/T Calculation

Table E-5 Calculation of System Noise Temperature

Table E-1

Rosman Ground Station RF Parameters

Antenna Gain (85')	
Transmit (@ 6150 MHz)	58.5 dB
Receive (@ 3950 MHz)	57.4 dB
Receive System Noise Temperature	
Preamplifier, T_P	132.9^{o} K
Antenna, T_A	73.5^{o} K
System Noise Temp ($T_P + T_A$)	206.4^{o} K
	23.1 $dB^{o}K$
Receive G/T	34.3 dB

Table E-2

Spacecraft - Earth Station Geometry

		4 June 80	20 Nov 80
S/C to Earth Sta LOS (Km)		37,000	37,700
Free Space Loss (dB)			
C-B uplink @ 6212 MHz	(dB)	199.8	199.9
C-B downlink @ 4120 MHz	(dB)	196.2	196.3
L-B downlink @ 1550 MHz	(dB)	187.9	
S/C to Earth Sta Off Beam Center			
Degrees	(0)	6	13
Ant Gain allowance			
C-Band	(dB)	0.5	2.0
L-Band	(dB)	1.0	
Polarization Loss (L/B only)	(dB)	0.2	

Table E-3

Sample S/C EIRP Calculation

From Ground Station C/N_0 measurement (Rosman, 04 June 1980)

S/C Configuration: C-Band WBDM, Planar Array Antenna, TWT 1 & 2

Ros Received C/N_0 (dB)	85.5	measured value
Ros G/T	34.3	measured value
Boltzmans Constant, K ($dBm\ Hz^{-1}\ K^{-1}$)	-198.6	
F.S. (Free Space Loss) (dB)	196.2	
S/C Antenna Off Beam (Lp) (dB)	0.5	
S/C EIRP(1)	(dBm) 49.3	calculated value

(1) $EIRP = C/N_0 - G/T + K + F.S. + Lp$

Table E-4

Sample S/C G/T Calculation

S/C Configuration: C-Band, FT Mode, Planar Array Antenna TWT 1 & 2

Ground Station Tx Power, Pg (dBm)	Ground Station Received Carrier (dB)	Correction[1] Factor, C.F. (dB)	G/T (dB)
60	0 (REF)		
43	-1	-5.2	-17.5

(1) The Correction Factor, C.F., accounts for the noise power sharing of the spacecraft transmitter output and is derived as shown in Appendix F

(2) $G/T = K + S/C\ NPBW + F.S.\ Loss - G_{ant} - P_g + L_p - C.F.$

where: K = Boltzmans Constant = $-198.6\ dBm^{o}K^{-1}\ Hz^{-1}$

$S/C\ NPBW$ = S/C noise power bandwidth = 35.5 MHz = 75.5 dB Hz

F.S. = Free Space path loss = 199.9 dB

G_{ant} = Ground Staion transmit antenna gain = 58.5 dB

P_g = Ground Station Transmitter Power Output = 43 dBm

L_p = S/C Antenna off Beam pointing loss = 0.5 dB

C.F. = Correction factor (from Appendix 1 @ 1 dB suppression) = -5.2 dB

Calculation of System Noise Tempoerature from Specification and Prelaunch Measured Values

The spacecraft system noise temperature is dependent upon several factors; primarily the earth noise temperature, noise figure of the transponder and the receive losses of the transponder. The following formula is used to calculate the spacecraft system noise temperature referred to the preamp inputs.

$$T_S = T_A + T_T + T_o (L - 1) + (F - 1) L t_o$$

where T_A is the antenna sky noise, T_T is the noise spillover from the transmitter in the receiver band, L is the losses from the antenna to the front end of the receiver, F is the noise factor of the receiver, T_o is the actua temperature of the coupling network between the antenna and the receiver and is 290^oK (reference temperature)

The spacecraft repeater specification and measured noise figures and receive antenna losses are shown in Table E-5. Based upon ATS-1 data for a similar repeater we would expect the temperature of the coupling network to be about 285^oK while 30^oK is a reasonable assumption for the degradation due to transmitter thermal noise out of band. The antenna sky noise is taken to be 290^oK when looking directly at the earth using an Earth Coverage antenna, and is assumed to be $\approx 20^o$ using the omni antenna. Using these values in the formula above yields the spacecraft system noise temperatures referred to the electronics inputs. The G/T for the Spec and prelaunch parameters is determined by dividing the measured gain by the calculated system noise temperature.

Table E-5 shows the results of the Ts calculation for the ATS-5 antennas

Table E-5

Calculation of T_s and G/T

	C-Band			L-Band	
	Planar Array		Omni		
	Spec	Prelaunch	Prelaunch	Spec	Prelaunch
T_A (^oK)	290	290	20	290	290
T_T (^oK)	30	30	30	30	30
T_L (^oK)	246	216	324	199	99
T_R (^oK)	1711	1596	1941	1255	790
T_S (^oK)	2277	2132	2315	1774	1209
(dB^oK)	33.6	33.3	33.7	32.5	30.8
G_{ant} (Net)(dB)	16.3	16.6	-2.0	12.7	14.3
G/T (dB)	-17.3min.	-16.7	-35.7	-19.8min.	-16.5

Appendix F

In-Orbit Measurement of G/T

This appendix contains a derivation of a technique for in-orbit measurement of the G/T of a hard-limiting transponder.

Pages F-2 through F-8 are the original work presented to the ATS Project as Westinghouse memo #75-163.

Pages F-9 through F-11 are an addendum to the original memo which provided a refinement to the analysis to account for the S/N transfer characteristic of a bandpass limiter.

From F. J. Kissel
WIN #75-163 (corrected #75-137 and reissued)
Date 19 December 1975
Subject In-orbit Measurement of G/T of a Hard-limiting Transponder with AGC

Ref: Memo #75-085, 21 July 1975, "ATS-6 L-band G/T and Receiver Sensitivity Performance"

To M. Geller
WESTINGHOUSE ELEC. CORP.

Background

The referenced memo contains a derivation of a technique for in-orbit measurement of the G/T of a hard-limiting transponder with AGC (Appendix 1 of referenced memo). In order to reduce the complexity of the derivation, the intervening steps between equations (2) and (3) were omitted. Interest has been subsequently expressed in this area and the entire Appendix is herein reproduced with the intervening steps, equations (2A) through (2F) included. Corrections and clarifications have also been made in equations 6 and 7 and in Figure -1. Additional numerical examples have also been added.

F. J. Kissel
WESTINGHOUSE ELECTRIC CORPORATION

Attachment

cc: R. Baldridge
J. P. Corrigan
I. Galicinao
J. Meenen
R. Moore
D. Neudecker
L. Nicholson

In-orbit Measurement of G/T of A Hard-limiting Transponder with AGC

The technique of measuring G/T is essentially one of measuring the system noise temperature. This is readily accomplished for a linear amplifier using well established techniques developed for measuring amplifier noise figure, i.e., measure amplifier output power with no input, then measure change in output with a known input. The problem becomes more complex if the amplifier has AGC, and some assumptions must be made as follows:

1. The total output power is constant for all input levels;
2. The IM products due to front end noise are negligible.*

Using the above assumptions, the spacecraft noise power input, P_n, referred to the preamp input is:

$$P_n = KTB \qquad (1)$$

where:

K = Boltzman's constant = 1.38 $(10)^{-23}$ w/°/Hz (-198.6 dBm/°/Hz)

T = Spacecraft system noise temperature (°Kelvin)

B = Spacecraft bandwidth = 40 MHz (76 dB-Hz)

The spacecraft output power, P_{out}, is proportional to the signal power input, P_s, multiplied by the antenna gain, G, plus the noise power input, P_n;

$$P_{out} = P_{s\ out} + P_{n\ out} \propto P_s\ G + P_n \qquad (2)$$

where:

P_s = Ground station EIRP (dBm) - path loss (dB)

*"Hard-limiting of Two Signals in Random Noise" IEEE Transactions on Information Theory, January 1963.

For large P_sG (on the order of -70 dBm), P_n becomes negligible, and the total output power may be considered to be due to the signal input, P_sG. The signal power output, $P_{s\ out}$, may be observed and measured on a spectrum analyzer or a narrowband tuned voltmeter. As P_s is decreased, a decrease in $P_{s\ out}$ will occur, and $P_{n\ out}$ must then increase in order to maintain a constant P_{out}.

From equation (2):

at high power: $P'_{out} = P'_{s\ out} = C'P'_sG$ (2A)

and at low power: $P'_{out} = P_{s\ out} + P_{n\ out} = C(P_sG + P_n)$ (2B)

where C is a constant of proportionality and (') is used to indicate the high power condition.

From the above, since $P_{out} = P'_{out}$, we have:

$$P'_{s\ out} = P_{s\ out} + P_{n\ out} \quad (2C)$$

$$C'P'_sG = C(P_sG + P_n)$$

from which:

$$P'_sG = \frac{C}{C'}(P_sG + P_n) \quad (2D)$$

From equation (2C):

$$P_{n\ out} = P'_{s\ out} - P_{s\ out} \quad (2E)$$

Also, from (2B) and (2A):

$$P_{n\ out} = CP_n \quad \text{and} \quad P'_{s\ out} = C'P'_sG$$

which substituted into (2D) gives:

$$P'_sG = \frac{P_{n\ out}}{P_n}\ \frac{P'_sG}{P'_{s\ out}}\ (P_sG + P_n)$$

Substituting for $P_{n\ out}$ from (2E) gives:

$$P'_sG = \frac{(P'_{s\ out} - P_{s\ out})\ P'_sG}{P_n\ P'_{s\ out}} \quad (P_sG + P_n)$$

dividing through by P'_sG gives:

$$1 = \left(\frac{P'_{s\ out} - P_{s\ out}}{P'_{s\ out}}\right) \left(\frac{P_sG + P_n}{P_n}\right)$$

or

$$1 = (1 - P_{sr}) \left(\frac{P'_sG + P_n}{P_n}\right) \tag{2F}$$

where $P_{sr} = \frac{P'_{s\ out}}{P_{s\ out}}$

Expanding (2F) yields:

$$P_n = P_n - P_{sr}\ P_sG + P_sG - P_{sr}\ P_n$$

From which

$$P_{sr}\ P_n = (1 - P_{sr})\ (P_sG)$$

or

$$P_n = \frac{1 - P_{sr}}{P_{sr}}\ P_sG \tag{3}$$

For the special case where $P_{rs} = 0.5$ (3 dB drop), $P_{n\ out}$ is equal to $P_{s\ out}$, and P_n is equal to P_sG as follows. Equation (3) evaluated for $P_{rs} = 0.5$ becomes:

$$P_n = \frac{1 - 0.5}{0.5}\ P_sG = P_sG$$

or

$$P_n \Big|_{P_{rs} = -3\ dB} = P_sG \tag{4}$$

Substituting for P_n in equation (1) gives:

$$P_sG = KTB \text{ or } \frac{G}{T} = \frac{KB}{P_s}$$

Assuming 40 MHz spacecraft BW:

$$G/T\ (dB) = -198.6 + 76 - P_s = -122.6 - P_s \qquad (5)$$

where:

P_s = Ground station EIRP (dBm) - path loss (dB)

The more general case of equation (5) becomes:

$$G/T\ (dB) = -122.6\ dB - 10 \log \left(\frac{1 - P_{sr}}{P_{sr}}\right) - P_s\ (dB) \qquad (6)$$

Calculation of equation (6) is simplified by use of the nomogram shown in Figure A-1 (attached) which solves for the correction factor, C.F.;

$$C.F. = 10 \log \left(\frac{1 - P_{sr}}{P_{sr}}\right) \qquad (7)$$

EXAMPLE

For synchronous altitude (spacecraft subsatellite point at 94° west longitude), Rosman L-band transmitter:

$$P_s = P_{gnd}\ (dBm) + G_{gnd}\ (dB) - L\ (dB) \qquad (8)$$

where:

P_{gnd} = Rosman T_x power (dBm)

G_{gnd} = Rosman antenna gain = 33.4 dB

L = Path loss at 1650 MHz = 188.2 dB

Thus:

$$P_s = P_{gnd}\ (dBm) - 154.8\ dB$$

Substituting (7) and (8) into (6) gives the expression for the ATS-6 spacecraft G/T as a function of Rosman transmitter power:

$$G/T\ (dB) = -122.6 - C.F. - P_{gnd}\ (dBm) + 154.8$$

$$G/T\ (dB) = 32.2 - C.F. - P_{gnd}\ (dBm) \qquad (9)$$

Similarly, for the Madrid Hybrid station (spacecraft at 35° east longitude) we have:

HYB L-band T_x

$$G/T\ (dB) = 32.6 - C.F. - P_{gnd}\ (dBm)$$

HYB S-band T_x

$$G/T\ (dB) = 36.5 - C.F. - P_{gnd}\ (dBm)$$

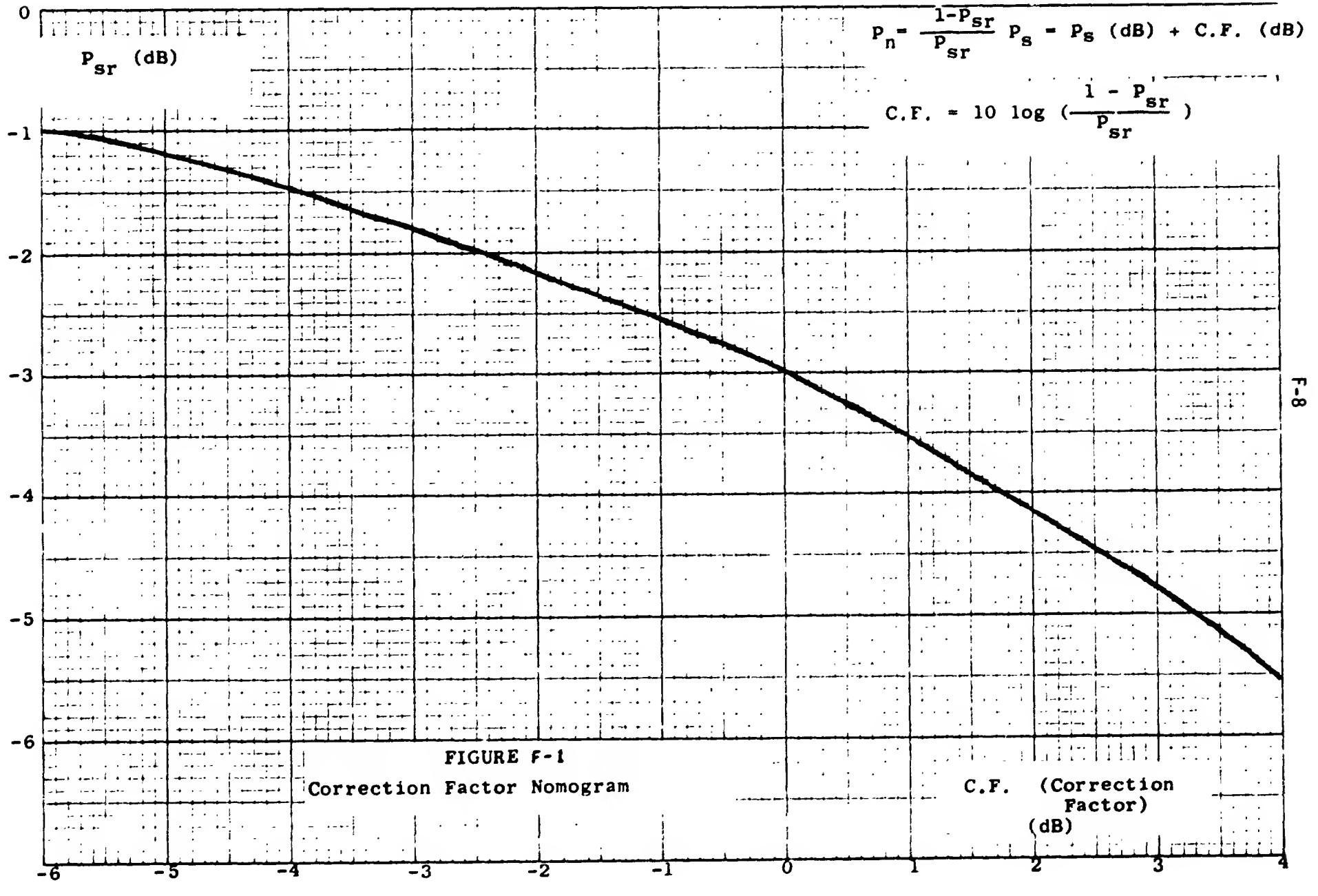

FIGURE F-1
Correction Factor Nomogram

Addendum to Westinghouse memo #75-163

(In-Orbit Measurement of G/T of a Hard-Limiting Transponder with AGC)

Background

The subject memo (W #75-163) assumed:

A basic assumption in the derivation presented in the subject memo was that the signal-to-noise ratio was unchanged through the spacecraft limiter (essentially performing as a linear device with regard to S/N). Figure 1 shows that the S/N transfer characteristic of a hard limiter is not linear [1]. This effect has been used to modify the Correction Factor curve presented as Figure A-1 in the subject memo. The revised curve is presented herein (Figure 2).

[1] Davenport, Jr. Applied Physics, June 1953

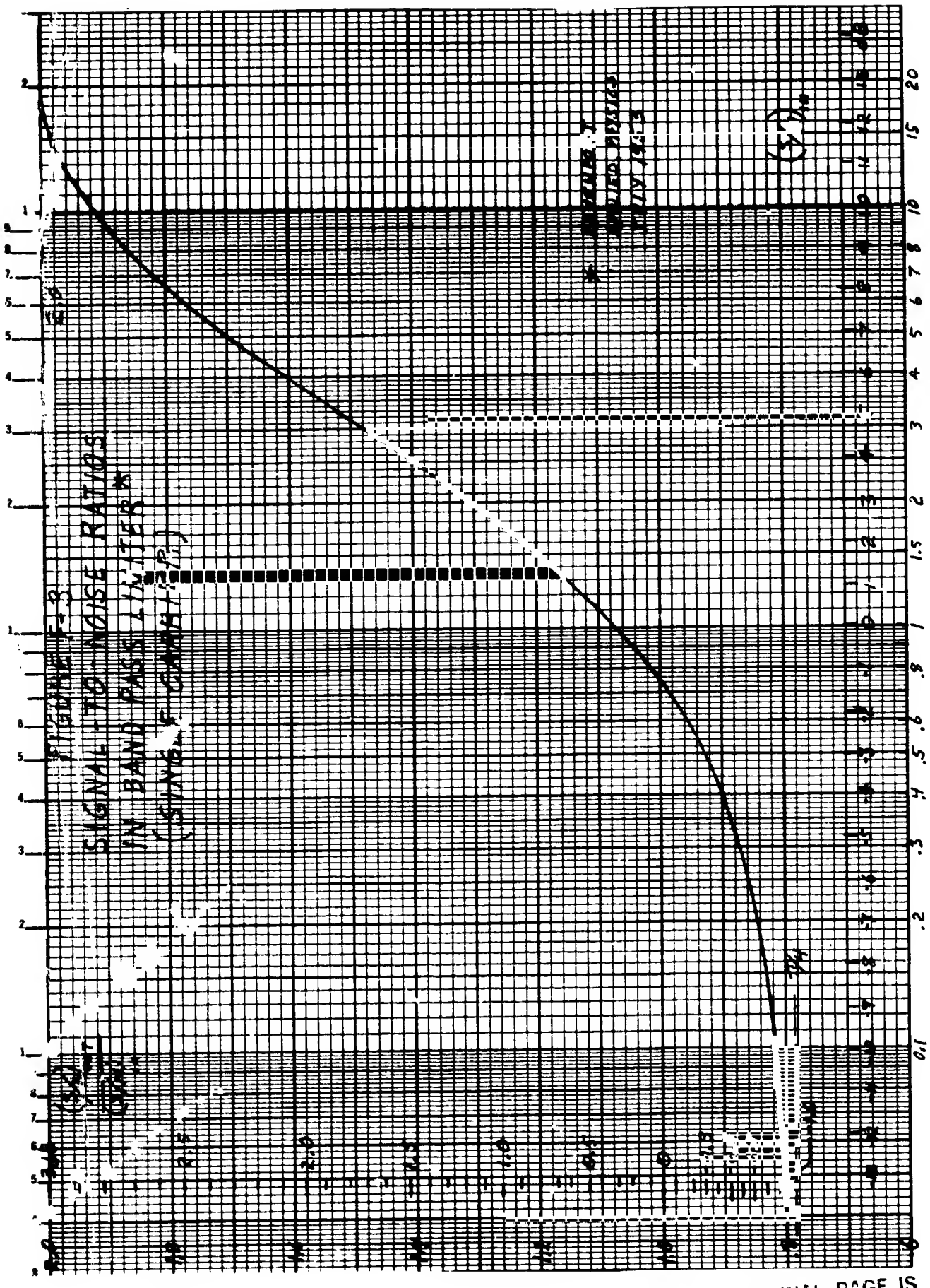

F-10

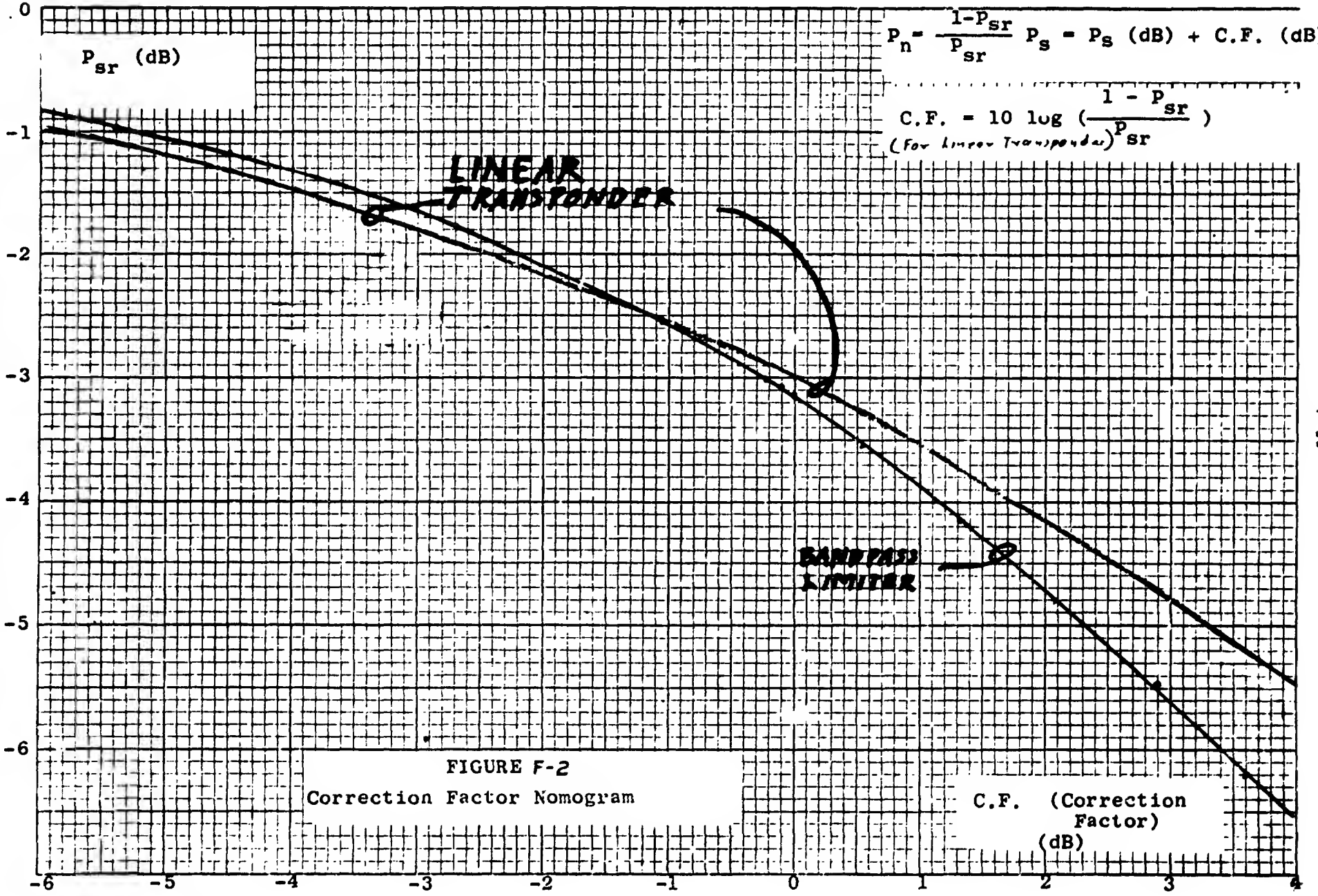

FIGURE F-2

Correction Factor Nomogram

APPENDIX G

Post Launch Tests

This appendix consists of a Westinghouse field report in which many of the first ATS-5 performance tests were performed. Much of the included data was used for in-orbit comparisons with the EOL tests.

FORM BA 5451

FIELD ENGINEERING TRIP REPORT

DATE 11-17-69

REPORT NO

WESTINGHOUSE ELECTRIC CORPORATION — BALTIMORE DEFENSE CENTER — FIELD ENGINEERING & SERVICE

AGENCY VISITED: NASA Mojave Stadan Site	This form may only be used to report the results of a field visit not normally covered in Field Reports (Form BA 5414) and for in-plant meetings involving non-Westinghouse personnel.	JOB NO:	
LOCATION: Barstow, California		ARRIVAL DATE: 10-20-69	DEPARTURE DATE: 10-24-69
TYPE OF TRIP: ATS-5 Tests		DISTRIBUTION LIST NO:	DISTRIBUTION LIST ATTACHED

PURPOSE OF TRIP: To perform L-band propagation and antenna pattern tests.

PERSONS PRESENT: F. J. Kissel, D. R. Rau, W. H. Asplund, T. Stores

SUMMARY

The primary purpose of the trip was to perform L-band propagation tests using the ATS-5 spacecraft. In addition to the propagation tests, the S/C transmit and receive antenna patterns were to be measured as well as other S/C parameters such as VCO offset frequency and drift rate.

The primary objectives of the trip were accomplished: Propagation data was obtained for the up and down links, and S/C transmit and receive antenna patterns were measured. The latter was measured in the L-C cross-strap (SSB/FM) mode using the omni-directional C-band antenna. At this time it was discovered that RF leakage from the C-band planar array antenna was interacting with the omni radiation pattern to cause signal enhancement and cancellation. The effect was a function of S/C orientation such that the signal cancellation caused the FM receiver to operate below threshold during a 2 to 3 millisecond time interval. Measurements were also made of S/C VCO offset and drift rate.

Trarsmit Antenna Pattern

The L-band transmit antenna pattern was measured with the S/C in the wideband data mode (WBDM). The S/C VCO was unmodulated, the S/C transmitter was internally saturated to provide maximum drive to the TWT amplifier (two TWT's were used). The received L-band signal was down converted to 70 MHz and passed through a 500 KHz IF filter (709 KHz noise BW). The signal was then amplified in Jerrold model LA-5100 log amplifier and AM detected. The detected output was displayed on a Honeywell 1508 Visicorder(see figure 1 for a block diagram of the test setup).

Calibration of the received signal strength was performed by injecting an L-band signal of known power level into the parametric amplifier. The calibration signal was varied in known increments to provide calibrated steps on the strip chart. A low pass filter was used at the input to the recorder to remove the effects of thermal noise which was present in the L-band oscillator output.

Table 1 presents pertinent data obtained from the transmit antenna pattern, and figure 2 shows a polar plot of the pattern.

Receive Antenna Pattern

The L-band receive antenna pattern was measured with the test set up shown in figure 3. The system was configured for L-C (SSB/FM) cross-strap operation using the C-band omni-directional antenna on the downlink. The uplink SSB signal was generated using a 70.550 MHz IF signal derived from an HP 5100 synthesizer. This resulted in a 550 KHz modulation on the C-band downlink which was AM detected using the Jerrold Log Amplifier and detector. The detector output was displayed on the Honeywell visicorder. The first efforts to record the receive antenna pattern appeared to be unsuccessful. This was because the recorder pattern showed a "dip" in the main lobe which moved very slowly across the pattern. Subsequent investigation showed that the "dip" was caused by the FM receiver operating below threshold because of distructive interference in the downlink between the C-band omni antenna and leakage from the C-band plannar array antenna. By careful selection of a time of measurement, it was possible to obtain a receive antenna pattern which was free of the "dip". The measured receive antenna pattern is shown in figure 4. Table 2 presents an analysis of the pattern.

SSB/FM Modulator Sensitivity

The sensitivity of the SSB/FM modulator was measured by determining the SSB transmitter power output which was required to cause an FM deviation of 2.64 radian peak on the downlink (this point was determined by observing the downlink IF on a spectrum analyzer and noting when the first and second sidebands were equal. Subsequent tests have been performed which utilize a narrow band (20 KHz) tuned receiver to determine the point of first and second carrier null (2.40 and 5.52 rad peak mod index, respectively). The results of these tests indicate S/C sensitivity to be between -111.5 dbm to -114.5 dbm (as compared with the specification of -113.0 dbm $\pm$2.5). Further testing and analysis will be performed in this area which will also take into account the change in off beam center allowance due to S/C orientation.

Transponder Saturation

The saturation point of the S/C transponder was determined for the narrow band FT mode of operation. The uplink (unmodulated) power level was varied by changing the transmitter power output from 32 dbm to 60 dbm and recording the received downlink power. The saturation point is defined as that S/C input power level which when increased by two db, results in a one db increase in S/C power output (also referred to as the 1 db compression point). Figure 5 shows a curve of the S/C transponder input/output response characteristics. The 1 db compression point was determined to be -100.9 dbm.

S/C Oscillator Drift and Frequency Offset

The drift rate of the S/C oscillator was determined by monitoring the downlink IF frequency while the S/C was operated in the WB DM. In this mode, any frequency drift or offset is due to the WB VCO and the S/C master oscillator. Since the stability of the master oscillator is considerably greater than the VCO, its effect may be neglected (subsequent measurement of master oscillator frequency offset and drift has validated this assumption). The VCO offset as a function of time after S/C driver turn on is shown in figure 6. The offset after 3 hours warm-up was -140 KHz.

Downlink Carrier-to-Noise Ratio

The downlink carrier was measured at several receiver gain settings, resulting in measurements of 12.9 to 17.4 db with the higher CNR corresponding to the higher RCVR gain setting. The cause of this effect is under investigation.

Table 1

ATS-5 L-BAND TRANSMITT ANTENNA PATTERN
(WIDE BAND DATA MODE, S/C TO EARTH STATION LINK)

		Earth Station Received Signal Strength*	Antenna Pattern Beam Width	Time Earth Station is Illuminated**
Main Beam	Max	-98.2 dbm	-	-
	-1db	-99.2 dbm	10°	21.9 ms
	-3 db	-101.2 dbm	24°	52.5 ms
	-6 db	-104.2 dbm	36°	78.7 ms
	-10 db	-108.2 dbm	48°	105.0 ms
1 st Side Lobes (Max)				
	-15.3 db	-113.5 dbm	-	-

(side lobes occure $\pm 55^{\circ}$ from peak of main beam)

* Power at input to Earth Station Preamp (Earth Station Antenna Gain = 35.7 db)

S/C Transmitter Power = 24 Watts (Two TWT's)

** Based on a S/C spin period of 787.6 ms (76.2 rpm)

Table 2

ATS-5 L-BAND RECEIVE ANTENNA PATTERN
(L to C CROSSTRAP MODE, C BAND OMNI ANTENNA)

		Antenna Pattern Beam Width	Time Earth Station is Illuminated*
Main Beam	-1 db	10°	21.9 ms
	-3 db	23°	50.4 ms
	-6 db	35°	76.6 ms
	-10 db	48°	105.0 ms

1 st Side Lobes (Max)

-13.7 db and -15 db

(side lobes occur at +57°and -48° from main beam peak)

*Based on a S/C spin period of 787.6 ms (76.2 rpm)

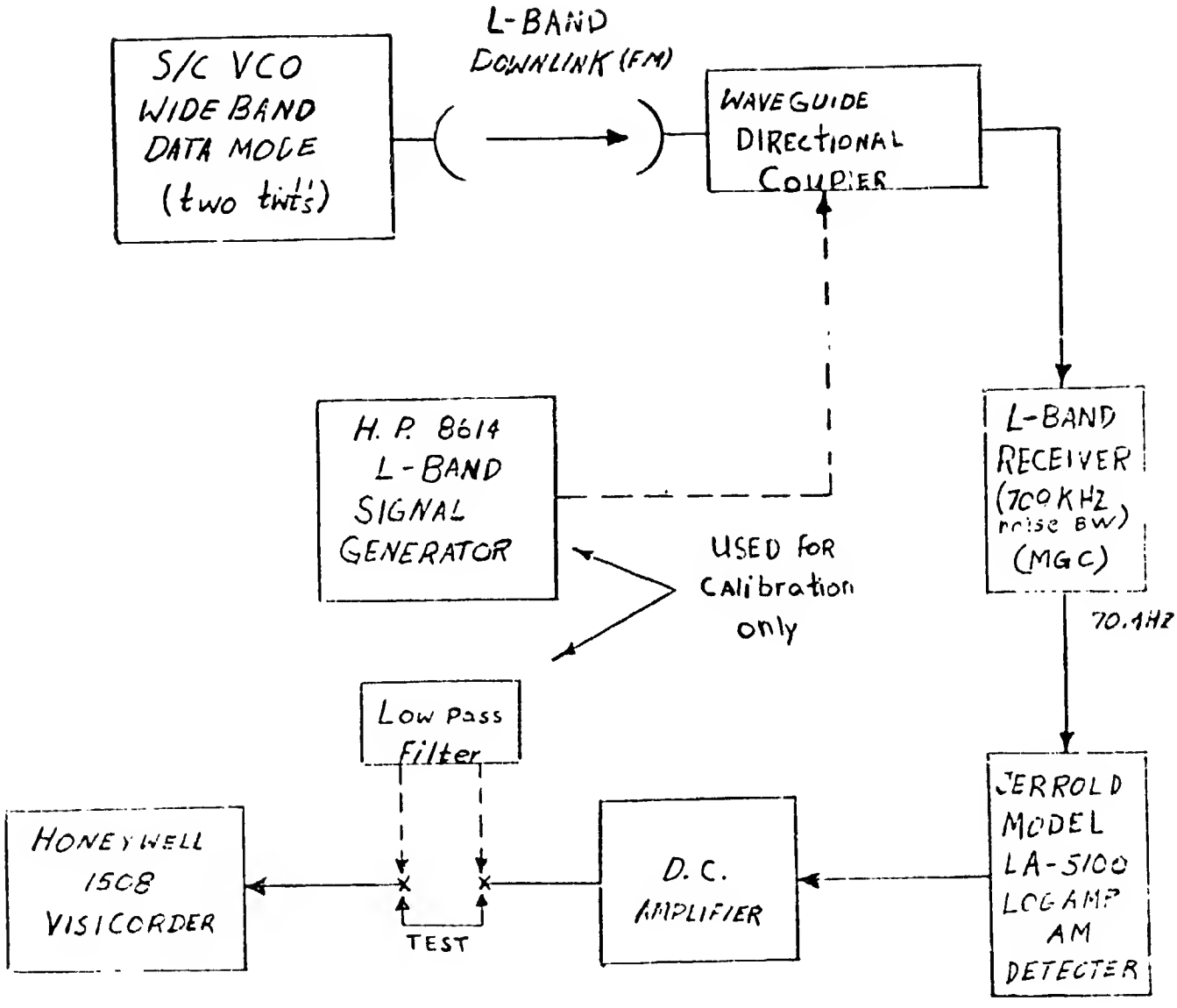

FIGURE 1 BLOCK DIAGRAM

S/C L-Band Transmit Antenna Pattern Test Setup

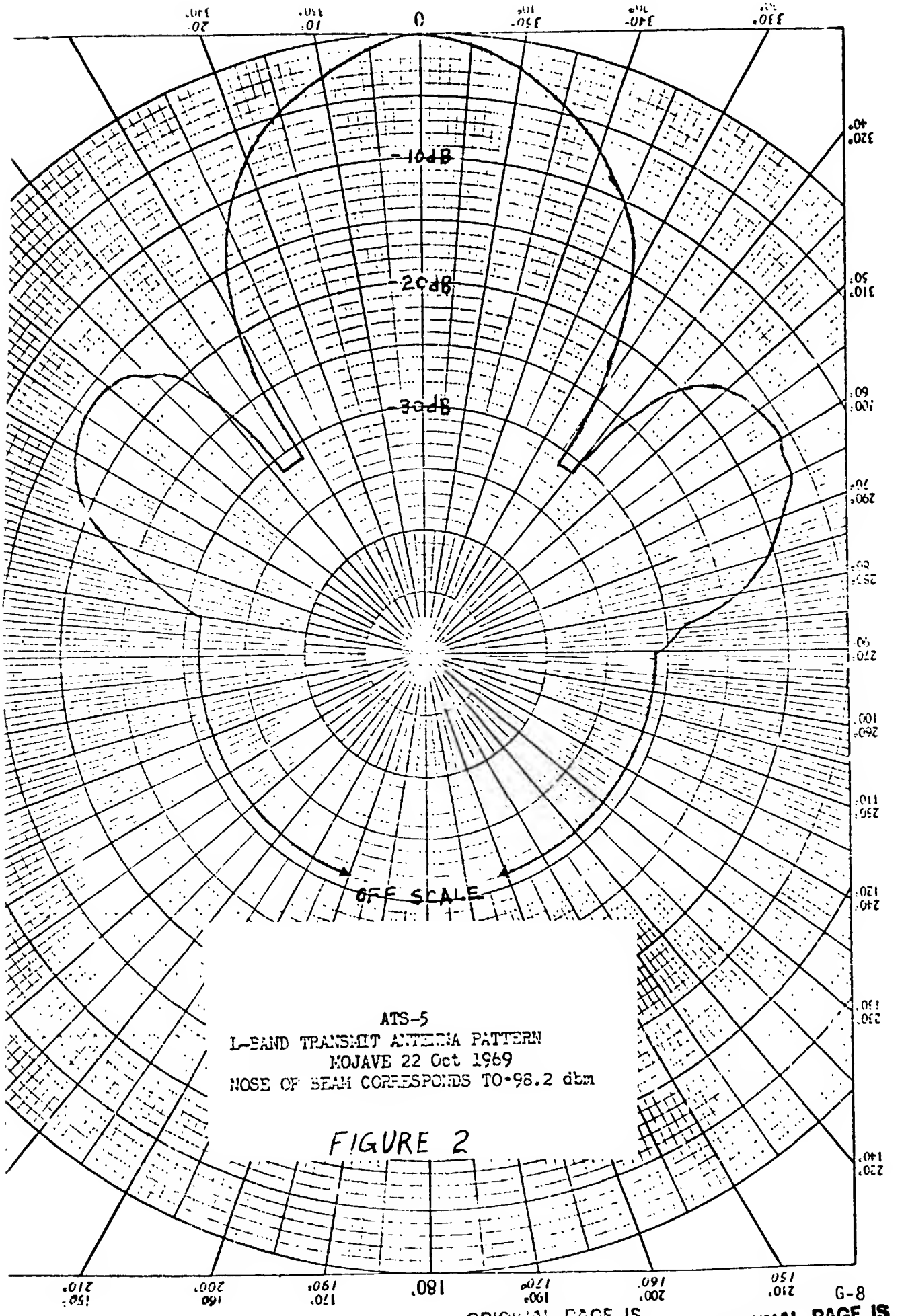

ATS-5
L-BAND TRANSMIT ANTENNA PATTERN
MOJAVE 22 Oct 1969
NOSE OF BEAM CORRESPONDS TO -98.2 dbm

FIGURE 2

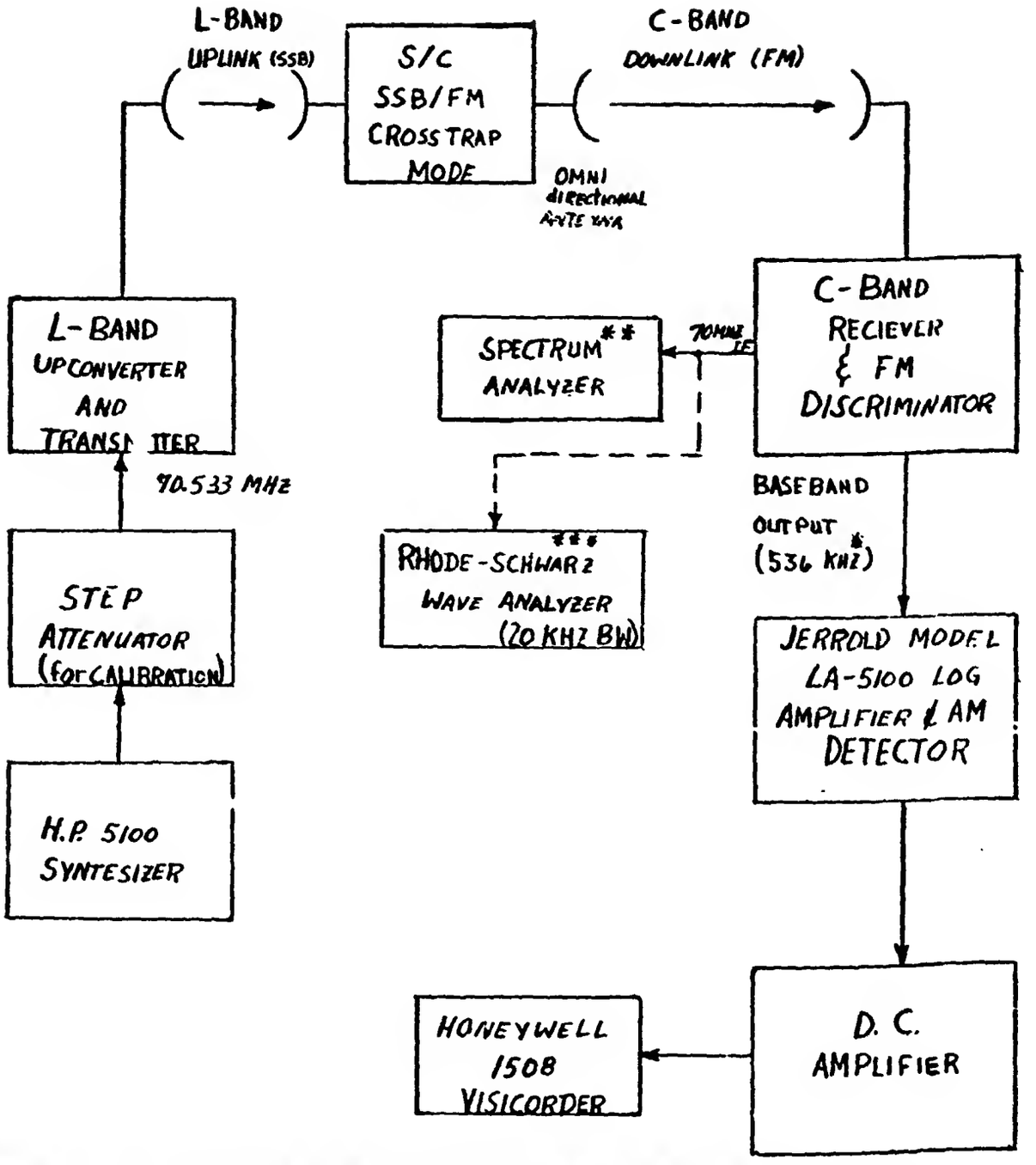

* Note: 3 KHz shift in baseband frequency is due to frequency offset in S/C master oscillator.

** The spectrum analyzer is used to calibrate the uplink power (when first and second sidebands are equal, the mod index is 2.64 rad peak)

*** Subsequent tests used the wave analyzer to determine carrier null as a method of calibration of uplink S/C received power (first carrier null occurs at a mod index of 2.40 rad peak).

FIGURE 3 BLOCK DIAGRAM

S/C L-Band Receive Antenna Pattern Test Setup

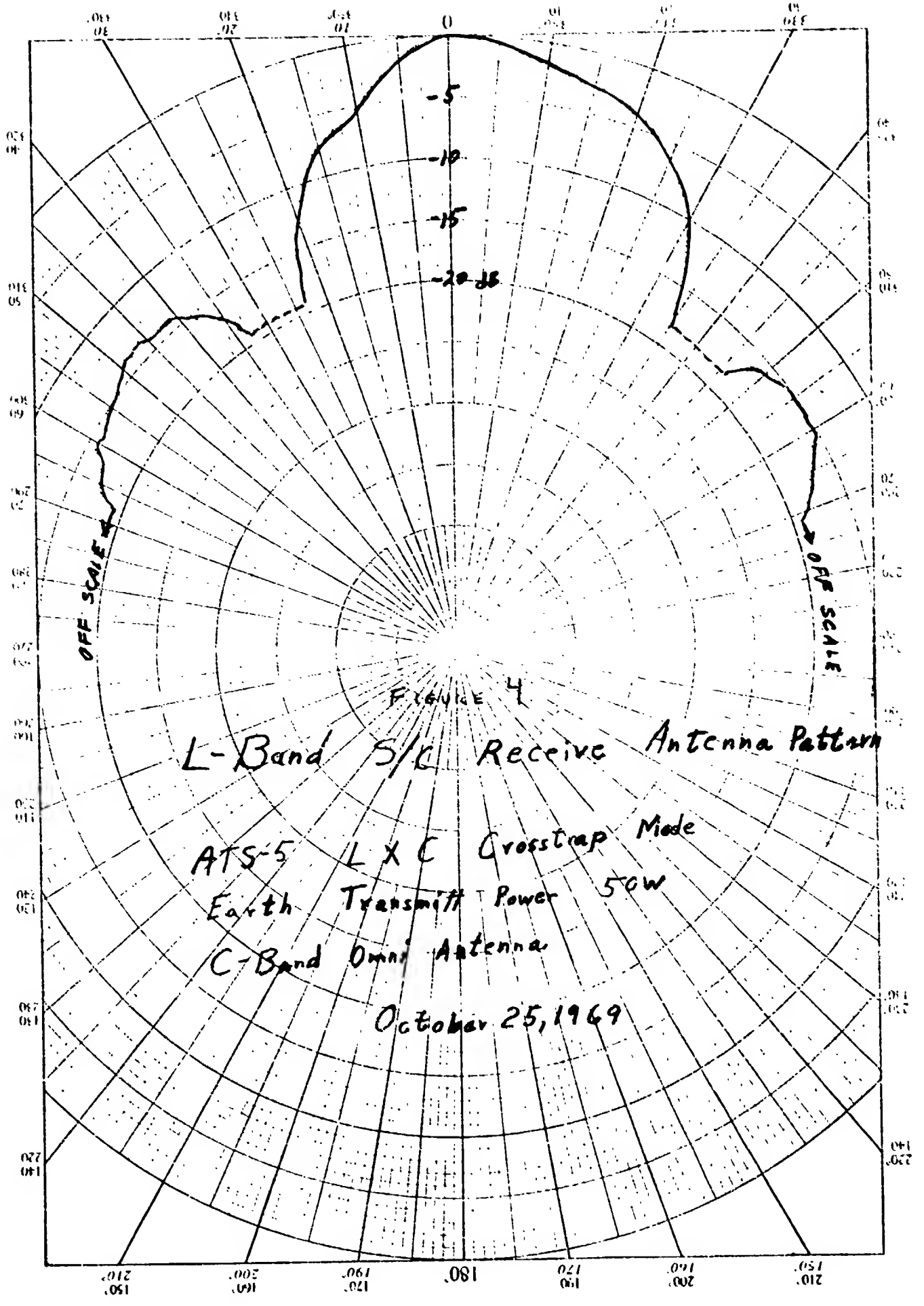

FIGURE 4

L-Band S/C Receive Antenna Pattern

ATS-5 L X C Crosstrap Mode

Earth Transmit Power 50W

C-Band Omni Antenna

October 25, 1969

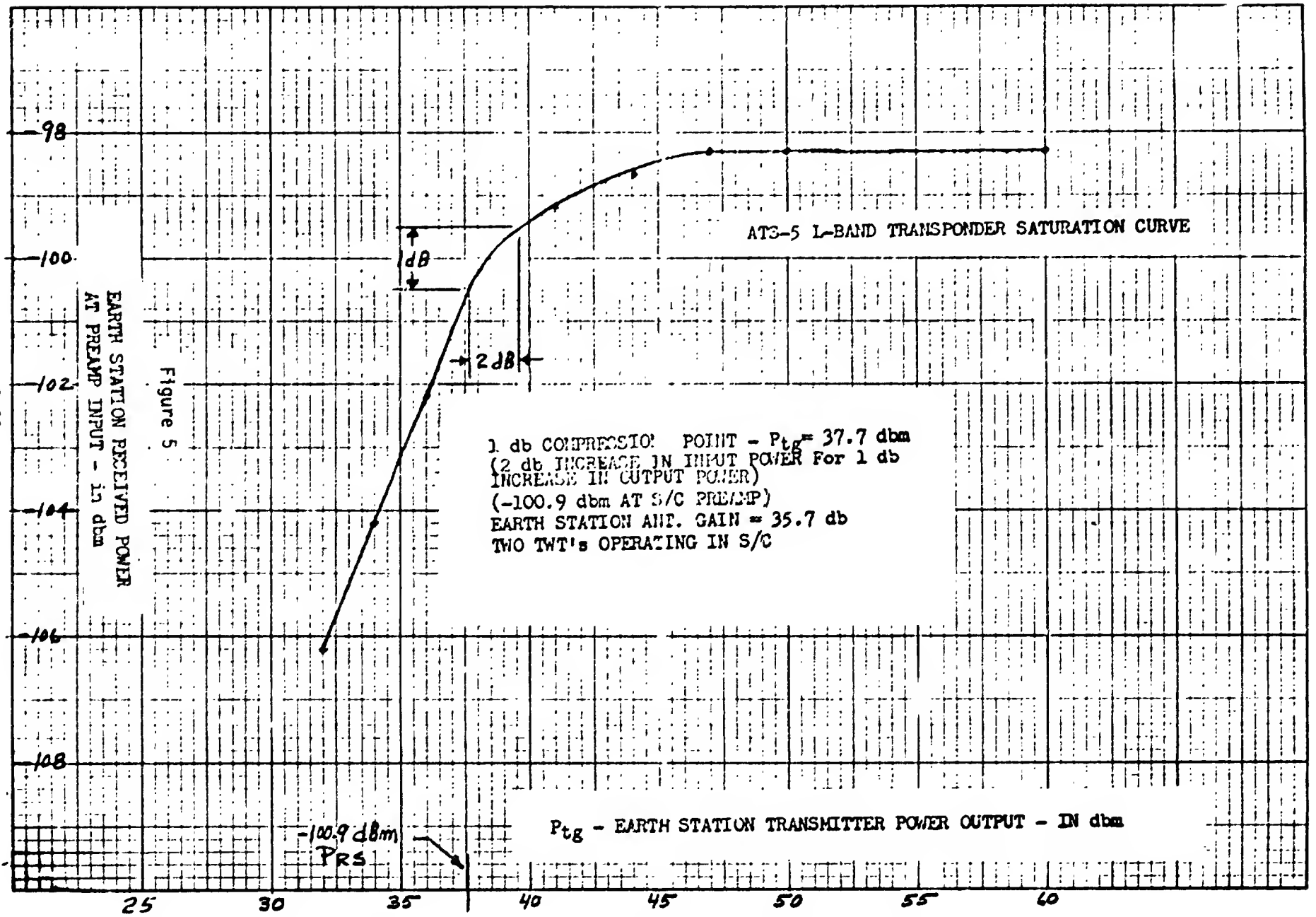
AT3-5 L-BAND TRANSPONDER SATURATION CURVE
1 dB
2 dB
1 db COMPRESSION POINT - Ptg = 37.7 dbm
(2 db INCREASE IN INPUT POWER For 1 db
INCREASE IN OUTPUT POWER)
(-100.9 dbm AT S/C PREAMP)
EARTH STATION ANT. GAIN = 35.7 db
TWO TWT's OPERATING IN S/C
-100.9 dBm
PRS
Ptg - EARTH STATION TRANSMITTER POWER OUTPUT - IN dbm
EARTH STATION RECEIVED POWER AT PREAMP INPUT - in dbm
-98
-100
-102
-104
-106
-108
25
30
35
40
45
50
55
60

Figure 5

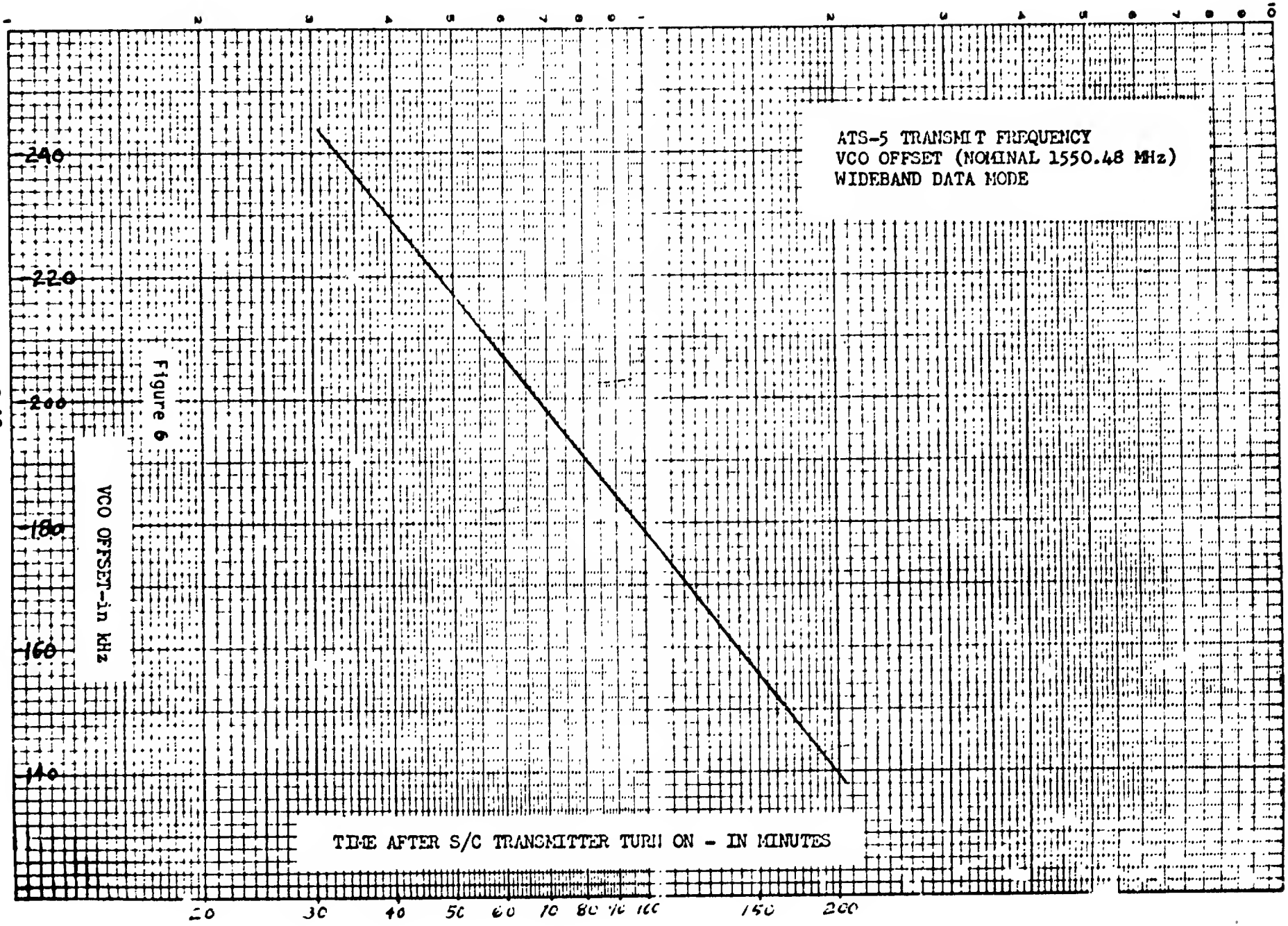
ATS-5 TRANSMIT FREQUENCY
VCO OFFSET (NOMINAL 1550.48 MHz)
WIDEBAND DATA MODE
VCO OFFSET-in kHz
240
220
200
180
160
140
TIME AFTER S/C TRANSMITTER TURN ON - IN MINUTES
20
30
40
50
60
70
80
90
100
150
200

Figure 6

APPENDIX H

SOLAR ARRAY BUS CURRENT

This appendix presents dwell telemetry data of the solar array current (Solar Array Bus 1 and 2). The telemetry data was recorded on a stripchart, portions of which are shown in Figures H-1 through H-4.

Figures H-1 and H-2 show the solar bus current as the spacecraft leaves the Umbra portion of the earth's shadow. Figures H-3 and H-4 show the solar bus current during a noneclipse time. The spacecraft power load is constant except as noted. The Ordinate (Bus Current) on Figures H-1 through H-4 is approximate and is not corrected for sensor nonlinearity.

The chart speed is 1 cm/sec except as indicated; the S/C PCM sync pulses occur in all figures at a repetition rate of 2.97 seconds, the S/C spin period is 0.765 sec (3.9 rotations between sync pulses).

The two solar-cell arrays are mounted on the outer cylindrical shell at either end of the spacecraft as shown in Figure H-5. The forward array (Solar Bus No. 1) is composd of 44 parallel connected subgroups of silicon solar cells. Each subgroup is composed of there parallel strings of 80 cells in series divided into two sections, one of 54 cells extending the full length of the array and the other of 26 cells sharing the length with the adjacent subgroup. The remaining space is used for the parallel high conductance silicon diodes which connect the subgroups to the unregulated bus. The aft array (Solar Bus No. 2) is similar except that it consists of 46 parallel subgroups.

Examination of Figures H-1 and H-3 (Solar Bus Current No. 2) clearly shows the effect of damage to the aft solar array (caused by

collision with the apogee motor during apogee motor jettison). The damaged solar cells causes the output of the aft array to fluctuate at the S/C spin period.

The fluctuation in the forward solar array output current (Solar Bus No. 1) is due to the asymetrical positioning of the solar cells around the spacecraft (the area reserved for the Libration dampers causes a variation in the available output current which occurs twice each spin period).

Solar Bus Current (S.B.#2)
(amp)

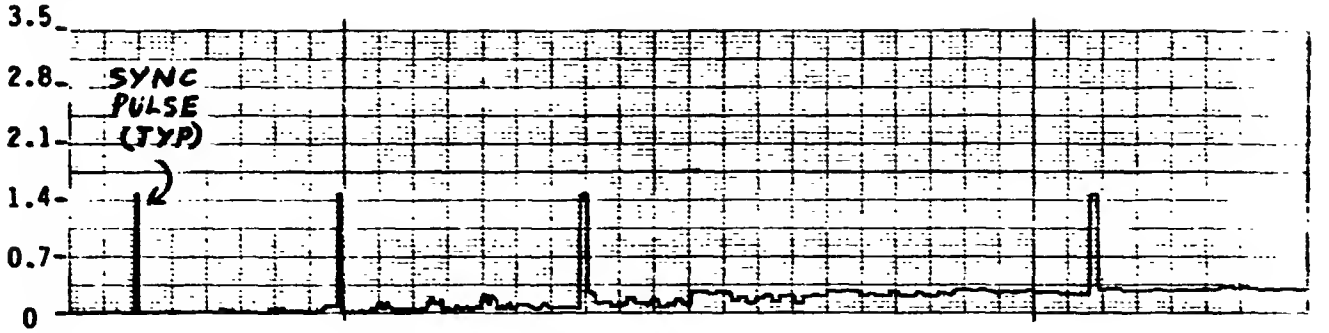

Figure 1A Remarks: S/C moving from Umbra to punumbra; note change in

Day/Time 071 / 0519:52 (Z) chart speed (from 1 cm/sec to 2.5 cm/sec)

Solar Bus Current
(amp)

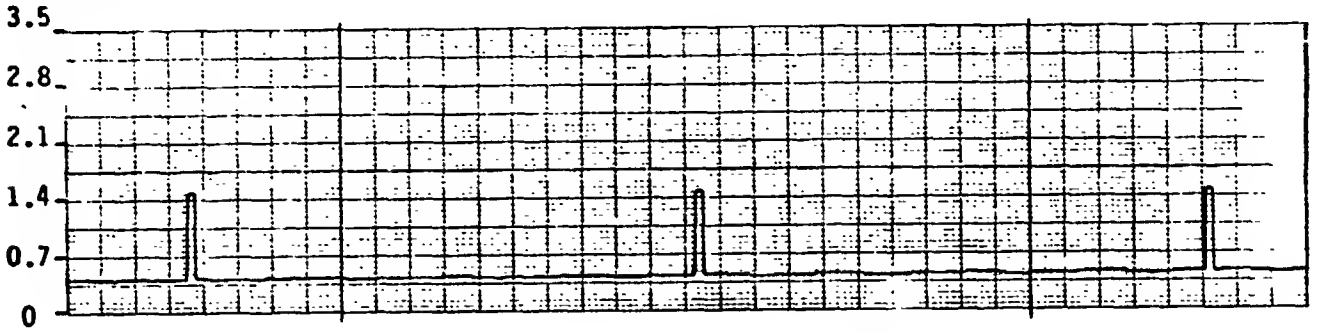

Figure 1B Remarks: Very little ripple (24 sec after Umbra exit)

Day/Time 071/0520:16(Z)

Solar Bus Current
(amp)

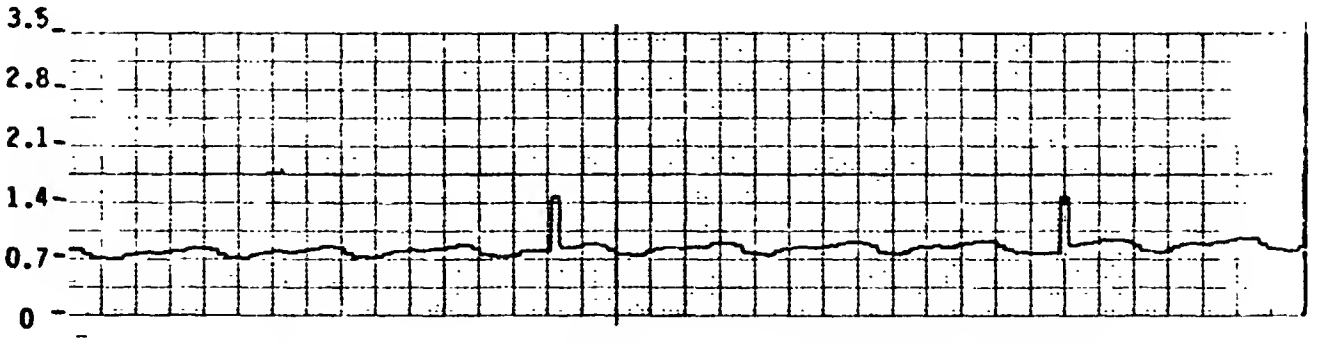

Figure 1C Remarks: Onset of ripple at S/C spin period (54 seconds after

Day/Time 071/0520:46(Z) umbra exit)

FIGURE H-1 Post Eclipse Solar Bus 2 Current

Solar Bus Current (S.B.#2)
(amp)

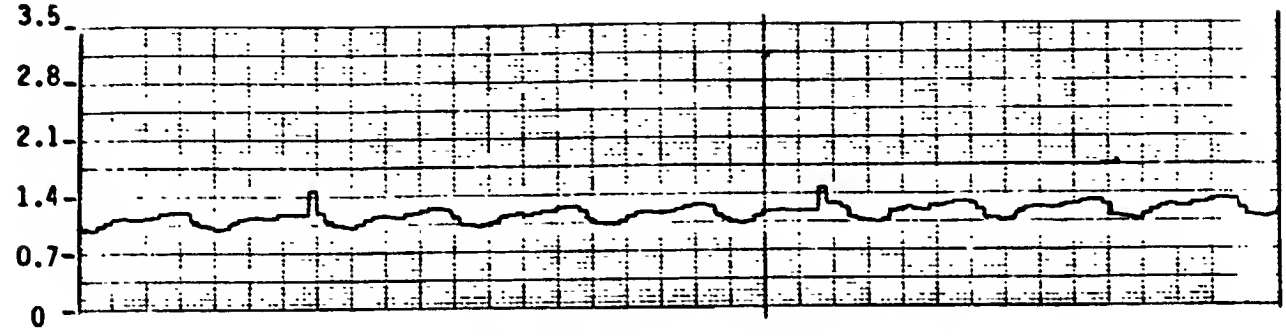

Figure 1D Remarks: S/C spin modulation is becomming more pronounced

Day/Time 071/0521:06(Z)

Solar Bus Current
(amp)

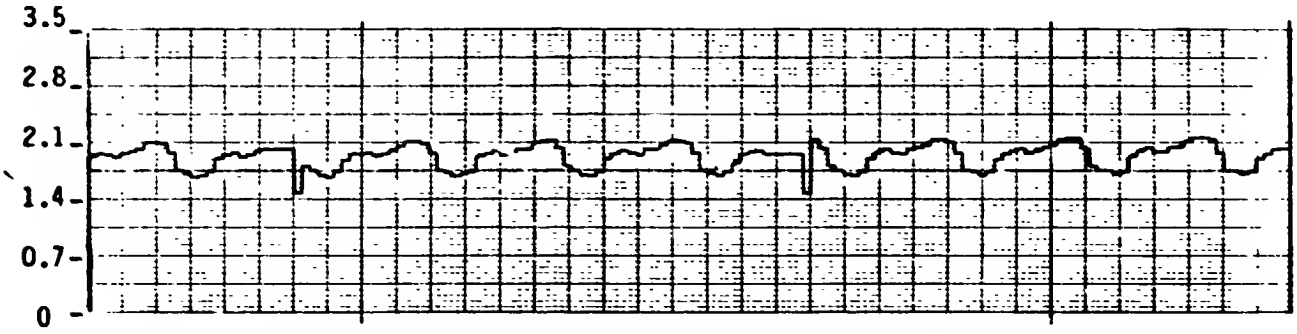

Figure 1E Remarks: Near Max Solar Bus Output; note that sync pulses

Day/Time 071/0521:56(Z) are inverted

Solar Bus Current
(amp)

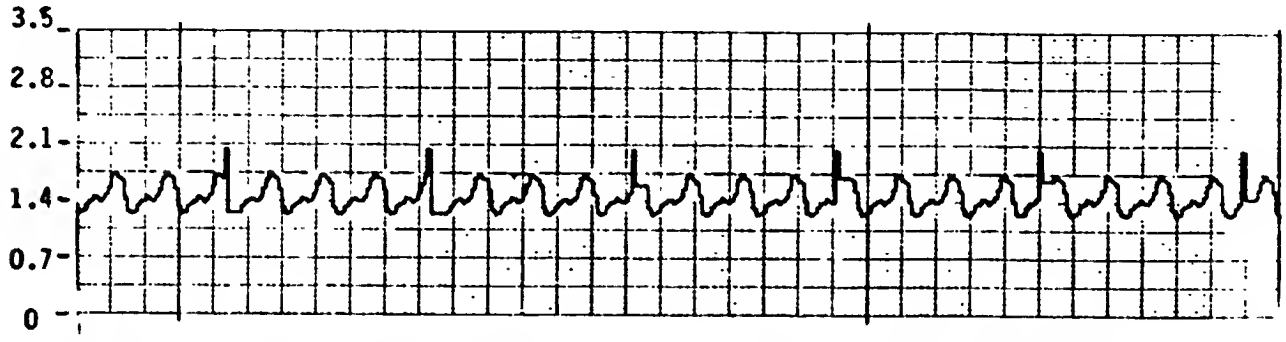

Figure 1F Remarks: Note decrease in S.B. Current (S/C loads were held

Day/Time / : (Z) constant; also note change in chart speed from 2.5 cm/sec to 1 cm/sec

FIGURE H-1 Post Eclipse Solar Bus 2 Current (continued)

Solar Bus Current (S.B.#1)
(amp)

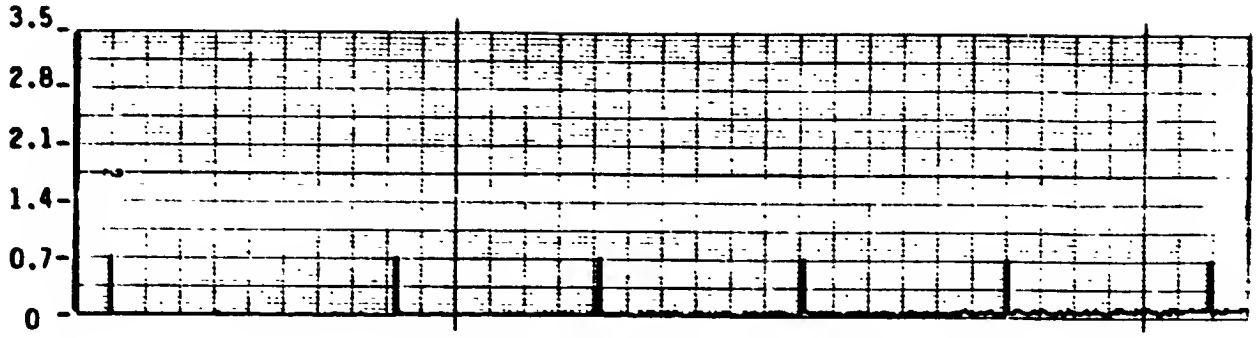

Figure 2A Remarks: S/C Moving from Umbra to Punumbra, Solar Bus 1 & 2

Day/Time 086/0459:09(Z) Paralleled (Note change in chart speed to 1 cm/sec)

Solar Bus Current
(amp)

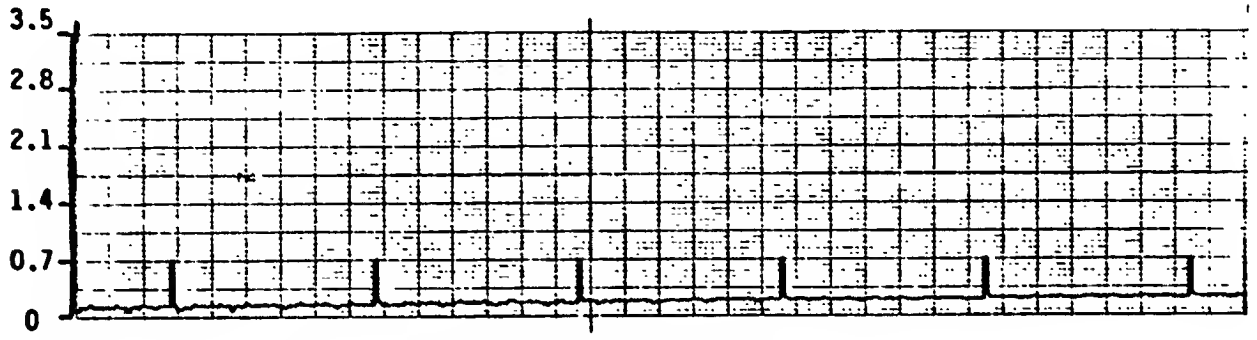

Figure 2B Remarks: Continuation of Figure 2A

Day/Time 086/0459:30(Z)

Solar Bus Current
(amp)

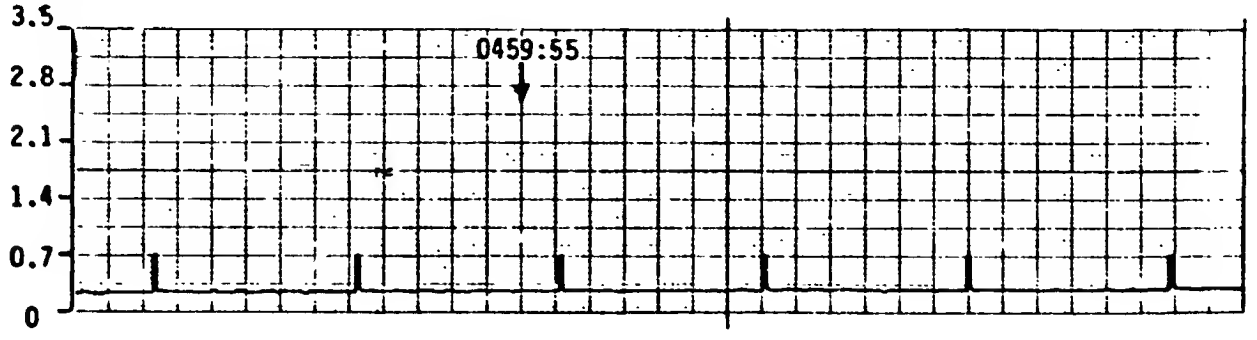

Figure 2C Remarks: Continuation of Figure 2B, S.B. 1 & 2 unparalled

Day/Time 086/0459:48(Z) at 045955

Figure H-2 Post Eclipse Solar Bus 1 Current

Solar Bus Current (S.B.#1)
(amp)

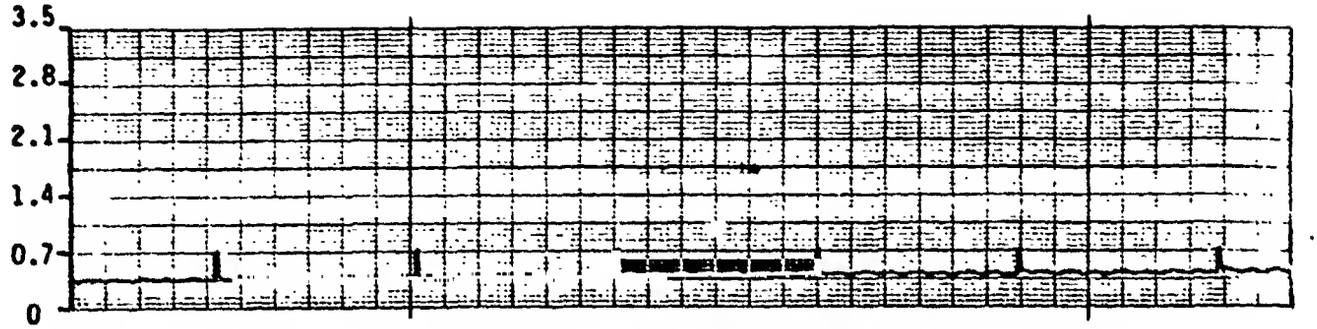

Figure 2D Remarks: Spin modulation is decernable (at twice the S/C

Day/Time 086 /0500 :23(Z) spin rate)

Solar Bus Current
(amp)

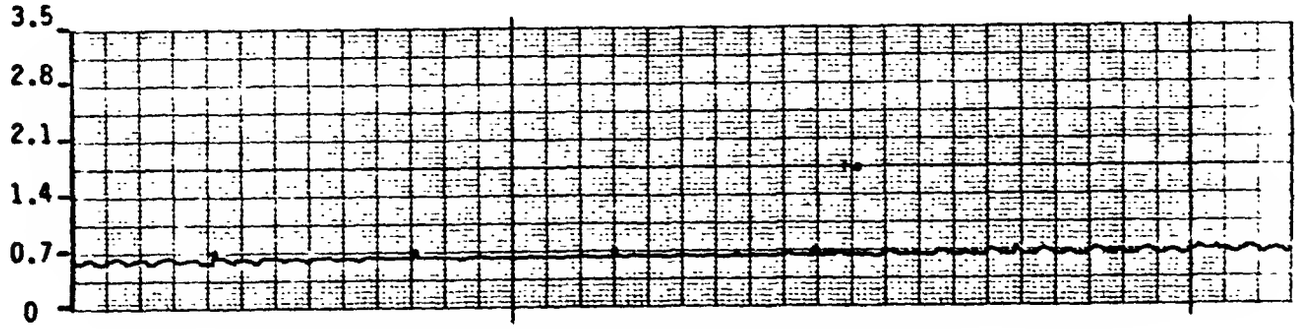

Figure 2E Remarks: Spin modulation decreases then returns

Day/Time 086 / 0500:51(Z)

Solar Bus Current
(amp)

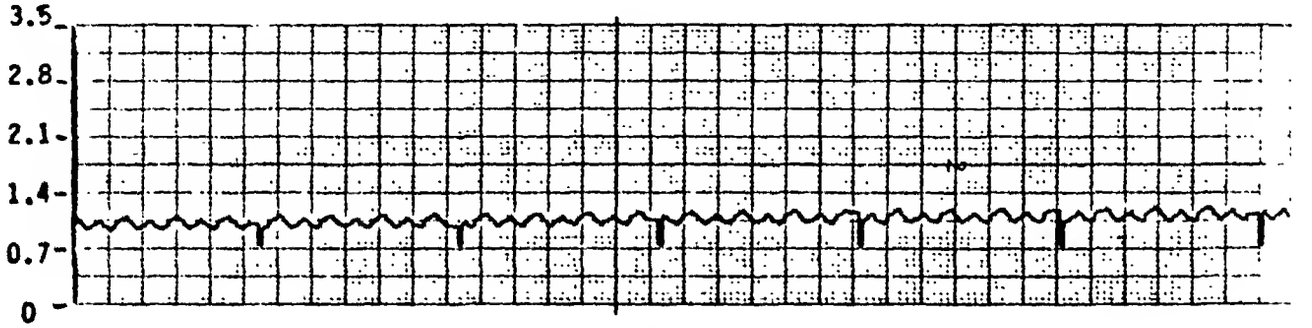

Figure 2F Remarks: Spin modulation is very pronounced

Day/Time 086/0502 :00(Z)

FIGURE H-2 Post Eclipse Solar Bus 1 Current (continued)

Solar Bus Current (S.B.#1)
(amp)

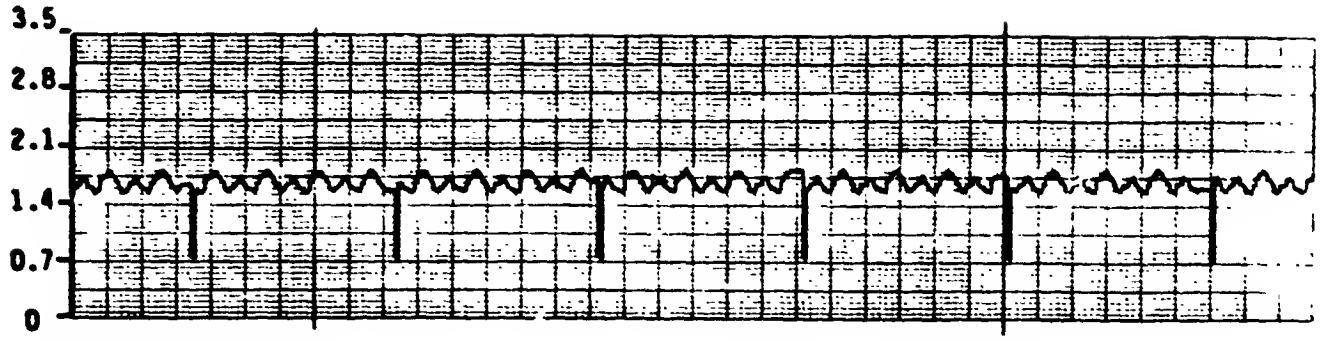

Figure 2G Remarks: _____

Day/Time 086 /0503 :45(Z)

Solar Bus Current
(amp)

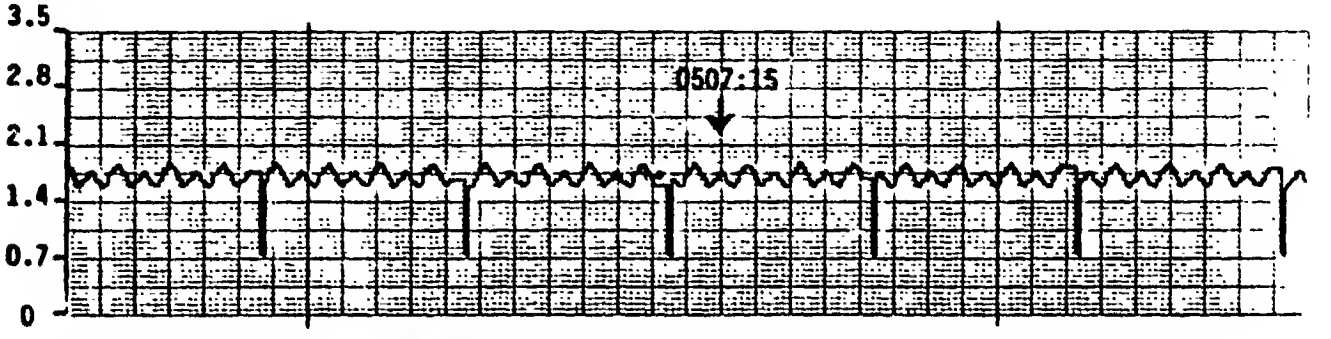

Figure 2H Remarks: Current Control Unit ON (0507:15)

Day/Time 086 /0507:05(Z)

Solar Bus Current
(amp)

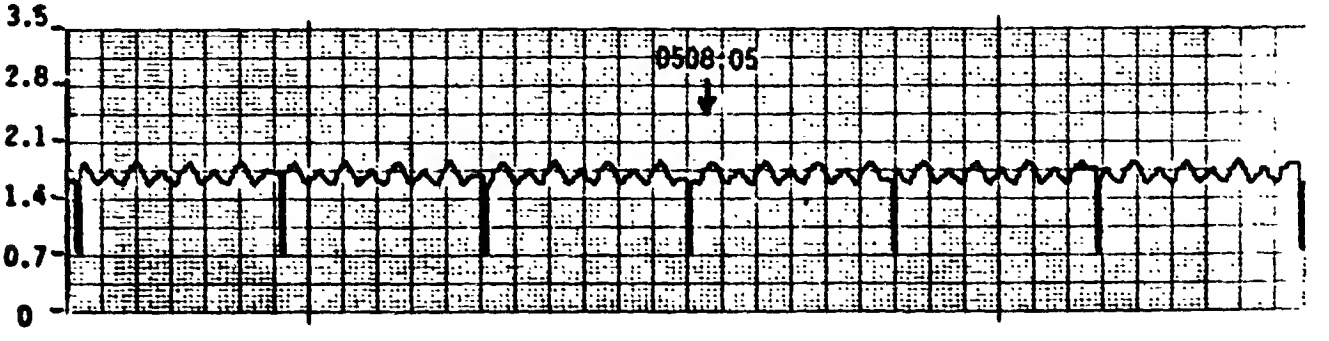

Figure 2J Remarks: MWW Reg #1 ON (0508:052)

Day/Time 086 / 0507;55(Z)

FIGURE H-2 Post Eclipse Solar Bus 1 Current (continued)

Solar Bus Current (S.B.#2)
(amp)

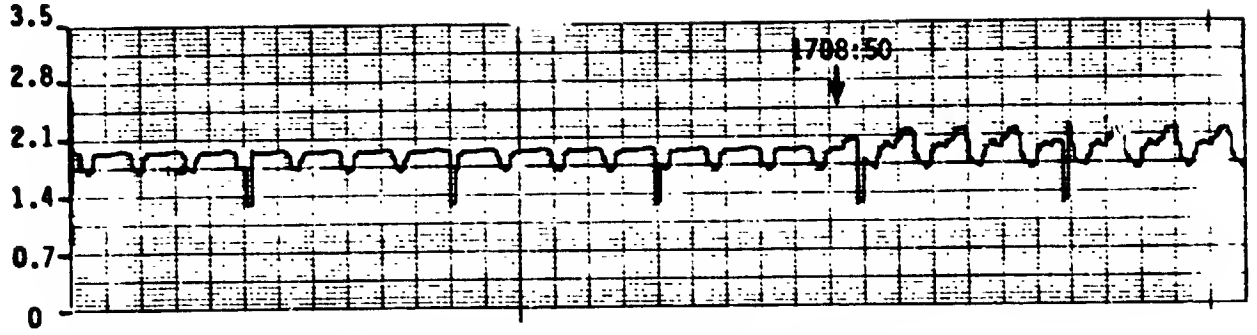

Figure 3A Remarks: Repeater 2 ON (FT Mode) at 1708:50

Day/Time 139 / 1708:39(Z)

Solar Bus Current
(amp)

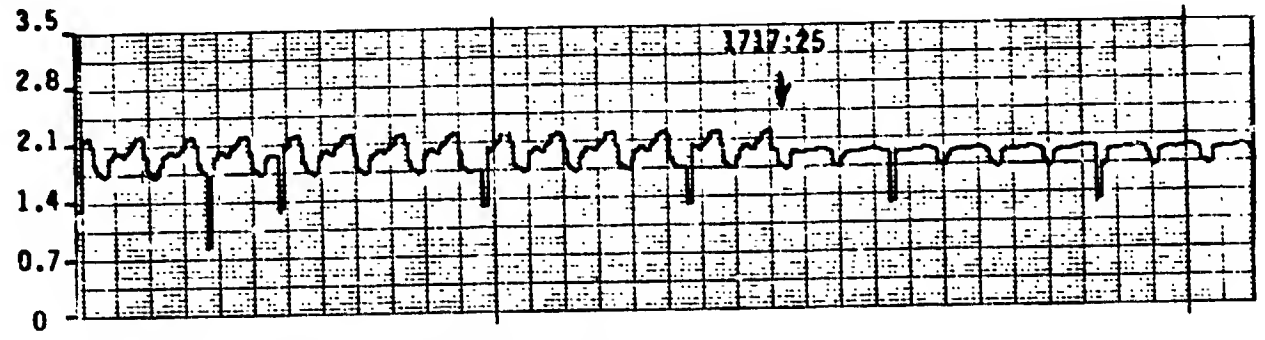

Figure 3B Remarks: Repeater 2 OFF at 1717:25

Day/Time 139 / 1717:15(Z)

Solar Bus Current
(amp)

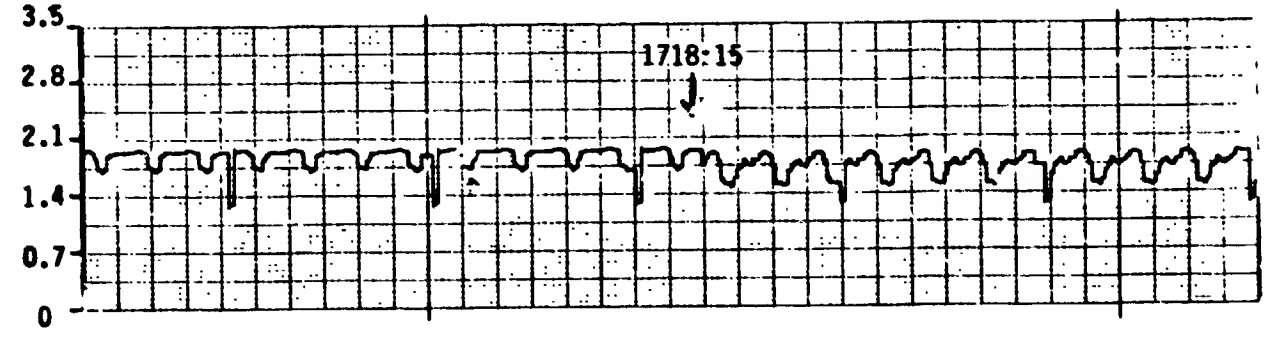

Figure 3C Remarks: Repeater 1 OFF at 17:18:15

Day/Time 139 / 1718:06(Z)

Figure H-3 Solar Bus 2 Current

Solar Bus Current (S.B.#1)
(amp)

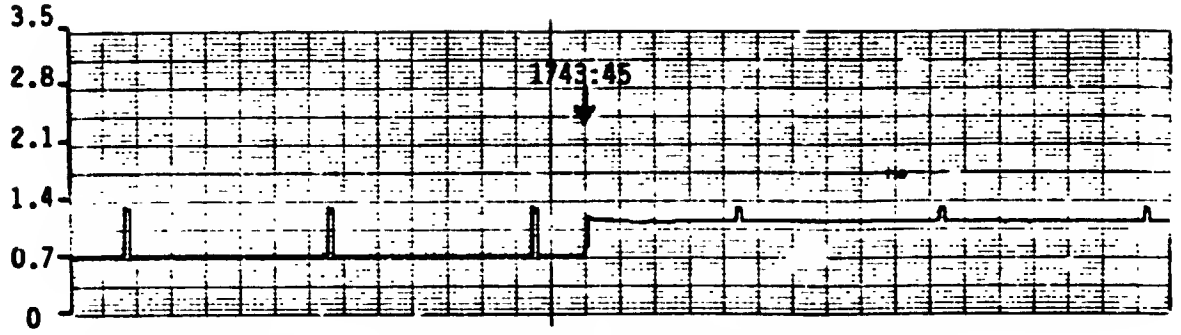

Figure 4A Remarks: Current Control Unit on at 1743:45(Z)

Day/Time 139 / 1743:38(Z)

Solar Bus Current
(amp)

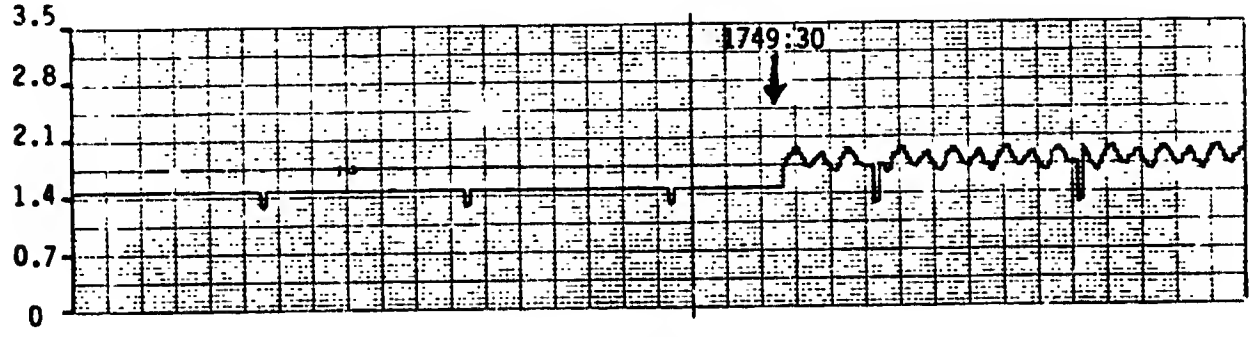

Figure 4B Remarks: RPTR 1 HV on at 1749:30

Day/Time 139 / 1749:20(Z)

Solar Bus Current
(amp)

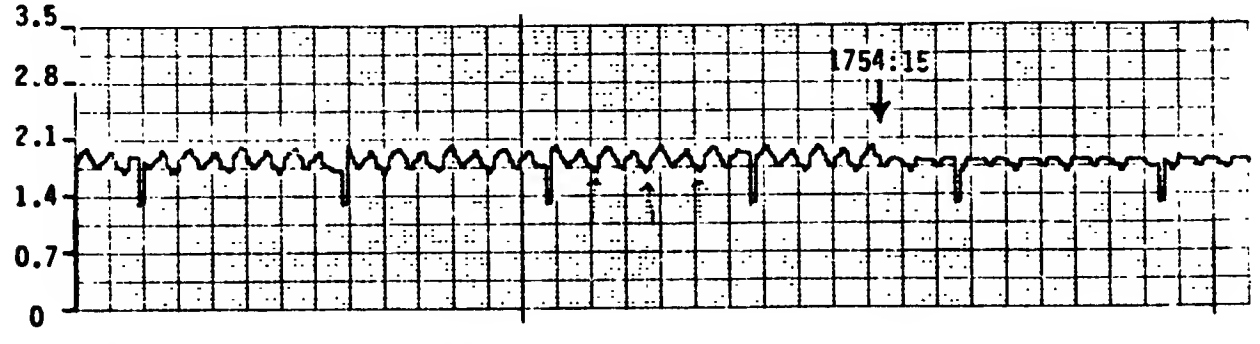

Figure 4C Remarks: Current Control Unit Off at 1754:15(Z)

Day/Time 139 / 1754 :03(Z)

FIGURE H-4 Solar Bus 1 Current

Solar Bus Current (S.B.#1)
(amp)

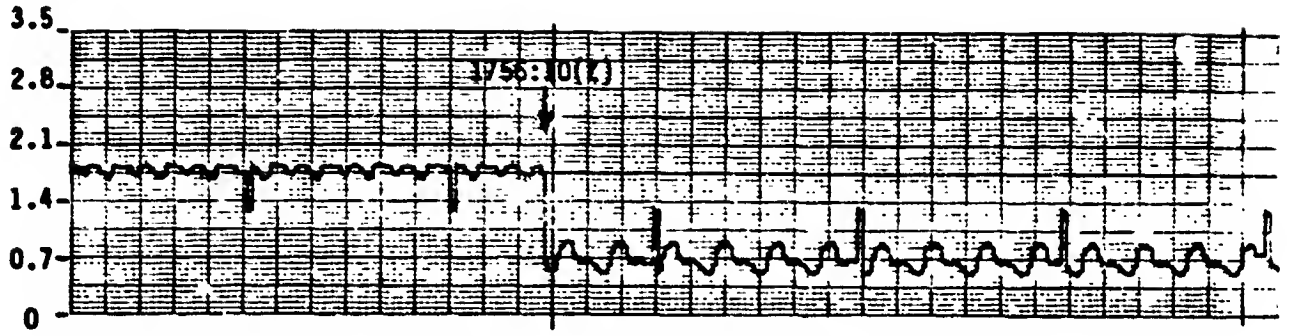

Figure 4D Remarks: Solar Bus 1 & 2 Paralleled at 1756:10(Z)

Day/Time 139 / 1756:03(Z)

Solar Bus Current
(amp)

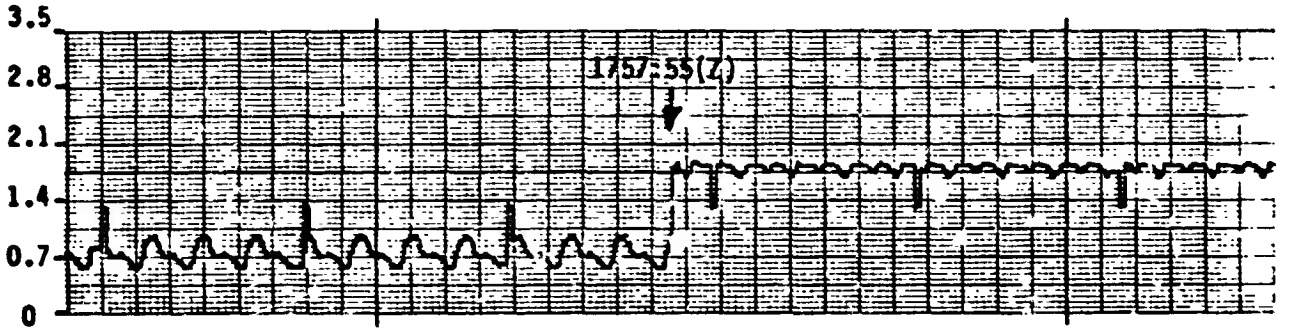

Figure 4E Remarks: Solar Bus 1 & 2 Unparalleled at 1757:55(Z)

Day/Time 139 / 1757:46(Z)

Solar Bus Current
(amp)

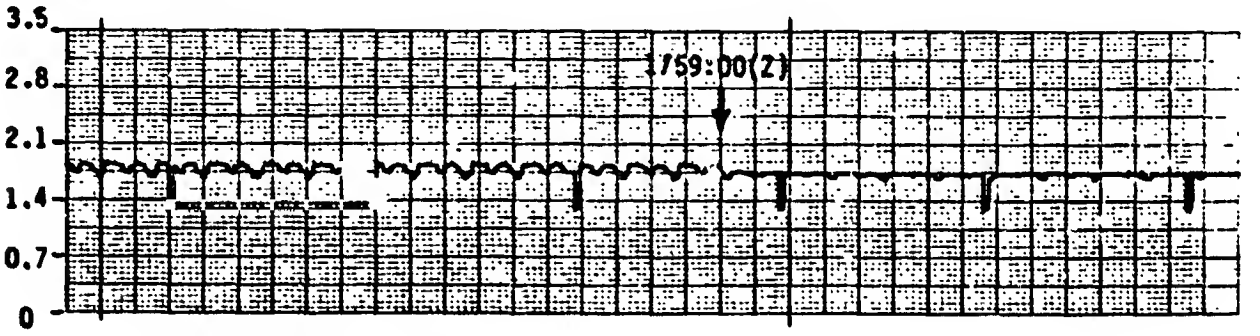

Figure 4F Remarks: ION Engine 1 Reg OFF at 1759:00(Z)

Day/Time 139 / 1758:50(Z)

FIGURE H-4 Solar Bus 1 Current (continued)

Solar Bus Current (S,B,#1)
(amp)

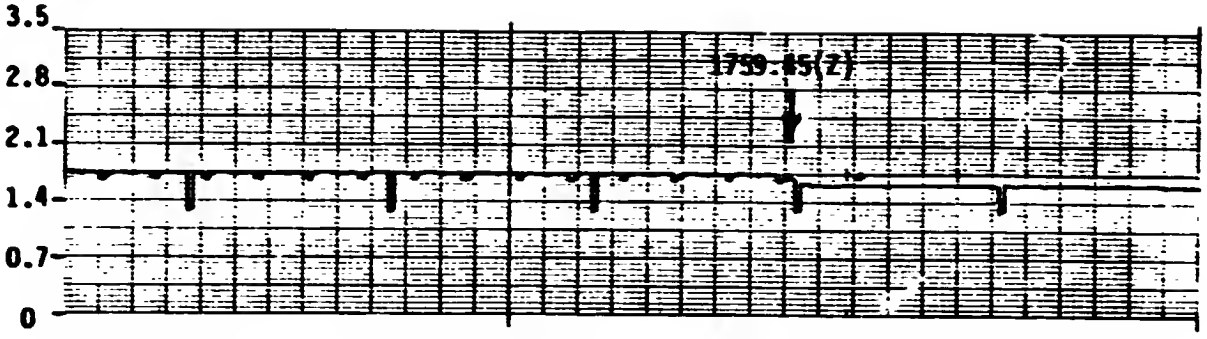

Figure 4G Remarks: Resistor Jet Exp Reg OFF at 1759:45(Z)

Day/Time 139 / 1759:35(Z)

Solar Bus Current
(amp)

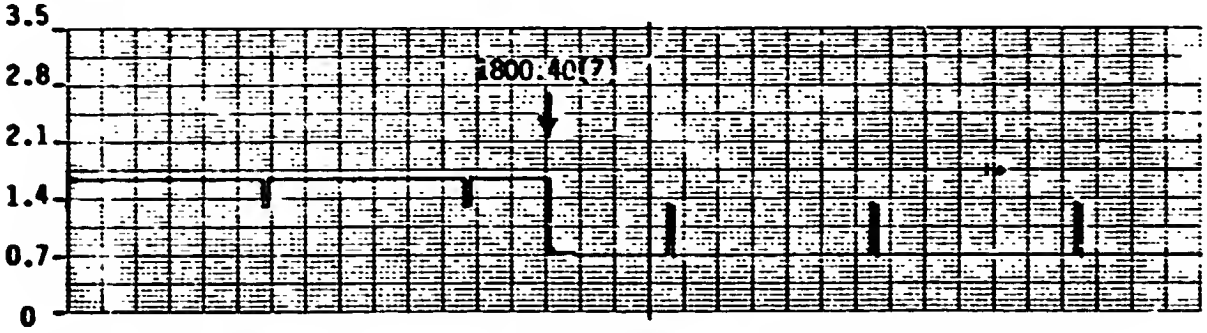

Figure 4H Remarks: Repeater No. 1 OFF at 1800:40(Z)

Day/Time 139 / 1800:33(Z)

Solar Bus Current
(amp)

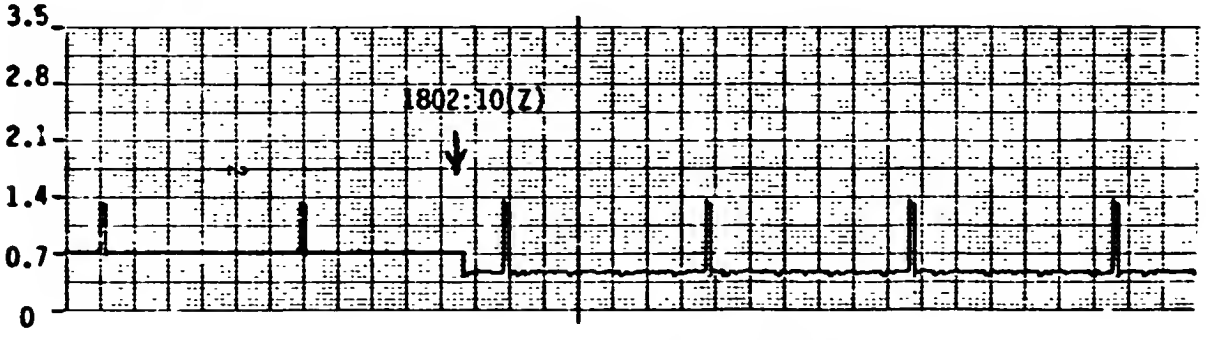

Figure 4J Remarks: Solar Bus No. 1 and 2 Paralleled at 1802:10(Z)

Day/Time 139 / 1802:04(Z)

FIGURE H-4 Solar Eus 1 Current (continued)

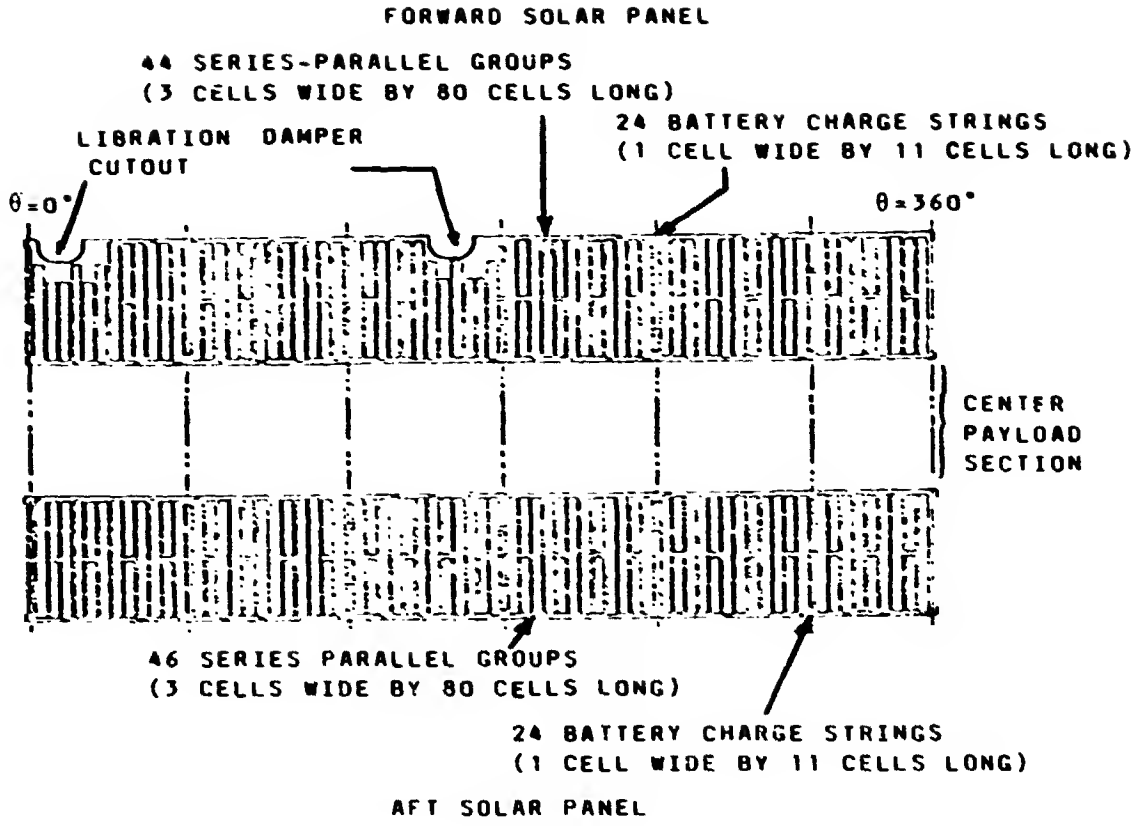

FIGURE H-5 Solar Cell Panel Layout